Представляем научные достижения миру. Естественные науки

Saratov State University

Presenting Academic Achievements to the World. Natural Science

Papers from the IV international conference
for young scientists
«Presenting Academic Achievements to the World»

March 15–16, 2013
Saratov

Issue 4

Saratov University Press
2013

Саратовский государственный университет им. Н. Г. Чернышевского

Представляем научные достижения миру. Естественные науки

Материалы IV международной
научной конференции молодых ученых
«Presenting Academic Achievements to the World»

Март 15–16, 2013
Саратов

Выпуск 4

Издательство Саратовского университета
2013

УДК 5(082)
ББК 20я43
П71

П71 **Представляем научные достижения миру. Естественные науки :** материалы научной конференции молодых ученых «Presenting Academic Achievements to the World». – Саратов : Изд-во Сарат. ун-та, 2013. – Вып. 4. – 164 с. : ил.

В данном сборнике опубликованы материалы участников секции естественных наук IV международной научной конференции молодых ученых «Presenting Academic Achievements to the World», которая состоялась в Саратовском государственном университете 15-16 марта 2013 года. В сборник включены статьи с результатами исследований в области физики, химии, географии, геологии и информационных технологий.

This publication assembles papers given at the IV international conference for young scientists «Presenting Academic Achievements to the World» which was held in March 15-16, 2013 at Saratov State University. The articles present the results in such fields of natural science as Physics, Chemistry, Geograghy, Geology and Information Technology.

УДК 5(082)
ББК 20я43

Работа издана в авторской редакции

ISSN 2305-2937

THE MORPHOLOGICAL CHARACTERISTICS OF HEAVY FRACTURED MINERALS OF SANDY ROCKS IN BOBRYKOVSKIY HORIZON WITHIN BEREZOVSKAYA GROUP OF UPLIFTS NEAR THE SARATOV VOLGA REGION

K.M. Antonov

Saratov State University

The main task of detecting the paleogeographic features of sedimentation in paleobasins is to establish the provenance of the source area and composition of destructible rocks, which were major suppliers of terrigenous material in the paleobasins (Гроссгейм, 1984). The composition and morphological features of heavy fractured minerals are the essential sign of their origin and serve as the proof of terrigenous links as indicators of provenance of the source area (Бергер, 1987). Following this purpose we analyzed the composition of the heavy sandy rocks fraction in Bobrykovskiy horizon within Berezovskaya group of uplifts.

Tectonically Berezovskaya group of uplifts is located in the northwestern part of the pre-edge area of Caspian depression, at the junction zone of Zolotovsk-Kamenskaya raised area and Stepnovskiy complicated swell (Шебалдин В.П. 2008).

According to the reflecting horizon nC1bb within the investigated area on the background of monocline immersion to the southeast, three structures can be traced: Berezovskaya, Eastern- and Western- Berezovskaya, representing the anticline wrinkles.

Analyzes of the morphological features of sandy rocks heavy fractured minerals in bobrykovskiy horizon were performed in the following wells : Z-1

(range 2360.3-2361.9 m), W-2 (intervals 2356.7-2357 m and 2369.7-2375.5 m), B-1 (interval 2402.0-2405.9 m), B-2 (interval 2398.7-2400.7 m), C-1 (intervals 2416.0-2418.0 m and 2420.0 -2422.0 m).

While studying the mineral composition of the heavy fraction, it was established that, independently on granulometric composition, the highest content of the heavy fraction outputs has the dimension of 0.063 - 0.08 and 0.08 - 0.1 mm.

According to the classification of the physical and chemical stability of the heavy fraction minerals three groups are distinguished: 1 - highly resistant igneous minerals and stable metamorphic (rutile, tourmaline and zircon), 2 - unstable and interstage (garnets), 3 - Ore minerals (chromite, ilmenite and leucoxene).

In almost all samples there were detected tourmaline, rutile, zircon, leucoxene. Ore minerals are represented by ilmenite and chromite. Garnets and anatase, which occur as individual grains, behave differently.

Tourmaline is found in sediments as prismatic crystals and its debris. Crystal's figure is elongated and shortgated. In its cross section the mineral has the spherical triangle, the panes are often with vertical hatching and sometimes have a smooth (clean) surface. The mineral color is mostly brown to dark brown, sometimes gray to black. The ubiquitous presence of tourmaline in the heavy fraction is typical for the bobrikovskiy deposits.

Rutile occurs in sediments as crystals of various forms, their debris and grains of various rounding degrees. The crystals usually have an elongated prismatic shape, sometimes in combination with bipyramid. Rutile prismatic crystals' surface is smooth and is often characterized by a vertical (thin) or diagonal hatching. Debris are usually irregular in shape and of various degrees of rounding, sometimes there are oblong-oval grains. By color crystals are red, cherry red, with reddish-brown, golden-yellow, yellow-brown varieties. Rutile grains are mostly pure, rarely with leucoxene.

There are three morphological types for rutile. Rutile as the most widespread placers mineral, occurs as prismatic crystals of the columnar shape. They are characterized by complex prisms forms (tetragonal and ditetragonal) with bipyramid and sometimes truncated bipyramid (in combination with pinacoids). The cross-section often takes shape through pseudoround complications faces in prismatic zone. This kind of rutile forms is typical for metamorphic rocks and much less common for igneous rocks. The second rutile type is represented by toggle doubles, which is most typical for the pegmatite veins. The third type of rutile is granular aggregates of rounded and angular-rounded

forms are usually built in the weathering process from different magnesium-iron-formations.

Rutile is usually observed in all the investigated core samples.

Zircon is founded in studied deposits as pink and yellow-brownish grains, less often as clear and uncolored, of various degrees of roundness, from the well-faceted crystals to oval-rounded grains. Sometimes grains with zonal structure are found, as well as hatching on the edges. Due to its stability, zircon is a widespread mineral and exists in nearly every analysis of any sample.

There are three morphological types of zircon which clearly indicate different conditions of their formation. The first "zircon" prismatic type is characterized by a combination of two tetragonal prisms and a tetragonal dipyramid, sometimes in combination with a skalenoedr. This type is widespread in syenites and alkaline syenites, and sometimes occurs in gabbro as the accessory mineral. "Hyacinth" prismatic type of zircon is characterized by the combination of three tetragonal prisms with a tetragonal bipyramid. It is typical for common granites and associated vein rocks. The third type of zircon, isometric is defined by approximately the same development of its tetragonal prisms of different orders and edges of the main dipyramid. This type is common in moderately acidic igneous rocks, such as granodiorites.

Ilmenite is presented in almost all samples as grains of irregular shape, which are sometimes leycoxenized. Minerals' color is dark gray to black. Its role in the heavy fraction is quite mosaic.

Garnets in the sediments are presented by transparent, uncolored or pink colored crystals. Grains are of angular debris, rarely rounded. Sometimes garnets are found in the form of well-faceted crystals (rhombododecahedrons). The surface of the grains is mostly clean, but there can be small cracks on it sometimes.

Anatase is presented by crystals of tabular forms or bipyramidal habitus, sometimes in the form of crystal fragments and irregular grains, of blue and azure colours. The mineral is transparent or semi-transparent due to the hatch on the surface of the grains. Anatase is found in the well samples.

In the section of the well 1 the mineral composition of the heavy fraction is mainly represented by tourmaline, rutile, zircon, ilmenite, and leycoxen. There are sometimes single grains of garnet and anatase. A complex morphological set of accessory minerals in the heavy fraction shows different sources of terrigenous material, which could be either igneous or sedimentary. Zircon and rutile's form conforms in their morphological features to the rocks of the Voronezh crystalline massif (metamorphic granites, granite-syenite, veined formation and volcanic-sedimentary rocks). It is necessary to mention the fact

of prevalence of the rounded mineral grains' edges, which suggests a sedimentary complex of more ancient rocks as the source.

Taking into account the frequency of occurrence of the identified minerals in the heavy fraction's composition, there can be identified a zircon-rutile-tourmaline mineral association.

The composition of the heavy fraction and morphological features of the minerals in samples from well 2 of the interval 2356.7-2357.7 m do not differ from the composition and morphology of the minerals in samples from well 1. For the given interval a zircon-rutile-tourmaline association is also typical.

In the interval 2369.7 – 2375.5 m (well 2) the role of ore minerals – ilmenite, and chromite appears.

Considering the role of the ore minerals in the heavy fraction of the samples in the given interval, we can conclude that the main mineral association is rutile-tourmaline-ilmenite.

An obvious difference in the set of minerals in the heavy fraction of the upper and lower intervals and their morphological differences indicate that the source of the terrigenous material in the interval 2356.7-2357.7 m was a more ancient sedimentary complex, and for the interval 2369.7-2375.5 m – it was the metamorphic and igneous complex of the Voronezh crystalline massif.

The mineral composition of the heavy fraction of sandy rocks in well 1 is tourmaline, rutile, zircon, ilmenite, and leycoxen. There are sometimes single grains of anatase. The prevailing association is zircon-rutile-tourmaline.

The mineral composition of the heavy fraction of the rocks of bobrykovskiy horizon in well 2 is mainly tourmaline, rutile, zircon, ilmenite, and leycoxen. Prevailing association is zircon-rutile-tourmaline.

For mineralogical analysis of the heavy fraction of the rocks of bobrykovskiy horizon in well 1 eight samples were selected from the interval 2416.0-2418.0 m and 2420.0-2422.0 m.

The composition of the heavy fraction and morphological features of the minerals in the samples from well 1 of the interval 2416,0 -2418.0 m do not differ from the composition and morphology of the mineral samples from well 2 of the interval 2356.7-2357.7 m. Except the core set of minerals (tourmaline, rutile, zircon, leucoxene), single grains of garnet are identified. For the given interval a zircon-rutile-tourmaline association is also typical.

In the interval 2420.0-2422.0 m the role of ore minerals, ilmenite, is increased and chromite appears. Increasing of the ore minerals' role in the heavy fraction of the rocks in the interval 2420.0-2422.0 m allows allocating a tourmaline-rutile-ilmenite association.

Thus, the complex morphological set of the accessory minerals in the heavy fraction's composition indicates different sources of the terrigenous material's entry, which could be either igneous, metamorphic, and sedimentary rocks. The forms of tourmaline, zircon and rutile in this case are consistent with the morphological characteristics of Voronezh crystalline massif rocks (metamorphic granites, granite-syenite, veined formation and possibly volcanic-sedimentary rocks). The presence among the well-faceted crystals of rounded grains of minerals shows that the source was a sedimentary complex of the older rocks.

REFERENCES:

1. *Бергер М. Г.* Терригенная минералогия. М. : Недра, 1986
2. *Гроссгейм В. А.* Методы палеогеографических реконструкций, 1986
3. *Шебалдин В. П.* Тектоника Саратовской области. Саратов: ОАО «Саратовнефтегеофизика», 2008

BIOMECHANICAL ANALYSIS OF CAROTID PATHOLOGICAL BENDING

A.V. Aristambekova, A.A. Goliadkina, O.E. Pavlova

Saratov State University

Cerebrovascular disease has been the leading cause of morbidity and mortality for many years. At present cerebral stroke ranks second to cardiac infarction among the causes of death. There are about half a million strokes in Russia every year and 35% of them are fatal, 50% of people become handicapped and only 10% fully recover. However most of them have the second stroke in next 5 years. It should be noted, that the highest death rate is among 30 – 50 aged people.

At present time it is estimated that 80% of strokes has ischemic genesis. The cause of the ischemic stroke can not only be ischemia associated with abrupt reduction of blood flow due to vessel stenosis or occlusion induced by atherosclerotic lesion but misperfusion induced by pathological tortuosity of carotid and vertebral arteries.

Unfortunately surgical treatment of such diseases is the only effective method. However there are no objective indications to the employment of specific surgical procedure of optimal blood flow reconstruction. The devel-

opment of such recommendations for carotid plasty requires construction of as much as possible acute mathematical model and investigation of vessel biomechanics from the point of view of hemodynamic theory of atherogenesis. It is also necessary to take into account individual features of the patient such as vessel geometry, mechanical properties of the wall, velocity and pressure of blood in different sections of vascular bed. This allows to conduct 'virtual operation' at the stage of preoperative examination of the patient in order to choose the most appropriate type of surgery from the biomechanical point of view. It will also serve the basis for clinical trial for the purpose of surgery results prediction.

Model construction

The construction of three-dimensional geometry models based on magnetic resonance imaging in the specialized program package SolidWorks was conducted. It was supposed that all vessel cross-sections are circles. Smooth surface based on these circles using directional and axial lines (Fig. 2) was created.

Geometry models of healthy carotid artery (Fig. 1) and carotid artery with pathological C-bending (Fig. 2) for different bending angles: 90, 100, 110, 120 and 130º were constructed.

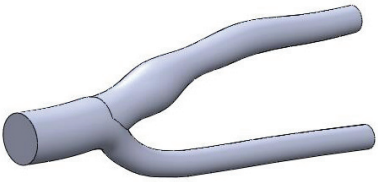

Fig. 1. Model of healthy carotid artery

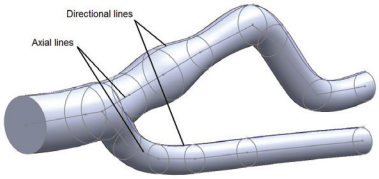

Fig. 2. Model of carotid artery with pathological C-bending

Numerical experiment

Obtained models were then imported into Ansys Multiphysics for further finite-element simulation. They were meshed with tetrahedrons because of the geometry complexity. The size of tetrahedrons was 0.0005 m.

Blood was assumed to be homogenous, incompressible and Newtonian fluid. The material of the wall was assumed to be homogenous, isotropic and perfectly elastic. Wall behavior is described with the help of Newton's second law of motion.

There was rigid attachment on the wall butts. There was condition of equality of velocity of fluid particles that are adjacent to the wall and corresponding wall particles on the artery wall. Zero pressure was applied at the

outlets from internal carotid artery (ICA) and external carotid artery (ECA). We apply velocity at the inlet to common carotid artery (CCA) (Fig. 3).

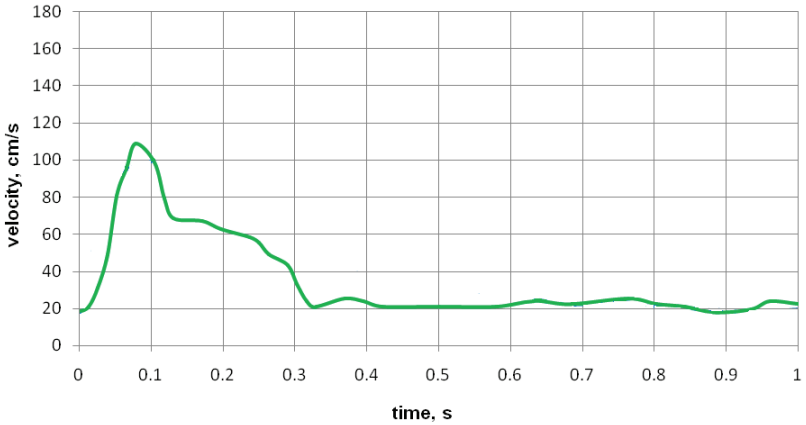

Fig. 3. Blood velocity during cardiac cycle

Mechanical data of blood and artery wall were accepted as following: blood density is 1050 kg/m^3, viscosity is 0.0037 Pa·s, vessel wall density is 1378 kg/m^3, Poisson's ratio is equal to 0.4, Young modulus is $5.5 \cdot 10^6$ N/m^2 (Павлова и др., 2010).

Results and discussion

Analysis of numerical results was conducted in accordance with phase of the cardiac cycle: systolic phase (SP) and diastolic phase (DP).

Analysis of blood flow in DP shows that there is similar distribution of velocity in all six models. In SP the decreasing of bending angel causes appearance of velocity minimum in the area of most bending of ICA.

Pressure maximum in DP shifts from CCA to carotid bulb while decreasing of bending angel. In SP pressure maximum locates in the bulb and the area of most bending near the convex surface of the wall.

Low wall shear stress (WSS) is located in carotid bulb and in contrast to normal CA there is the region of low WSS in the area of most bending in pathologically tortuous carotid arteries.

Analysis of stress-strain state shows that distribution of strain in DP coincides with the distribution of stress. In SP maximum of strain and stress is located in carotid apex and it appears in the area of most bending for carotids with 90º and 100º bending.

Numerical analysis allows to draw the following conclusions:

1. There are low WSS and blood flow velocities in the carotid bulb. According to the atherogenesis theory it indicates to possible formation of atherosclerotic lesions. In addition high stress and strain in apex point to artery epithelial layer injury, which also leads to pathological alteration of carotid artery.

2. Decreasing of ICA bending angle forms the second critical region of atherosclerotic lesion in the area of most bending, which is confirmed by low WSS and blood velocity.

This research allowed to obtain knowledge of blood flow in consideration of the wall stress-strain state for healthy carotid artery and artery with pathologies and reveal the features of the processes that take place in this biomechanical system. Numerical experimental results enable operating surgeon to take into account this features to choose surgery method correctly and avoid potential errors during the operation.

ACKNOELEDGMENTS:

This work was supported by grant «У.М.Н.И.К.»

REFERENCES:

1. *Павлова О.Е., Иванов Д.В., Грамакова А.А., Морозов К.М., Суслов И.И.* Гемодинамика и механическое поведение бифуркации сонной артерии с патологической извитостью// Известия Саратовского ун-та. 2010. Т.10, №2. С. 66-73.

3D VISUALIZATION USING SCANNING ELECTRON MICROSCOPY

V.S. Atkin, N.O. Bessudnova

Saratov State University

INTRODUCTION:

Scanning electron microscopy (SEM) is widely being used for object visualization at micro- and nano- scales (Dykstra M. J. and Reuss L. E., 2003). However, SEM images are just two-dimensional plains of three-dimensional objects, which makes it difficult to determine their metric characteristics such as volume and depth of observed structures.

Principles of 3D model reconstruction are similar in applied software and human brain. The world around us is perceived in three dimensions due to binocular vision. Two pictures of the same object are formed at different angles of

view and merged into a single pattern in the visual center of the human brain, reconstructing a three-dimensional object.

Alicona 3D MeX software (Alicona Imaging GmbH) (Alicona Imaging GmbH, 2009) is based on the principle in the process of 3D model reconstruction, described earlier. The program calculates three dimensional models from plain SEM images.

The present study aims 1) to develop a novel technique of 3D pattern reconstruction and evaluate its optimal parameters; 2) to determine trends in error appearance on the steps of a 3D model design.

MATERIALS AND METHODS:

The program suite Alicona 3D MeX was used for 3D-processing of two-dimensional SEM microphotographs. Three-dimensional images were generated by reconstructing the volume from several two-dimensional plains produced at different angles of sample observation. It was essential to fix 2D images to keep the sizes of an electron beam irradiation area constant. The software algorithm automatically selected the homology points and calculated the distance between them to evaluate a unique roughness height.

A joint application of Alicona software and selected microscope revealed the problem of image defocusing at high magnifications along with the changes in the angle of sample observation. The problem was mainly caused by absence of the eucentric tilt function in the microscope's software. Fig. 1 il-

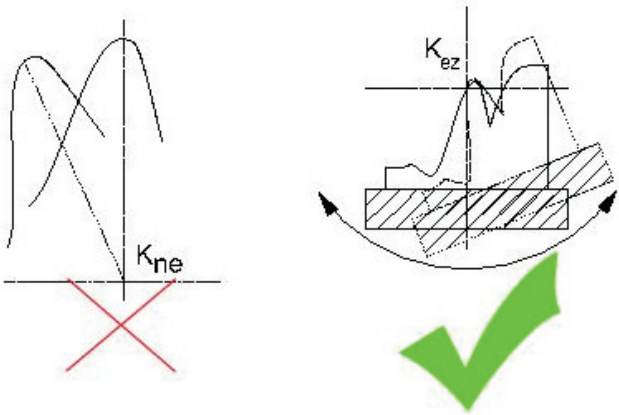

Fig. 1. The tilting mode programmed in the scanning electron microscope software, K_{ne} – the tilt axis (on the left) and the eucentrical tilting, K_{ez} – the eucentrical tilt axis (on the right)

lustrates the eucentric tilting when an object table's tilt axis intersects with the electron beam's impact position. The eucentric tilt function could be simulated gradually changing the tilting angle along with an object table shift. In this case, to reconstruct a 3D model most accurately, it is important to hold the view field value constant.

RESULTS:

To construct 3D models three samples were selected: a razor blade, a shell of a bullet, and a calcium-phosphate crystal on dentine surface. All samples were of different size and shape and made of different kinds of materials.

Fig. 3 shows the results of 3D visualization of the razor blade (Fig.2).

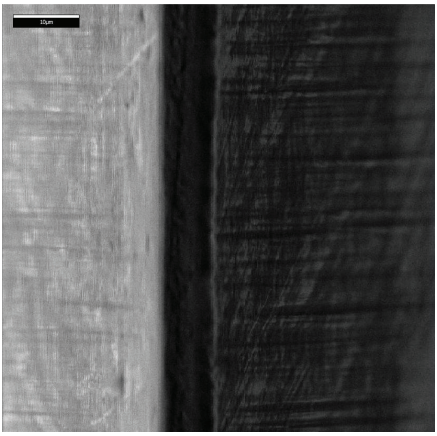

Fig. 2. A SEM image of a razor blade (top view)

As for the size and shape, the generated 3D model concurred with a real object and did not have noticeable cracks in model reconstruction. Defocusing was not observed due to the object's large sizes and quite low magnification.

Another research object that was studied is a fired bullet shell (Fig. 4) or, more precisely, traces and scratches on its surface caused by friction between the bullet and barrel as well as high temperature at the moment of a shot. The peculiarity of the object is a great amount of irregularities on its surface. The results of calculations are presented in Fig. 5.

The 3D models of shot traces accurately reflect real scratches and grooves on the shell surface and even pieces of melted metal that are formed as soon as incandescent gases are expanded. It is worth noticing that it is the 3D model that makes it possible to identify cavities and convexities in the SEM image.

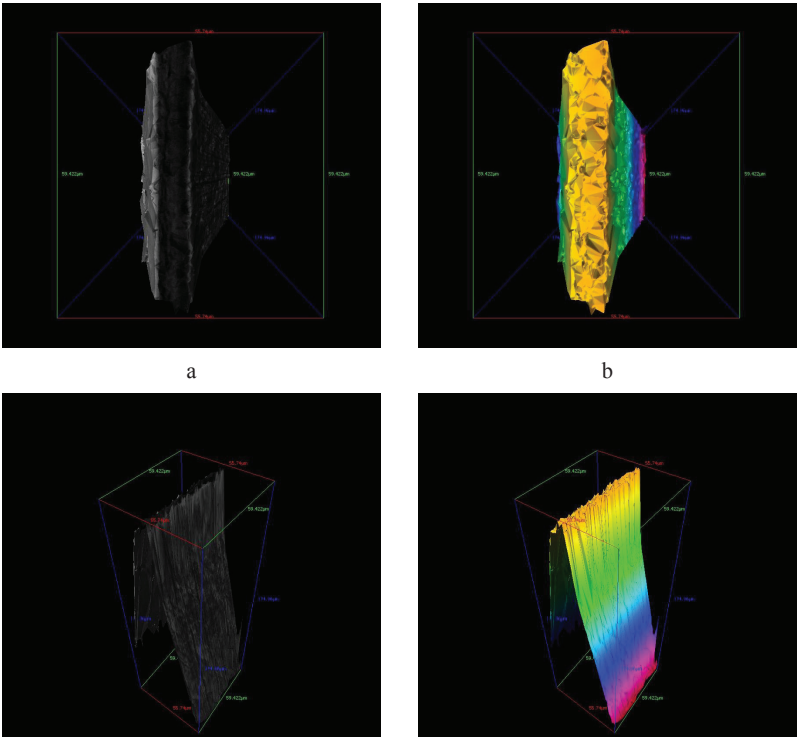

a b

c d

Fig. 3. The 3D model of a razor blade (a, c) and the color/height distribution (b,d)

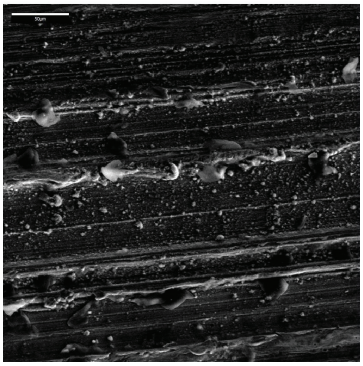

Fig. 4. A SEM image of surface morphology of a bullet shell

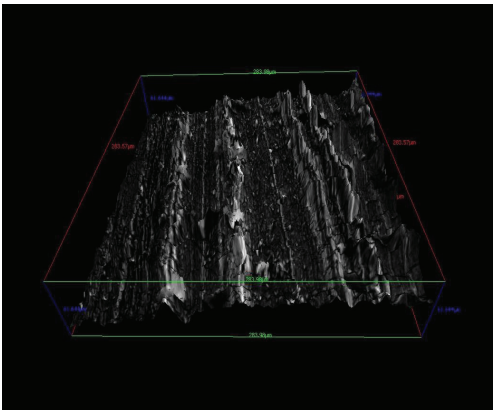

Fig. 5. The 3D model of the bullet shell surface

Last object that was researched is a crystal formation grown on dentine surface (Bessudnova N.O. etc., 2013). The example of SEM visualization of an aster-like crystal and its 3D model are shown in Fig. 6 and Fig.7, 8 respectively.

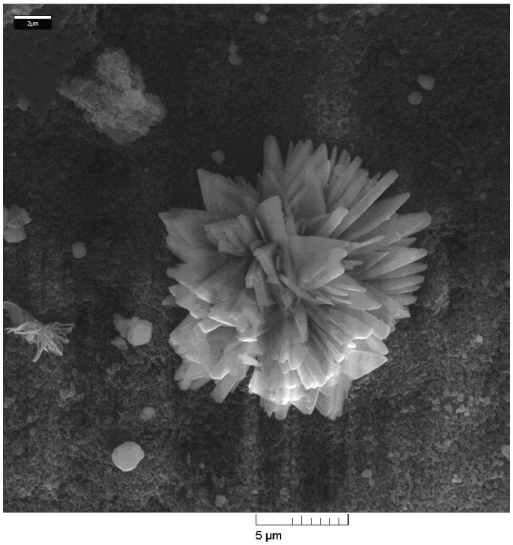

Fig. 6. A SEM-image of surface morphology of a single crystal on dentine substrate

The evaluated model contains the crystal itself and surrounding surface fragments. The reconstructed three-dimensional image made it possible to visualize the shape of the crystal.

However, it was impossible to reproduce a real object's shape in full in the generated model, which was caused by the loss of the object's fine details (Fig. 7a). In particular, the noticeable peaks and "petals" in crystal morphology were not built, while being visible in 2D microphotographs. Image details did not come out because the electron beam was shielded by the protruded parts of the crystal even at significant tilting angles. As a result, there was no available information about the surface under this crystal's parts and the reconstruction was completed in a random manner.

Usually, if data loss occurs, it is necessary to make a comparison between a 3D model and 2D images as well as to perform the procedure of interpolation to collect the lost data and completely reconstruct the model. An example of the three-dimensional crystal model after the procedure of interpolation is shown in Fig. 7b.

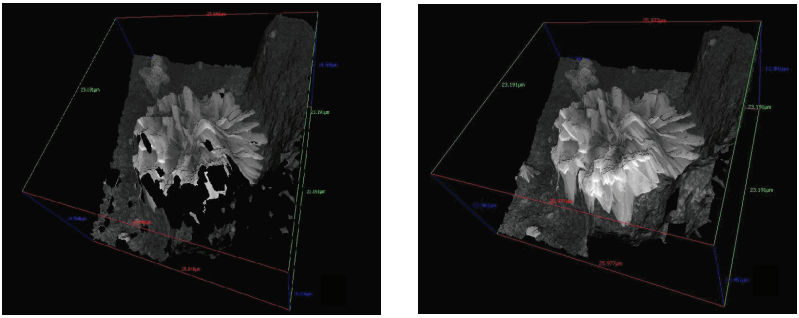

a *b*

Fig. 7. A three-dimensional model before (a) and after (b) the procedure of interpolation

CONCLUSION:

3D visualization of various objects at micro- and nanoscales has been performed using a scanning electron microscope and Alicona 3D MeX software. The nature of possible errors in the steps of model design has been studied:

1. It was shown that defocusing at high magnifications, which occurs under object table tilting is a significant problem in model generation. The problem is mainly caused by the lack of the eucentric tilt function in the microscope software. Fortunately, the eucentric tilt function could be simulated changing gradually the tilting angle along with the object table shift. In this case, to re-

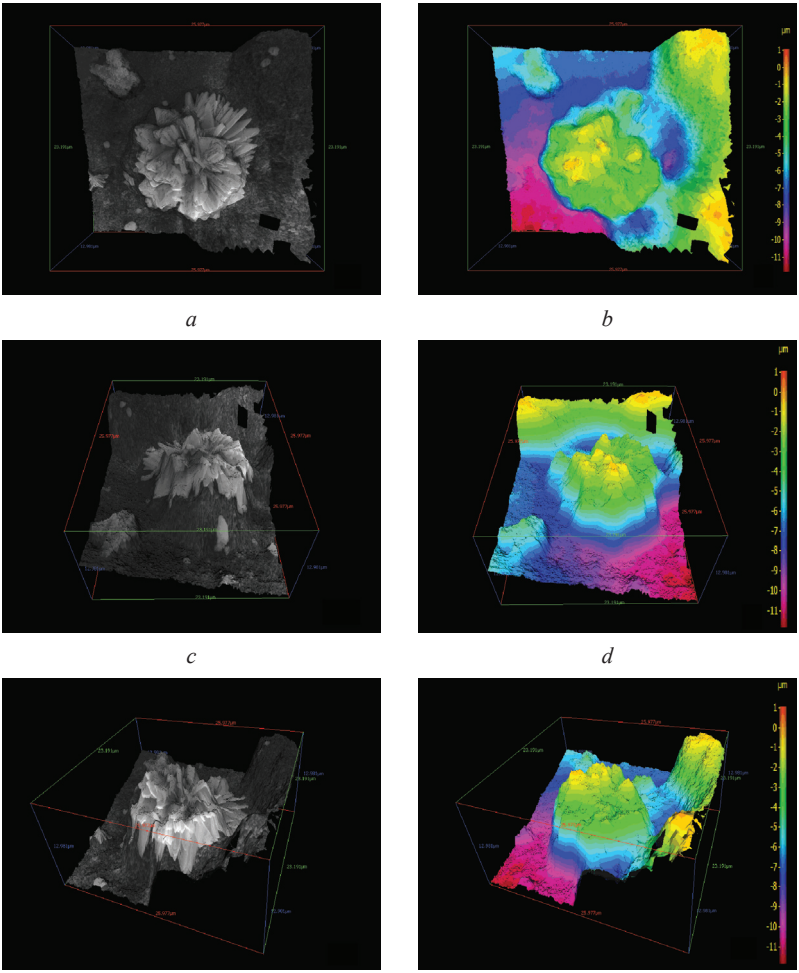

Fig. 8. Three- dimensional models of the crystal after the procedure of interpolation in three different planes (a, c, e) and the corresponding height distribution in color (b, d, f).

construct a 3D model most accurately, it is essential to hold the field of view constant.

2. While reconstructing 3D-objects with complicated geometry, it is necessary to keep in mind possible data loss, especially partial loss of the model's

fine details. The sources of errors were mainly the crystal's protruded parts reflecting an electron beam.

REFERENCES:

1. Alicona Imaging GmbH. Alicona 3D MeX User's Guide / Brno, Czech Republic, 2009.
2. *Bessudnova N.O., Bilenko D.I., Venig S.B., Atkin V.S., Galushka V.V., Zakharevich A.M.* 3D visualization of calcium-phosphate crystals observed on dentine surface // Proc. SPIE. 2013. 86990J, doi: 10.1117/12.2018762.
3. *Dykstra M.J., Reuss L.E.* Biological Electron Microscopy: Theory, Techniques and Troubleshooting / Springer publishing, 2003.

THE ROLE OF OXYGEN IN BRIGGS–RAUSCHER AUTO OSCILLATING REACTION

A.V. Bondarenko, A.P. Rytik, D.A. Usanov

Saratov State University

The first observations of sustained oscillations in real chemical systems belong to the beginning of the last century, but the real interest to the subject has been arising for the past 40 years (Жаботинский, Огмер, Филд и др., 1988). There are several reasons to explain it. Firstly, phenomena occurring in Belousov-Zhabotinsky reaction attracted the attention of experimentalists and theorists working in the field of chemistry and engineering. Secondly, the discovery of the fact that rhythmic processes occur at any level of biological organization, have attracted to this problem also biologists. Finally, the modern theory of dynamical systems has reached such a level when its use has provided an opportunity to propose an effective means for the analysis of complex systems. Now in literature all the main stages of the liquid-phase auto oscillating chemical reactions, including Belousov-Zhabotinsky, Libava-Bray, Briggs-Rauscher (BR), and other reactions are rather good and detailed described. (Рытик, Усанов, Гребенников, Бондаренко, 2012) Also there are sources that represent the studies of similar processes in living systems: at the cell level (Белоцерковский, Опарин А, 2000; Буданов, 2001; Хакен, 1991), and at the organism level (Андреев, Белый, Ситько, 1984, Кольцов, 1936, Корзухин, 1976). In 1965, Graven SN, Estrada S., Lardy HA (Коваленко, Тихонова, Яцимирский, 1988) discovered cyclic uptake and release of ions [K +] and [H +] in the suspension of mitochondria (of the heart muscle).

Changing the color of Briggs–Rauscher auto oscillating reaction occurs due to a periodic change in the concentration of iodide-starch complex. The reaction depends on the ratio of the chemical potentials of the ions in two phases (Жаботинский, Огмер, Филд и др., 1988). Alexander Kovalenko describes one of the possible stages of the reaction (Коваленко, Тихонова, 1989; Коваленко, Тихонова, Яцимирский, 1988).

$$I + O_2 \rightarrow IO_2,$$

Authors concluded that this particular stage is a source of active radicals [IO_2], independent on the concentration of the switch phase fluctuations - iodide ions. Reaction behavior on this stage can lead to the switch of oscillation phase or their complete inhibition, depending on the light effect. In (Жаботинский, Огмер, Филд и др., 1988) the «Unexplained effects Briggs-Rauscher reaction» (str.215) was noted that oxygen may well participate in the reaction, although not included in its main 13 stages.

Iodine is formed rapidly at low ion concentration [I-] - the solution turns yellow. Then, the concentration of [I-] increases with [I_2], and forms a blue complex starch iodide. Most part of oxygen and CO_2 is liberated during the formation I_2. I_2 concentration reaches its maximum and begins to fall, until, finally, the solution becomes clear. A sharp drop in [I-] makes possible the repetition of the cycle.

Earlier cooperative behavior in auto oscillating chemical reactions has been shown, for example, in (Киселев, 2001; Гольдштейн, Аксиров, Закржевская, 2008). So, in (Гольдштейн, Аксиров, Закржевская, 2008), cooperative active centers dynein causes oscillatory activity of a reaction agent. There is a description of the influence of terahertz electromagnetic radiation at frequencies of absorption molecular oxygen on auto oscillating_Briggs-Rauscher reaction. It is shown that the effect of radiation at these frequencies changes the nature of the oscillations and can increase the total time of the auto oscillating regime. However, this work didn't give investigation of the influence of dissolved oxygen from the environment to the reaction.

So, the purpose of this work was to investigate the effect of oxygen in the reaction of Briggs-Rauscher.

The Experimental Part

Ingredients for Briggs-Rauscher reaction was prepared by the method described in (Briggs, Rauscher, 1973). These were:

1) 100 ml of 30% hydrogen peroxide in a measuring flask, adjusted the volume to 250 ml with distilled water;

2) 1.1 ml of concentrated H_2SO_4, mixed with 50 ml of water and 3.52 g iodic acid, brought to 250 ml of distilled water;

3) dissolved by heating in 20 ml of distilled water, 0.08 g of starch, 3.9 g of malonic acid (CH_2 (COOH) $_2$) and 0.85 g of manganese sulfate (II), after cooling of bringing the addition of distilled water in a measuring flask to 100 ml.

After the preparation of solutions they were mixed in one chemical container and divided into two identical flasks of 20 ml, for the better separation of volumes pipettes were used.

With the help of Sony HDR-220E camera, video recording was made in the optical range of auto oscillating reaction. Online data were received through the USB port to the computer, where with the help of special software the recording of video frames, process, and results output. Before the analysis of series of video frames calibration balance of the white of each frame was held.

Reaction media in the flask was irradiated with one generator of electromagnetic oscillations on Gunn diode operating at frequencies of the first zone of absorption of atmospheric oxygen (129 GHz). Generator power was 100 μW. With the help of flare beam of electromagnetic waves was formed, completely covering the media. The power density of finding a solution to the flask is 0.012 mW/cm2. Generation mode is continuous.

Stirring of BR reaction environment was done by a magnetic stirrer. All measurements were performed at a pressure of 760 mm Hg. Art. and room temperature. For registration of the chemical changes in the environment of reactions, including changes in the amount of dissolved oxygen, pH-meter-ionomer series “Expert-001” 8 with sensors was used.

1. Ion-selective electrode “iodine”;

2. Dissolved oxygen sensor DKTP integrated with temperature sensor.

At the time of video recording of the visible vibrations BR reaction, an analysis in the program Exp2pr was held, working with liquid analyzers series “Expert-001”, in which online reflect the dynamics of dissolved oxygen, the electrical potential iodine-selective electrode and temperature in the media (Graven, Estrada, Lardy, Proc., 1965; Melikhov, Vanag, 1995). Aeration agent reaction was performed using a nebulizer of compressor with a flow rate of 20 cm / s. These data were further analyzed using the program MathCad v.14.

To determine the influence of molecular oxygen on the characteristics of auto oscillating Briggs-Rauscher reaction three series of experiments were performed, with each at least two comparison among the control flask with experimental:

1) with artificial aeration with oxygen in the reaction medium;

2) The EMR irradiation at frequencies of the absorption spectrum of oxygen environment;

3) the combined action of EMR radiation and aeration.

Artificial Aeration of Briggs-Rauscher Reaction environment

In the first series of experiments oxygen was given in the environment of reaction with regular mixing. In this case amplitude of electrode potential was instable that perhaps was connected with the process of mixing. The total number of oscillations of BR reaction for aerated solution is less than in the control, Figure 1 (aeration curve). As for irradiated microwave - an increase of the total time a auto oscillating by radiation of environment reactions was shown, as it was noted in the work earlier (Рытик, Усанов, Гребенников, Бондаренко, 2012).

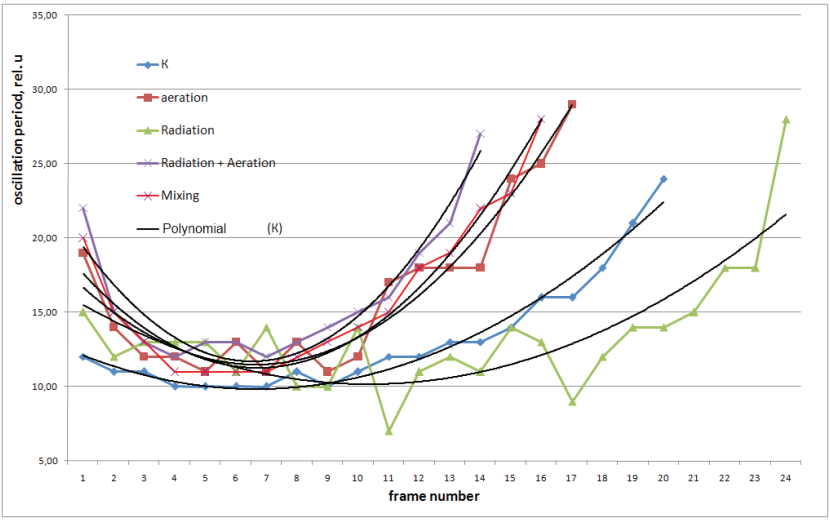

Fig.1. The dependence of the oscillation period from its number for all the cases of stimulus

It should be noted that the rate of output in the saturation of the reaction has a great meaning in the case of «Irradiation + Aeration» (Fig. 1). These results show an increase of the rates of auto oscillatory process in this case.

Separately, an experiment to measure the values of the electrode potential for the cases of aeration and mixing was held. It was found that amplitude of

the oscillations of the potential in the case of aeration is significantly less than in the control.

From these results can be concluded that the auto oscillating aeration is characterized by a decrease of the oscillation period, compared with the control. The absolute speed of movement can affect the behavior and the final product of complex nonlinear homogeneous chemical reactions in this media. (Melikhov, Vanag, 1995).

Acceleration mechanism of BR reaction in the series of experiments with artificial aeration is probably connected with changes in the process of mixing the reaction media.

Irradiation with Electromagnetic Radiation at Frequencies of the Absorption Spectrum of Oxygen

For this series of experiments, one of the flasks was exposed by electromagnetic radiation at frequencies, characterised for absorption spectrum of oxygen.

In this case the total time of auto oscillating mode is more as compared with the control, as the number of oscillations themselves, this effect has already been found and described in the work (Рытик, Усанов, Гребенников, Бондаренко, 2012). The distance between the oscillations decreases with time slower than in the control, Figure 1. This may be connected with the absorption of radiation and the change in the parameters of the endogenous oxygen, in particular the diffusion capacity.

Consequently we can suggest that the irradiation regulates the cycle of oscillations, but the amplitude was also lower than in the control.

Development of iodine dioxide in the presence of iodine reactive oxygen when exposed to radiation at frequencies of oxygen leads to the intensification of the oscillation process.

The Combined Effect of Irradiation and Aeration Media BR

Checking the effect of the combined effects of radiation at the frequency of maximum oxygen uptake and aeration reaction media is shown in Figure 2. For this experiment, one of the flasks with the reaction, except irradiation with electromagnetic radiation at frequencies is characteristic of the absorption spectrum of oxygen, further subjected to aeration.

From the results shown in Figure 2 can be concluded that the number of oscillations decreased. Figure 1 shows that the period between the oscillations decreased as compared with the control almost twice, which, in turn, said the acceleration of the auto oscillating reaction.

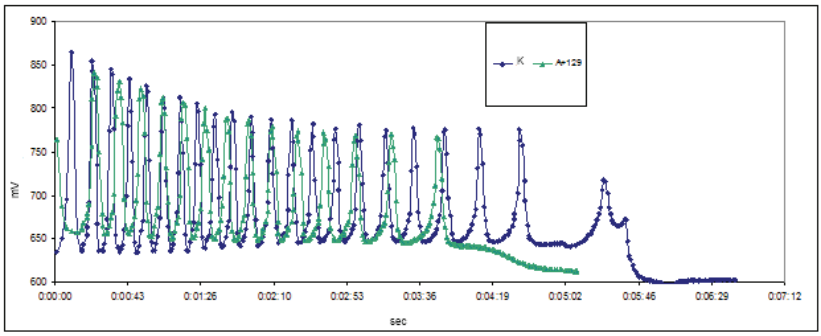

Fig.2. The dependence of the electrode potential (mV) versus time (s) for irradiated and aerated reaction media in comparison with control

So, it was found that not only the concentration of reactants and the fluctuations in media intermediates in reaction environment, electromagnetic field, etc affect the behavior of Briggs-Rauscher reaction. It is shown that artificial aeration helps coming out of oxygen bubbles formed during the reaction. Moreover the reaction is faster, that can be connected with the fact that in the control of the reaction only the dissolved oxygen is involved which already present in the environment, while the process of aeration needs an additional mixing, which could contribute to the variability of oxygen concentration involved in the reaction.

The results prove the fact of the possibility to control oscillations in auto oscillating reaction. In the case of Briggs-Rauscher reaction can also be said that the release of endogenous oxygen in the environment occurs with oscillations, that can be used to control the auto-oscillating process, prolongation and restart of oscillations in particular.

ACKNOWLEDGMENTS:

This work was supported by a grant of the President of the Russian Federation for support young Russian scientists - PhD MK-1382.2012.4

REFERENCES:

1. *Андреев Е. А., Белый М. У., Ситько С. П.* Проявление собственных характеристических частот организма человека // Доклады АН УССР, № 10, 1984. С. 56–59.
2. *Белоцерковский О. М., Опарин А. М.* Численный эксперимент в турбулентности: От порядка к хаосу. Издание 2-е, доп. М.: Наука. 2000. 223с.

3. *Буданов В. Г.* Мезопарадигма синергетики: моделирование человеко-размерных систем и метод ритмокаскадов / Синергетика. Труды семинара. Том 4. Естественно-научные, социальные и гуманитарные аспекты. М.: Изд-во МГУ. 2001. С. 54–57.
4. *Гольдштейн Б. Н., Аксиров А. М., Закржевская Д. Т.* Простая кинетическая модель колебательной активности динеина // Молекулярная биология, 2008, том 42, № 1, С. 138–142
5. *Жаботинский А. М., Огмер Х., Филд. Р. и др.* Колебания и бегущие волны в химических системах: Пер. с англ. / Под ред. Р. Филда и М. Бургера. М.: Мир, 1988, 720 с.
6. *Киселев М. А.* Размер молекулы сывороточного альбумина человека в растворе / М. А. Киселев, Ю. А. Грызунов, Г. Е. Добрецов, М. Н. Комарова // Биофизика. 2001. Т. 46, вып. 1. С. 423–427.
7. *Коваленко А. С., Тихонова Л. П., Яцимирский К. Б.* Влияние молекулярного кислорода на концентрационные автоколебания и автоволны в реакциях Белоусова-Жаботинского // Теор. и экспер. химия. 1988. Т.24. № 6. С. 661–662.
8. *Коваленко А. С., Тихонова Л. П.* Сложные колебательные режимы и их эволюция в реакции Белоусова-Жаботинского // Ж. физ. химии. 1989. Т.63. № 1. С. 71–73
9. *Кольцов Н. К.* Организация клетки. М,; Л.: Биомедгиз, 1936. 652 с.
10. *Корзухин М. Д.* Колебательные процессы в биол. и химич. системах / Ред. Г. М. Франк. М., 1967. С. 231.
11. *Рытик А. П., Усанов Д. А., Гребенников В. А., Бондаренко А. В.* Влияние терагерцового электромагнитного излучения на частоте поглощения молекулярного кислорода на автоколебательную реакцию Бриггса-Раушера // Бюллетень медицинских Интернет конференций. 2012. Том 2. Выпуск 6 (Июнь). С.410-413
12. *Хакен Г.* Информация и самоорганизация. Макроскопический подход к сложным системам. М.: Мир, 1991. 298 с.
13. *Briggs T. S., Rauscher W. C.* An oscillating iodine clock. J. Chem. Educ., 1973, V.50, № 7, P.496
14. *Graven S. N., Estrada S., Lardy H. A., Proc. Natn.* Acad. Sci. U. S., 53, 1076 (1965).
15. *Melikhov D. P., Vanag V. K.* «Study of Possible Macromixing Effects in Photoinduced Phase Transitions in the Briggs-Rauscher Reaction under Batch Conditions» Russian Journal of Physical Chemistry 1995, No. 11, 2064.

COMPUTER MODELING OF OPTICAL PULSE SHAPING IN SLOT WAVEGUIDES

E.V. Borisov, E.A. Romanova

Saratov State University

Slot waveguides (Fig. 1a) are prospective structures of the modern photonics as building blocks for photonic chips (Baehr-Jones, Hochberg, Wang et el., 2005; Fujisawa, Koshiba, 2006). Such waveguides have some unique properties in comparison with three-layer waveguides. Using the slot waveguides allows to achieve high energy localized within the slot. That

means it gets possible to increase the intensity locally without increasing the light source power.

Transmittance of nonlinear guiding structures based on the slot waveguides is power dependent. This effect can be used for shaping of high-intensity optical pulses propagating in the structures.

In this work, numerical model of nonlinear waveguide excitation by its linear mode has been used for evaluation of the waveguide transmittance depending on the input power. Transmittances of the nonlinear slot and three-layer waveguides have been evaluated and compared. The waveguides with step refractive index profile have been considered (Fig.1). The refractive index was considered to be intensity dependent:

$$n = n_0 + n_2 I, \tag{1}$$

in all regions of each of the waveguides according to the □err nonlinearity (□□□□□□□□, 1□□1). In (1) n_0 is linear refractive index n_2 is □err constant.

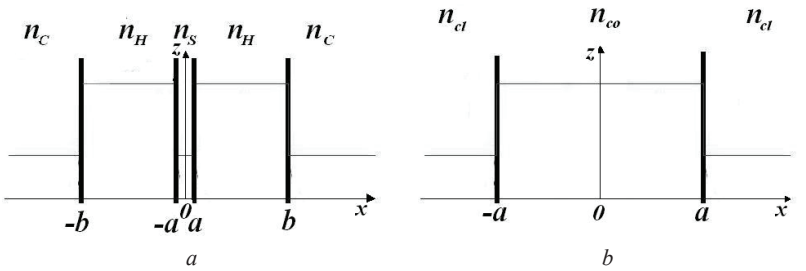

a *b*

Figure 1. □lot(*a*) and three-layer (*b*) waveguide geometries (vertical lines) and linear step-index profiles (hori□ontal lines)

The finite-difference beam propagation method (F□-□□□) was used for numerical solution of the parabolic wave e□uationsfor the slowly varying amplitudes of T□-mode electric fi eld components (□nyder, □ove, 1□□□):

$$2i\beta\frac{\partial \mathrm{e}_x}{\partial z}+\frac{\partial^2 \mathrm{e}_x}{\partial x^2}+\frac{\partial}{\partial x}\left\{\mathrm{e}_x\frac{\partial \ln n^2}{\partial x}\right\}+\left[n^2k^2-\beta^2+\varepsilon_{nl}\left(|\mathrm{e}_x|^2+\frac{2}{3}|\mathrm{e}_z|^2\right)\right]\mathrm{e}_x=0, \tag{2a}$$

$$2i\beta\frac{\partial \mathrm{e}_z}{\partial z}+\frac{\partial^2 \mathrm{e}_z}{\partial x^2}+i\beta\frac{\partial \ln n^2}{\partial x}\mathrm{e}_x+\left[n^2k^2-\beta^2+\varepsilon_{nl}\left(\frac{2}{3}|\mathrm{e}_x|^2+|\mathrm{e}_z|^2\right)\right]\mathrm{e}_z=0, \tag{2b}$$

where k is wavenumber in free space, β is longitudinal propagation constant, $\varepsilon_{nl} \approx \frac{k^2 n^2 n_2}{Z_0 n_{e\,ff}}$ characterizes the Kerr nonlinearity and $n_{e\,ff} = \frac{\beta}{kn}$, Z_0 Z_0 is the free space impedance□

□n the solution of the e□uations (2□), (2□□), the split□step method was used, so that the linear and nonlinear steps were considered consecutively□□□□ (2□□) contains some derivatives of the functions which are discontinuous at the core□cladding boundaries□□o avoid this problem, the second and the third terms of the left side of □□□ (2□□) were combined in the following way □□u, □uang, □□□□□□

$$\frac{\partial^2 \mathrm{e}_x}{\partial x^2} + \frac{\partial}{\partial x}\left\{\mathrm{e}_x \frac{\partial \ln n^2}{\partial x}\right\} = \frac{\partial}{\partial x}\left\{\frac{1}{n^2}\frac{\partial\left(n^2 \mathrm{e}_x\right)}{\partial x}\right\}. \qquad (□□□)$$

□t the linear step ($\varepsilon_{nl} = 0$□), □□□□□ (2□□) can be transformed into a □nite□dif□ ference e□uation by using the □ran□□□icolson scheme (□□□□□□□□□□, □□□7□□)

$$\begin{aligned} &a\,\mathrm{e}_x(x-\Delta x, z+\Delta z) - c\,\mathrm{e}_x(x, z+\Delta z) + b\,\mathrm{e}_x(x+\Delta x, z+\Delta z) = \\ &= -f\left(\mathrm{e}_x(x-\Delta x, z), \mathrm{e}_x(x, z), \mathrm{e}_x(x+\Delta x, z)\right). \end{aligned} \qquad (□□□)$$

□he □nite difference e□uation was solved by the sweep method□

□he longitudinal component of the electric □eld (e_z) was calculated by using the relationships between the electromagnetic □eld components (□nyder, □ove, □□□□□□

$$\mathrm{e}_z = \frac{i}{\beta n^2}\frac{\partial\left(n^2 \mathrm{e}_x\right)}{\partial x}. \qquad (□□□)$$

□henumerical scheme has been tested by modeling the waveguide e□cita□ tion by its linear □□$_0$□mode□

□t the nonlinear step, the phase self□modulation is ta□en into account by multiplying the □eld amplitudes to the nonlinear factors□

$$\mathrm{e}_x^{NL} = \mathrm{e}_x^{L} \exp\left\{i\frac{\varepsilon_{nl}}{2\beta}\left(\left|\mathrm{e}_x\right|^2 + \frac{2}{3}\left|\mathrm{e}_z\right|^2\right)\right\}, \qquad (□□□□)$$

$$\mathrm{e}_z^{NL} = \mathrm{e}_z^{L} \exp\left\{i\frac{\varepsilon_{nl}}{2\beta}\left(\frac{2}{3}\left|\mathrm{e}_x\right|^2 + \left|\mathrm{e}_z\right|^2\right)\right\}. \qquad (□□□□)$$

□he numerical modeling shows that the beam pro□le is changing at the □rst steps of the propagation distance due to the nonlinear effects□□s a result,

the intensity at the waveguide axis $I(0)$ is increasing. Finally, the beam gets the certain shape being transformed into a nonlinear TM-mode of the waveguide. When the beam shape gets stable (steady state regime of the light beam propagation), the intensity at the waveguide axis can be calculated as follows:

$$I(0) = \frac{n}{2n_{e\,ff}} \frac{1}{Z_0} \left| e_x(0) \right|^2 . \tag{7}$$

To evaluate the efficiency of nonlinear effect in the waveguide, the transmittance of the structure was calculated as the ratio $I(0)/I_0(0)$ depending on the input beam power:

$$P_0 = 2a \int_{-\infty}^{\infty} s_{z0} dx, \tag{8a}$$

$$P_0 = 2b \int_{-\infty}^{\infty} s_{z0} dx, \tag{8b}$$

where $s_{z0} = \frac{n}{2n_{e\,ff}} \frac{1}{Z_0} \left| e_x \right|^2$ is the longitudinal component of the Poynting vector, 2*a* and 2*b* are the effective linear size of the three-layer (Eq.8*a*) and slot (Eq.*b*) waveguides along the y axis. The dependence is shown in Fig. 2.

In the modeling, for the waveguide regions we have used the values of the refractive indexes corresponding to chalcogenide glasses of the system As-S-Se ($n_{co} = 2.830$, $n_{cl} = 2.437$ for the three-layer waveguide, and $n_H = 2.830$, $n_C = n_S = 2.437$ for the slot one), the value of the light wavelength in free space $\lambda = 1.55 \cdot 10^{-6}\, m$, half-width of the three-layer waveguide $a = 1.505 \cdot 10^{-7}\, m$, the linear dimensions of the slot waveguide: $a = 1.55 \cdot 10^{-8}\, m$ and $b = 1.505 \cdot 10^{-7}\, m$, and $\varepsilon_{nl} = 0.07\ V^{-2}$. Input power was tailored in the range: $0.2 \cdot 10^3\ W \le P_0 \le\ 5.3 \cdot 10^3\, W$, that was assumed corresponding to peak powers of femtosecond pulses of nJ energy levels.

As we can see from Fig.2, transmittance of the both nonlinear structures grows with input power but the line slope is greater in the case of slot waveguide. This means that at the output, the optical pulse will be compressed in comparison with the input one in the both structures. However the slot waveguide is more efficient in comparison with the three-layer waveguide.

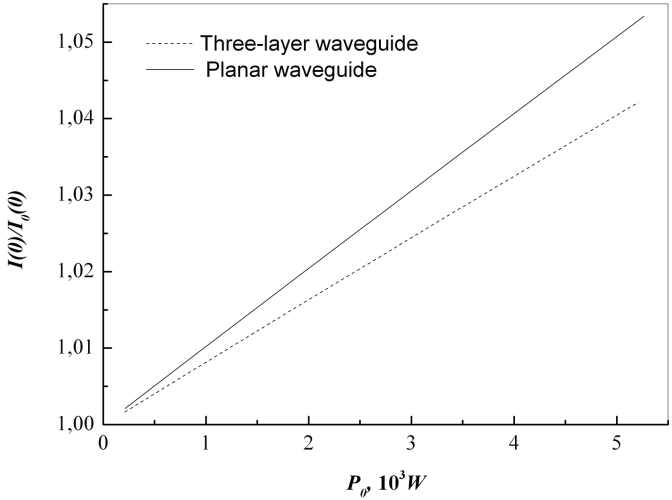

Fig. 2. The normalized intensity at the waveguide axis depending on the input beam power

REFERENCES:

1. *Самарский А. А.* Введение в численные методы. М.: Наука, 1987. 236 с.
2. *Сидоров Н. К.* Введение в волновую нелинейную оптику. Саратов: Издательство Саратовского университета, 1991. 17 с.
3. *Baehr-Jones T.*, *Hochberg M., Wang G. X. et el.* Optical Modulation and Detection in Slotted Silicon Waveguides // Opt. Express. 2005. Vol. 13, Issue 14. P. 5216–5226
4. *Fujisawa T., Koshiba M.* Guided modes of nonlinear slot waveguides // IEEE Photon. Technol. Lett. 2006. Vol. 18, № 14. P. 1530-1532
5. *Snyder A. W., Love J.* Optical waveguide theory. New York: Champan and Hall, 1983. 596 p.; 599 p.
6. *Xu C. L., Huang W. P.* Finite – difference beam propagation method for guide – wave optics // Progress in Electromagnetic Research. 1995. Vol. 11. P. 1–49

DEVELOPMENT OF THE GIGAHERTZ NANOOSCILLATOR MODEL BASED ON NANOPEAPOD

O.E. Glukhova, I.S. Nefedov, A.S. Kolesnikova, M.M. Slepchenkov, V.V. Shunaev, G.V. Savostyanov

Saratov State University

INTRODUCTION:

Gigahertz frequencies are widely used nowadays. The CPU of computers, logic devices [1], mobile phones, optical filters, which are used in spectroscopy, astronomy as telescopes and microscopes, work at these frequencies.

Currently, the actual problem is the creation of small-size systems of gigahertz frequency range. The theoretical model of ultrafast nanooscillators based on carbon nanoscrolls is presented in [2]. A carbon nanotube inside carbon scroll is able to move with the frequency of 10 GHz by the temperature 100K. Under the external electric field of 0.02 eV / Å nanotube can oscillate with the frequency of 100 GHz. Authors of [3] investigated that fullerene in nanotube can oscillate at the gigagertz range by temperature.

The aim of this work is to model the oscillator of gigahertz range based on nanopeapod filled with fullerenes C_{60} by means of an external electric field. The studies were conducted with the use of molecular mechanical method.

MOLECULAR-MECHANICAL MODEL:

Empirical model of grapheme is based on the theory of valence force field including the van der Waals iteraction for unbound atoms [4]. The total energy E_{tot} of finite graphene film is presented by a polynomial, each component of which has a weighting factor:

$$E_{tot} = \sum K_r (r - r_0)^2 + \sum K_\theta (\theta - \theta_0)^2 + \sum \left(\frac{K_a}{r^{12}} + \frac{K_b}{r^6}\right). \quad (1)$$

The first term in (1) corresponds to the change of the binding length between two atoms (r_0 =1.42Å), the second term – to the change of the valence angles between the bindings (θ_0 =120°), and the third term – to the Lennard-Jones potential which describes van der Waals interaction, K_r, K_θ, K_a, K_b – weight coefficients.

Atoms change their position due to the Newtons law, and by solving Newton's equation we find new coordinates and velocities on every step. Since the system interacts with environment, Newton's law will be written as

$$m\frac{d^2r}{dt^2} = F + F_0, \qquad (2)$$

where F_0 is radiation force of the considering stationary external electric field.

THE MODEL OF NANOOSCILLATOR:

In this paper we used an open nanotube (10, 10) with the length of 10.3 nm and the radius 1.35 nm. Two chains of three fullerenes C_{60} are encapsulated inside the nanotube from both ends. Fullerenes in the chain were connected by chemical bond with each other and with the wall of nanotube, distance between two chains equals 4.3 nm (Fig. 1). We chose this model because of the fact that it is impossible to produce nanotubes with closed ends experimentally.

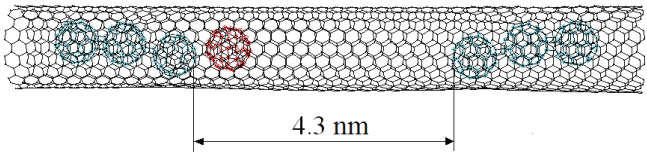

Fig. 1. The model of nanoremitter in gigahertz range.

Free fullerene C_{60} is located between two chains. If there are no external forces, it can be found in one of two potential wells of the energy distribution for van der Waals interaction (Fig. 2).

Under the influence of external electric field and of its own charge fullerene starts to move in potential well. The values of such electric field are rather small: $1\cdot10^3 V/m$. As fullerene oscillates at a certain frequency radiation, the frequency of the radiation is the main parameter of the nanooscillator.

In this study the frequency of C_{60} movement was calculated as the inverse value of the time of fullerene motion from one wall of the potential well to the other. Calculation of overshooting frequency was carried out for different values of the external electric field. With the increasing intensity oscillation period does not increase, it changes in unpredictable ways. This can be explained by the irregular form of the potential well.

At the initial moment the fullerene C_{60} had charge of +1e ($1.6\cdot10^{-19} Coloumbs$), the nanotube had charge -1e, therefore the structure retained in electrical neutrality. Gigahertz frequency range was observed when electrical field was equal to $1\cdot10^6 \div 1\cdot10^8 V/m$. The dependence of the oscillation frequency on the external electric field is shown in Fig. 3.

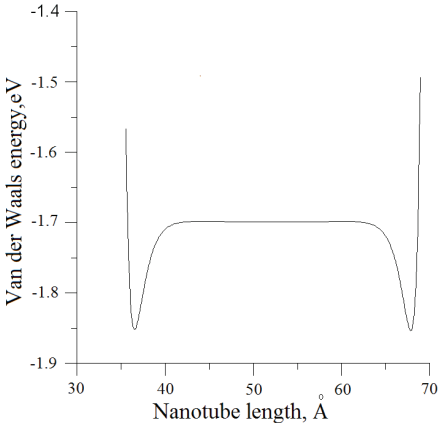

Fig. 2. Potential well of the nanotube.

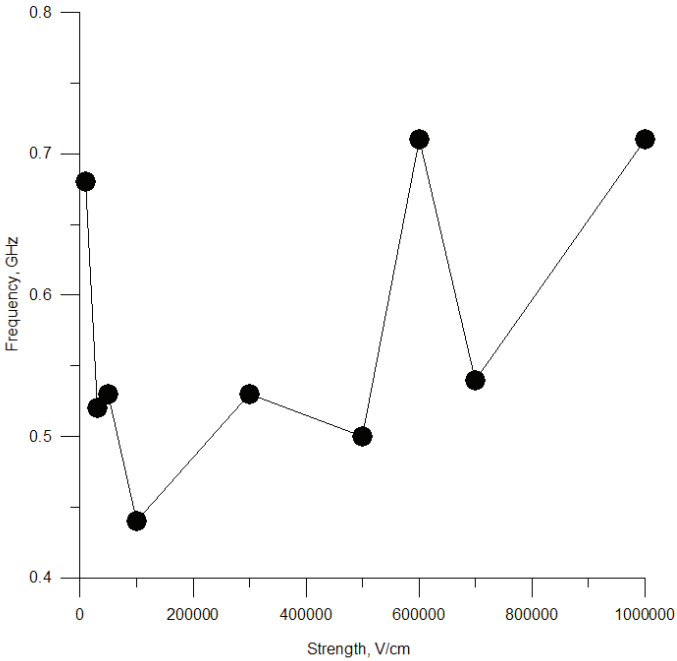

Fig. 3. Dependence of the C_{60} fullerene oscillation frequency with +1e charge on the electric field strength.

CONCLUSIONS:

The mathematical model of based on the carbon nanopeapod nanoemitter of gigahertz range was developed and presented in this paper. It was found that for generating the radiation in gigahertz range it is necessary to apply the external field with strength of $1 \cdot 10^6 \div 1 \cdot 10^8 V/m$. In this case the moving fullerene C_{60} has a charge of +1e, and the nanotube has a charge of -1e. Since the nanoemitter has small overall dimensions and a very high performance, we can note that the developed nanooscillator has no analogues nowadays.

REFERENCES:

1. *Levitan S. P., Fang Y., Dash D. H.* Non-Boolean Associative Architectures Based on Nano-Oscillators // 13th International Workshop Cellular Nanoscale Networks and Their Applications (CNNA), 2012. P. 1–6.
2. *Zhang Zh., Li T.* Ultrafast nano-oscillators based on interlayer-bridged carbon nanoscrolls // Nanoscale Research Letters, 2011. Vol. 6. P. 470
3. *Su H., Goddard III W. A., Zhao Y.* Dynamic friction force in a carbon peapod oscillator // Nanotechnology, 2006. Vol. 17. P. 5691.
4. *Glukhova O. E., Kolesnikova A. S., Kirillova I. V.* Investigation of the Effect of Bending on the Polymerization of Fullerenes Inside Carbon Nanotubes // Fullerenes, Nanotubes, and Carbon Nanostructures, 2012. Vol. 20. P. 391–394.

SYNTHESIS OF WATER-SOLUBLE CORE-SHELL QUANTUM DOTS

V.V. Goftman

Saratov State University

Quantum dots (QDs) are very small crystals of semiconductor materials. Their size ranges from about a hundred to a few thousand atoms. The diameter of QDs is approximately between 2 and 10 nanometers, which puts them in a special size range that retains some properties of bulk materials, as well as some properties of individual atoms and molecules (Fig.1) (Klimov V. I., 2003).

QDs possess high photostability and brightness, size-tunable emission with narrow and symmetrical peaks (Sung J. L., Bonghwan Ch., Taiha J., Seung K. Sh., 2008). In addition broad absorption spectra make it possible to use a single wavelength light source to excite fluorescence in nanocrystals with different sizes. The latter dramatically simplifies realization of multi-assay and imaging of biological objects using QDs as labels (Gill R, Zayats M, Willner I,

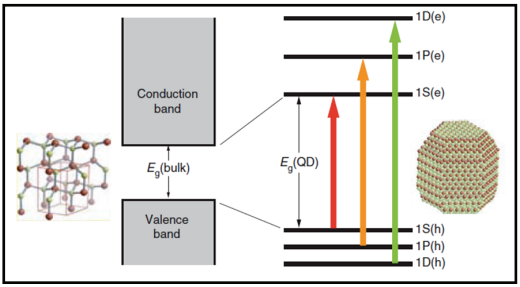

Fig. 1. Differences between bulk semiconductor and QDs

2003.). That is why QDs find great application both as biolabels for biological objects imaging and in immunoassay.

Cadmium selenide (CdSe)-based QDs are the most extensively used in biochemistry and immunoassay because their size-tunable emission lies in the visible region (450-650 nm) [2]. To improve quantum yield of QDs are covered with several wider band gap semiconductors (ZnS, CdS, ZnSe) that are used as shell materials. Due to this fact both photo-generated electrons and holes are efficiently confined in the nanocrystals' core and don't leak to ZnS shell (Xia X., Liu Z., Du G., Li Y., Ma M., 2010).

Method of colloidal fabrication of high-quality QDs allows to control shape, size, and fluorescence properties. The higher the temperature and the longer synthesis time the particles grow faster. The shape of QDs depends on stabilizer component. Usually, the quantum dots synthesized by colloidal fabrication of in organic solvents have hydrophobic surface ligands. For bioapplication QDs must to be water-soluble. A more promising approach for making water-soluble QDs is to use long chainlength amphiphilic polymers to form micelle-like structures. It lets to avoid decreasing of brightness using not expensive materials.

Cadmium oxide (CdO, 99,99%), selenium powder (Se, 99,99%), sulfur powder (S, 99%), zinc acetate (Zn (OAc)2, 99,99%), oleic acid (OA, 90%), 1-octadecene (ODE, 90%), oleylamine (OLA, 70%), poly (maleic anhydride-alt-1-octadecene) (PMAO) average Mn 30000-50000, JEFFAMINE M-1000, ethanol anhydrous were purchased from Sigma-Aldrich;, chloroform, toluene, buthanol, acetone were all of analytical grade.

CdSe quantum dots were prepared via a rapid hot-injection method in octadecene. The Se precursor was 0.1 M solution of S in ODE; the Cd precursor was 0.1 M solution of CdO and oleic acid in ODE.

A mixture of Cd precursor solution (5 ml) and octadecene (13 ml) in a three-neck flask was heated to 260^0C under argon. At this temperature 5 ml of Se precursor solution was quickly injected into the reaction flask. The temperature was lowered to 235^0C and remained at this value throughout the course of CdSe QDs growth.

For shell growth were prepared the S precursor solution (0.1 M) in ODE; the Zn precursor solution (0.1 M) was zinc acetate in a mixture of OLA and ODE.

The mixture of Zn-, S- precursor solutions and ODE was put in a flask. Then a concentrated toluene solution of CdSe QDs was added to the mixture and the temperature was increased up to 140^0C. The mixture was kept at this temperature for 2.5 hours. For CdSe/ZnS purification acetone was added to the CdSe/ZnS solution, the samples were centrifuged at 4000 rpm during 5 minutes. The precipitate was dissolved in a small amount of chloroform.

The mixture of polymers PMAO and Jeffamine M1000 was dissolved in chloroform in ratio 1:2.5 respectively. QDs CdSe/ZnS was added to polymer while stirring. After 12 hours of mixing the solution with 10 ml of 0.03M KOH was dryed under water injection pump.

UV-vis absorption spectra were measured with a SHIMADZU 1800 spectrophotometer. Photoluminescence (PL) spectra were measured with a Perkin Elmer LS55 fluorescence spectrometer.

Obtained CdSe cores are characterized with wide absorption spectra and narrow emission spectra that allow to use a single light source to excite QDs' fluorescence of different colors. The position of peak's maximum depends by size of CdSe nanocrystalls. Formation of CdS or ZnSe shell around CdSe cores results in a sufficient red shift of both the first absorption maximum and fluorescence. By this way shift is less than 10 nm (Fig. 2).

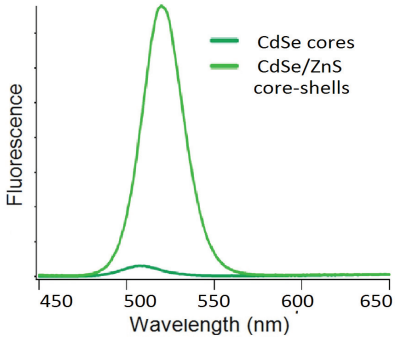

Fig.2. Fluorescence intensity of CdSe cores and CdSe/ZnS core-shells in toluene

Obtained water-soluble dots are characterized with intensive fluorescence and sufficient stability in solution with wide range of pH enough to use them as fluorescent biolabels in immunoassay. Shift of fluorescence peak is not observed (Fig. 3).

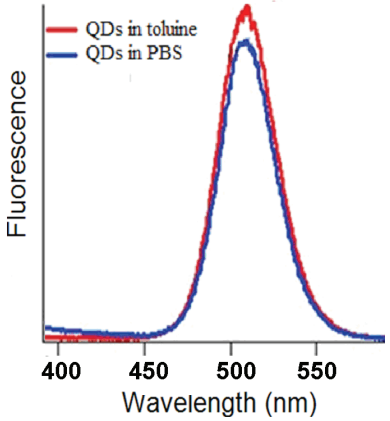

Fig.3. Fluorescence intensity of QDs CdSe/ZnS in toluene and polymer-coating QDs CdSe/ZnS in water

The research was supported by a grant from RFBR (project 12-03-91167-GFEN-a)

REFERENCES:

1. *Klimov V. I.* Nanocrystal quantum dots. From fundamental photophysics to multicolor lasing// Los Alamos Sc. – 2003. – V. 28. – p.214-220.
2. *Sung J. L., Bonghwan Ch., Taiha J., Seung K. Sh.* Synthesis and characterization of zinc-blende CdSe –based core/shell nanocrystals and their luminescence in water// J. Phys. Chem. C. – 2008. – V. 112. – № 6. – p. 1744–1747.
3. *Gill R, Zayats M, Willner I.* Semiconductor quantum dots for bioanalysis// Angew. Chem. Int. Ed. – 2008. – V. 47. – № 40. – p. 7602–7625,
4. *Xia X., Liu Z., Du G., Li Y., Ma M.* Structural evolution and photoluminescence of zinc-blende CdSe-blende CdSe/ZnS nanocrystals// J. Phys. Chem. C. –2010. –V. 114. –№ 32. – p. 13414–13420.

ABSORPTION AND REFLECTION SPECTRA OF NANOPARTICLE AQUEOUS SUSPENSIONS IN THE X-BAND OF MICROWAVE BANDWIDTH

E.E. Gulmanov, R.S. Sergeev, S.A. Sergeev

Saratov State University

Today semiconductor devices are widely used in all spheres of human activity. It is hard to imagine a world without semiconductor technologies. Cadmium sulfide is one of the semiconductors, which is actively used in the industry. Cadmium sulfide (CdS) is a direct semiconductor with a band gap of 2.42 eV (Holleman, Wiberg, 2001). The crystals have a color from lemon-yellow to orange-red with the crystal lattice of cubic and hexagonal types (Traill, Boyle, 1955). CdS is used in optoelectronics, photosensitive and photovoltaic devices. It can be used as an active medium in semiconductor lasers, the material for the manufacturing of solar cells, photodiodes and LEDs. It is also used as a phosphor mixed with zinc sulfide.

In the last decades cadmium sulfide finds its applicability in industry. It is used as an additive in alloy, electroplating, for cadmium pigments in the manufacturing of varnishes, enamels and ceramics, as a stabilizer for plastics in electric batteries and etc. (Орлов, Садовникова, Лозановская, 2002; Потапов, 2000; Петрова, Шантарин, Петров, 2003).

All compounds of cadmium are toxic. Maximum allowable concentration (MAC) of cadmium sulfide in water is 0.01 mg/m^3. It is classified as material of III dangerous group according to International Chemical Safety Cards.

In this work, we investigated the possibility of detecting water pollution with cadmium sulfide by microwave method of absorption and reflection spectra.

A few methods of measuring the dielectric and magnetic parameters of materials at microwave frequencies exist today (Брандт, 1963; Беляев, Лексиков, Тюрнев, 1995; Демянов, Семенов, Тамарин, 1974; Дьяконова, Казанцев, Маречек, 2011).

Wave guide technique is one of proper methods for measuring colloid and emulsion systems. In this work the value of attenuation and voltage standing wave ratio (VSWR) were measured for distilled water and water suspension of different concentration of cadmium sulfide (Брандт, 1963) (Fig. I). The experiments were performed at different temperatures ranging from 26 °C to 45 °C.

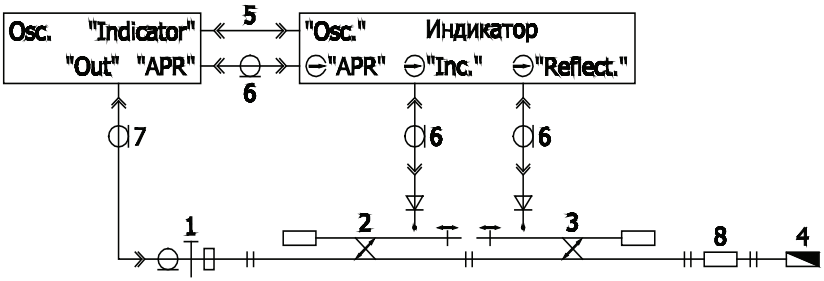

Fig. I. Experimental installation schematics for VSWR measurements: 1 – coaxial-to-waveguide conversion, 2 – «Incline» directional detector, 3 – «Reflected» directional detector, 4 – matched load, 5 – cable, 6 – K-9 cable, 7 – UHF cable, 8 – measured object

Waveguide section of 15 ml volume (length 5.5 cm) with thin weakly absorbing caps on flanges was used in the experiment. This fluid filled the space between the flanges completely. The resulting dependence of the voltage standing wave was determined in the X band of microwave bandwidth (wavelength range of 7.8 ÷ 10.2 GHz).

In this work, aqueous suspensions of CdS with concentrations 0.2 mg/m^3, 0.02 mg/m^3 and 0.002 mg/m^3 were used. The first two values exceed the MAC 20 and 2 times respectively. 0.002 mg/m^3 cadmium sulfide concentration was used to test the sensitivity of the detection method. Avarage particle size of cadmium sulfide was 550 nanometers. This result was obtained by the dynamic light scattering with Malvern Zetasizer Nano ZS device.

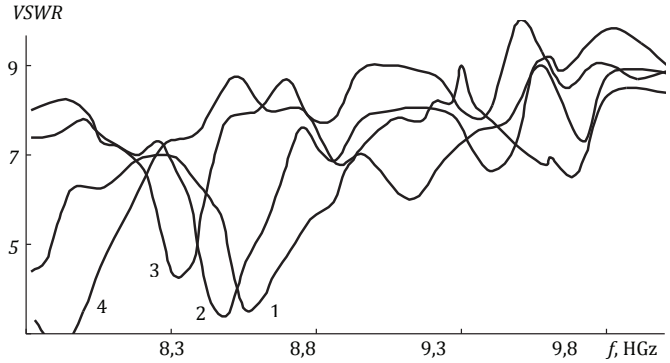

Fig. II. Dependence VSWR on the frequency for distilled water and aqueous suspensions with cadmium sulfide: 1 – water+CdS 0.002 mg/m^3, 2 – water+CdS 0.02 mg/m^3, 3 – water+CdS 0.2 mg/m^3, 4 – water

The frequency dependence of the VSWR for distilled water and the aqueous suspensions of cadmium sulfide with various concentrations is presented in Fig. II. Minimum VSWR is present on the frequency range from 8.3 GHz to 8.6 GHz. Minimum is shifted to the lower-frequency area with concentration increasing of cadmium sulfide. However a change of VSWR regularities doesn't occur in this field with increasing temperature. The maximum value of VSWR across the frequency ranges up to 10 at the frequency of 9.5 GHz for a suspension with a concentration of cadmium sulphide of 0.2 mg/m^3. The maximum difference between distilled water and water with cadmium sulfide is most evident in the area of 8.3 GHz to 8.9 GHz.

Absorption and transmission spectra measurements were obtained using VSWR and attenuation. Alleviation factor is equal to 37 dB. It's almost independent of frequency and temperature.

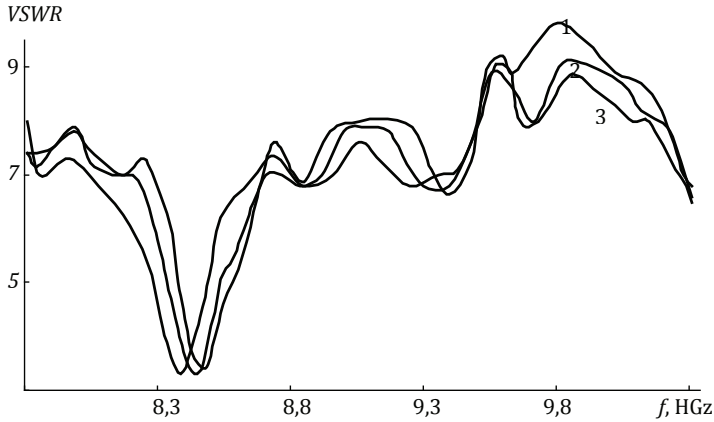

Fig. III. Dependence VSWR on the frequency for aqueous suspensions with cadmium sulfide concentration of 0.02 mg/m^3: 1–26 °C, 2–35 °C, 3–45 °C

The effect of temperature changing on the pattern of absorption of microwave radiation is shown in Figure III. The dependence of VSWR versus frequency for aqueous suspension of cadmium sulfide concentration of 0.02 mg/m^3 in the temperature range of 26 to 45 degrees was obtained. Minimum is presented on the curves in the frequency range from 8.4 GHz to 8.5 GHz. The minimum value of VSWR is 3.3. This is done for the suspension at a temperature of 45 °C, and 35 C. There is no change in VSWR in those minimums under suspension heating. But one can see that the minimum is shifted by heating in the lower-frequency region. Maximum in the frequency range from 9.8 GHz to

9.9 GHz for the suspension at all temperatures is also presented in this graph. The VSWR value was decreasing in the frequency characteristic minimum from 9 to 8.85 with the temperature increase.

Dependence of the frequency VSWR for distilled water and aqueous suspension of cadmium sulfide other concentrations (0.2 mg/m^3 and 0,002 mg/m^3) at temperatures ranging from 26 °C to 45 °C was also obtained.

According to our data distilled water can be distinguished from the water dispersion of various concentrations of cadmium sulfide. Thus the changing of properties of the suspension takes place with the temperature rising. It means that the wave method is sensitive to heating. The temperature of 26 °C was selected for a more evident detection. This is the temperature, at which the variation of the frequency dependence of VSWR is maximum.

REFERENCES:

1. *Беляев Б. А., Лексиков А. А., Тюрнев В. В.* Микрополосковый метод исследования диэлектрической проницаемости материалов на сверхвысоких частотах // Приборы и техника эксперимента. 1995. № 6. С. 123.
2. *Брандт А. А.* Исследование диэлектриков на СВЧ. М.: Физматгиз, 1963. 404 с.
3. *Демянов А. А., Семенов М. Г., Тамарин В. А.* Измерение комплексной диэлектрической проницаемости сильнопоглощающих жидкостей // Приборы и техника эксперимента. 1974. № 3. С. 132–133.
4. *Дьяконова О. А., Казанцев Ю. Н., Маречек С. В.* Измерения коэффициента генерации гармоник радиопоглощающим материалом в СВЧ-диапазоне // Приборы и техника эксперимента. 2011. № 2. С. 58–65.
5. *Орлов Д. С., Садовникова Л. К., Лозановская И. Н.* Экология и охрана биосферы при химическом загрязнении. М.: Высш. шк., 2002. 334 с.
6. *Потапов* А. Д. Экология. М.: Высш. шк., 2000. 445 с.
7. *Петрова Е. Ю., Шантарин В. Д., Петров Г. Л.* Окружающая среда и здоровье человека: Методические указания к практической работе по курсу «Экология». Тюмень: ТюмГНГУ, 2003. 21 с.
8. *Holleman A. F. Wiberg E.* Inorganic Chemistry. San Diego: Academic Press, 2001. 1884 p.
9. *Traill R. J., Boyle R. W.* The American Mineralogist // Jurnal of the mineralogical society of America. 1955. Vol. 40. P. 555–559.

THE CHARACTERISTIC OF WINTERS IN SARATOV FOR THE LAST DECADE

E.I. Guzhova, S.I. Pryakhina

Saratov State University

Climate and weather conditions are of great importance for the economic activities of a whole score and its regions. The most significant feature of the climate in XX and XXI centuries is global warming. It manifests itself in raising the global surface temperature and the temperature in the ocean (Пряхина С. И. и др., 2008). Global warming affects climate in Saratov region as well where over the past 30 years the temperature has risen by more than 1.5 °C. The most significant warming is observed in the winter period.

The authors have analyzed climate and weather conditions of the cold period on the daily meteorological material from station Saratov South-East over the last 10 years (2001-2010).

Table 1 presents the data of the monthly average air temperature in the winter period from November to March. We have seen that the average monthly temperature has been above long-term rates for the five winter months of the last decade. Significant warming is observed in January and February.The average monthly temperature of January has increased on 3.9˚C, and February – on 2.9˚C. The climate warming has also caused shift of winter season borders.

Table 1

The average air temperature (˚C) in the winter period (2001-2010 years).

Years	Months				
	November	December	January	February	March
Average long-term data (rate)	**-2.0**	**-8.3**	**-11.6**	**-11.0**	**-5.0**
2000-2001	-1.9	-2.0	-3.1	-6.2	-0.3
2001-2002	+0.9	-10.5	-4.9	-0.3	+3.0
2002-2003	+0.6	-15.0	-7.5	-10.5	-6.1
2003-2004	+0.5	-3.3	-6.8	-8.2	+1.7
2004-2005	+0.5	-4.2	-5.7	-8.8	-5.3
2005-2006	+1.1	-3.8	-13.8	-13.0	-2.6
2006-2007	-0.4	-0.8	+0.2	-9.2	-3.9
2007-2008	-2.5	-10.3	-11.3	-6.0	+3.4
2008-2009	+3.4	-5.2	-9.6	-7.4	-1.4
2009-2010	+0.4	-8.0	-14.1	-11.0	-3.6
Average for the ten years	**0.3**	**-6.3**	**-7.7**	**-8.1**	**-1.5**

As we can see from Table 1 the average January temperature for ten years ranged from +0.2 ºC (2007) to -14.1 º C (2006), and February temperature varied from -0.3 º C (2002) to -13.0 ºC (2006) (Table 1).

Meteorologists take the amount of time with the stable average daily temperature below zero for winter period that is on average from November 6 to April 3 (Бобров Г. П., 2001).

Table 2 shows the average duration of the winter season in the last decade. The average duration of the winter season for the last ten years has been 29 days shorter than the multi-year rates. That was reflected in the serverity of winters. We have calculated the average daily air temperature from November to March in each winter season from 2001 to 2010. The average amount of negative temperatures reached -825.0 ˚C per decade. According long-term data this sum is -1126.3 ˚ C. The average warming in the winter is about 300 ˚C.

Table 2

Data on temperature change in winter period and winter duration.

Years	Transition temperature through 0 ˚C in autumn period	Transition temperature through 0 ˚C in spring period	The duration of the winter period	The amount of negative air temperature, ˚C, November-March
Average long-term data (rate)	**6 XI**	**3 IV**	**149**	**-1126.3**
2000-2001	7 XI	1 IV	145	-516.6
2001-2002	16 XI	8 II	84	-557.7
2002-2003	5 XI	30 III	145	-1231.5
2003-2004	11 XI	18 III	128	-560.3
2004-2005	17 XI	4 IV	138	-808.9
2005-2006	21 XI	29 III	128	-1212.1
2006-2007	16 XI	15 III	119	-482.7
2007-2008	6 XI	23 II	109	-949.2
2008-2009	12 XII	26 III	104	-765.6
2009-2010	6 XII	21 III	105	-1163.1
Average for the ten years	**17 XI**	**17 III**	**120**	**-825.0**

All winters scored the amount of negative temperatures more than 120% of the average long-term rate have been attributed to the cold winters, and

scored less than 80% of the average long-term rate have been attributed to the warm winters.

Thus, a winter is considered to be warm if the amount of negative temperatures for period November-March is -900 ˚C and above a winter is considered to be normal in case of negative temperatures -900 ˚… -1350 ˚C. A winter is considered to be cold if it has scored amount of negative temperatures -1350 ˚ C and below.

Table 2 shows that in the last decade out of ten winters six were warm winters and four were normal.

The authors have constructed a distribution graph of average monthly air temperature amounts for different types of winters (Fig. 1). Fig. 1 shows that the normal winters are repeating course of long-term average data. Warm winters are significantly different from the normal winters on the thermal regime. In January the amount of negative temperatures in the warm winter is estimated to be -160 ˚C, and in a normal winter, the amount of negative temperatures is almost -350 ˚C.

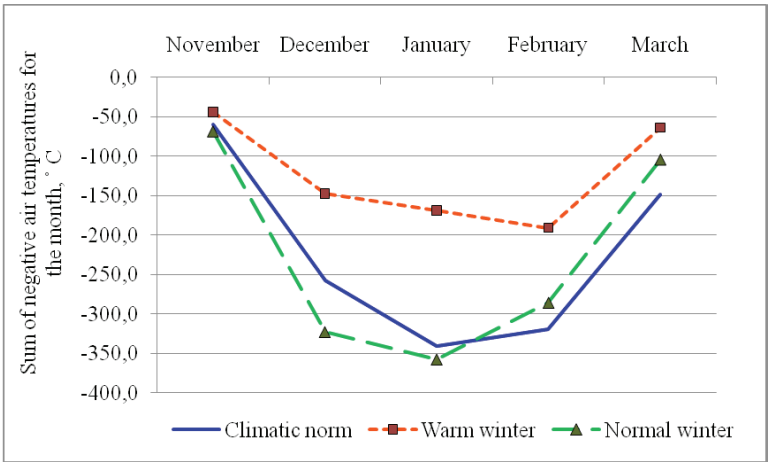

Fig.1. Distribution of average daily amounts of air temperature in period (November-March) for different types of winters

The data with a temperature below -20 º – (-25 ºC) and the number of days with this temperature are of considerably practical interest. Because these temperatures create uncomfortable conditions for the human body and unfavorable conditions for overwintering winter crops, as well as add up the difficult

conditions in the work of housing and communal services.In the cold winter of 2005-2006 years were observed 11 days with temperatures below -20 ºC and were observed 3 days with temperatures below -25 ºC. In were not observed warm winters days with temperatures below -20 ˚C.

Thaw caused the rise in temperature to 0 ˚C and higher with sustained freezing temperatures (Швер Ц. А., 198). Thaw of winter are extremely important. In January the number of days with thaw is 6 days on average in December the number of days with thaw is 4 days on average and in February the number of days with thaw is 1 day on average. In the warm winter of 2006-2007 the number of days with thaw for the three winter months (December-February) was 39 days.

The snow cover is extremely significant for functioning of the climate system.The snow cover is one of main measures in assessing the depth and extent of soil freezing as well as the loads on the roofs of buildings. The snow cover ranged from 19 to 49 cm in the last decade. The global warming is beneficial to the housing sector and road transport sector, but its effect for agriculture ambiguous.

REFERENCES:

1. *Бобров Г. П.* Погода и климат Саратова в вопросах и ответах. Саратов, 2001. 220 с.
2. *Пряхина С. И., Скляров Ю. А., Васильева М. Ю., Фридман Ю. Н.* Условия перезимовки озимых культур на фоне глобального потепления климата // Вавиловские чтения – 2008: Материалы Межд. науч. – практ. конф. Саратов, 2008. С. 190.
3. *Швер Ц. А.* Климат Саратова. Л., 1987. 152 с.

THE ANALYSIS OF UNEMPLOYMENT RATE IN RUSSIA: PROBLEMS AND WAYS TO MINIMIZE

A.S. Ivanova

Saratov State University

Nowadays unemployment is one of the most important problems in many countries and in global economy. The unemployment rate in European Union countries was 10,8% in February 2012, despite a set of measures to combat with it. These data were higher than the record of 1997. Accordingly even during severe crisis period from 2008 to 2009 unemployment situation was not as heavy as in the past years (3). At the same time it may be noted that the un-

employment rate in Russia is rather moderate. According to march 2012 data unemployment rate in Russia was 6.5%, while in Spain it made up for 24.1% and in Greece it was 21.7%. However, many researchers have noted that unemployment was «one of the most topical problems today, especially for Russian labor market» (1).

Thus the goal of the article is to analyze the level of unemployment in Russia, research the reasons of this problem, and consider ways to minimize unemployment.

In this article, we propose to consider the unemployment situation in period of 2008-2012, using the quarterly data to build the graph (Fig. 1)

Fig.1. Unemployment situation in period 2008-2012.

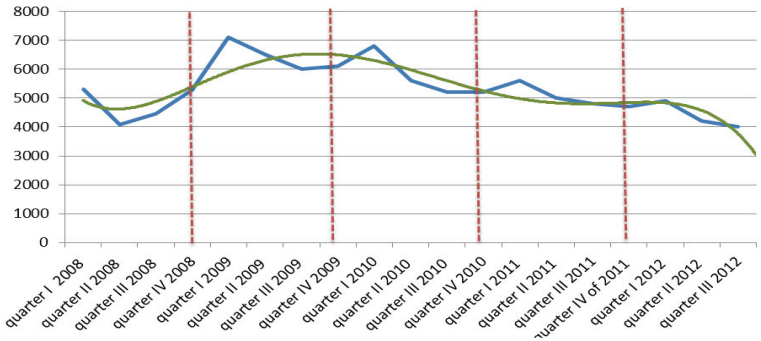

Fig.I Total number of unemployed 2008 – 2012 years.

For a clearer view of trends in the data changes and making some analytical predictions a polynomial trend line with the degree of polynom 5 (based on the number of extremes) was built. The vertical divide the graph into periods equal to one year.

The graph shows: in 2008, with the beginning of the global financial crisis, the number of the unemployed began to highly increase. In period of 2009-2010, the unemployment rate the highest, and then in 2009 the total number of the unemployed began to decline. The polynomial trend line also proves the fact that the unemployment rate was reduced. It peaked in quarter III of 2009, and then began to go down. At the same time the trend began more obvious in 2010. In quarter III 2012, the total number of the unemployed fell even slightly below the pre-crisis level (the minimum point in the II quarter of 2008 was 4097 thousand people and minimum point of the III quarter of

2012 was 4000 thousand people). Predictive analysis of the polynomial line also points to further reduction of unemployment rate.

So, the analysis of the unemployment rate in Russia gives quite a positive picture of the unemployment decline. However, more detailed research of separate regions such as the Ingushetia Republic of, the Chechen Republic demonstrates the extremely high level of unemployment rate (49.7%, 43.1%, respectively). Almost half of the population in those regions are unemployed. Either the unemployment rate in the Karachay-Cherkess Republic (10.3%), the Kurgan region (12.2%), Trans-Baikal region (11.4%) and others is not acceptable. At the same time, for example, in Moscow or St. Petersburg unemployment rate is 3.9% and 2.6% respectively. Thus, we can note the unevenness of employment in the regions of the Russian Federation.

The reasons for this situation can be following: poor integration of some regions in the production process, corruption, overpopulation. Another factors of unemployment are the lack of development of the economies or one-sided development of the economies of these regions. Therefore many people in these regions cannot find work.

In 2009, anti-crisis program was adopted by the President of the Russian Federation, 36.4 billion rubles were from the Russian budget allocated in support of regional labor markets. However, a large part of the funds allocated for the employment policy was directed to passive measures such as payment to the unemployed. This program also included the following directions: public work, job creation, giving loans to people to create their own business, internships for graduates, re-education.

Measures were taken by the government to defuse the unemployment situation. However they haven't solved the problem on the whole (namely, putting the unemployment rate to the acceptable level and equaling the number of the unemployed in regions). The most effective were the measures aimed at stimulating small and medium businesses and giving loans to people to create their own business (95 thousand of 6.5 million unemployed people found work due to the program for Small Business) (2). However, effective measures have a significant disadvantage. They are not available to everybody and to the destitute in particular.

In our opinion, it is necessary to continue struggling against unemployment in the following directions: developing a program of self-employment, at the same time making these activities more popular and available to the public; stimulating creation of new jobs in the field of small and large businesses. In case of small businesses with helping to establish own business, and in case of large businesses with helping to development. Moreover, to continue the

development of retraining programs, providing employment assistance and to take the necessary measures for the uniform distribution of population by sectors of the economy are also helpful. It is necessary to continue supporting people who temporarily left their workplace. It is important saving the moral and cultural level of the our population as well.

REFERENCES:

1. www.ibl.ru
2. www.rae.ru
3. www.top.rbc.ru

CORRELATION OPTICAL COHERENCE TOMOGRAPHY

O.A. Izotova, A.L. Kalyanov, V.V. Lychagov

Saratov State University

INTRODUCTION:

Nowadays a lot of people suffer from dangerous and even incurable diseases, such as diabetes, cancer, Alzheimer's, psoriasis etc. The burning issue for doctors and scientists is how to diagnose these diseases as early as possible and how to get a more convenient and qualitative way to control them. For monitoring these diseases a lot of attention is given to blood microcirculation. The microcirculation serves key functions within the body including regulation of blood pressure, body temperature, blood flow within tissues and delivery of nutrients and removal of metabolic waste products (Daly S. M., Leahy M. J., 2012). Therefore, its structural changes can lead to various diseases. And visualizing these changes, problem areas can be determined. There are several techniques to realize this, such as computed X-ray tomography and magnetic resonance angiography (MRA). Both of them are widespread in medicine and have their own advantages and disadvantages, for example computed tomography is less prone to motion artifacts, can provide more high-resolution images and is more accessible and cheaper than MRA, but in contrast to it MRA doesn't use X-ray waves. Both of these two methods use a contrasting agent for better visualization. Also, their spatial resolution is typically limited to a few millimeters in standard clinical practice.

In this case optical imaging techniques such as photoacoustic tomography or optical coherence tomography (OCT) are more preferable, because they en-

able high axial and transverse (≤1 μm) resolution imaging (Drexler W., Fujimoto J. G.). OCT provides a high resolution, non-invasive imaging of the microstructure in biological tissues and has a high speed – up to several tens of frames per second.

OCT techniques for microcirculatory system visualization can be divided into two groups. One of them is based on the Doppler effect, in which phase changes as a result of scattering of light by moving particles. But it has a number of disadvantages, such as dependence on phase changes of the signals, which appear when original signal is unstable, and dependence on the angle of the signal. The second way of imaging is based on the analysis of speckle-structure dynamics. This is the result of the interference of many waves of the same frequency, having different phases and amplitudes, which add together to give a result wave, whose amplitude, and therefore intensity, varies randomly (Daly S. M., Leahy M. J., 2012). In the course of time a speckle-structure of the object changes. Usually this effect appears only as a noise, but its changes can help to visualize blood vessels. Despite the fact that it isn't possible to measure the velocity of the particles by this method and it is only cross-sectional, it doesn't have the same disadvantages as in Doppler's method and is more practical. So, this paper is devoted to this method.

EXPERIMENT:

For this preliminary research we used a blood vessel model – a polypropylene capillary laying on microscope slide for speckle-correlation OCT method approving. The capillary was full of ink solution. Its scheme is shown in Fig.1.

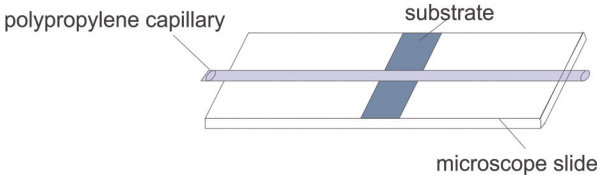

Fig.1. The scheme of the research object

The ink particles moved due to Brownian motion, which was exactly examined with Swept Source OCT System (OCS1300SS Thorlabs, Germany). For this a series of B-scans of the object was registered.

ALGORITM:

Algorithm of this method is based on the analysis of correlation coefficient. It values are on the range of 0 ± 1. If there are big structural changes

in the region, it takes the value of 0. If the regions are static, the correlation coefficient is 1. At the beginning of algorithm there is a stack of 2-D X–Z OCT frames, besides their period should be six times less than transverse resolution of the system (Enfield, Jonathan, Leahy,2011). One of the frames is shown in Fig.2.

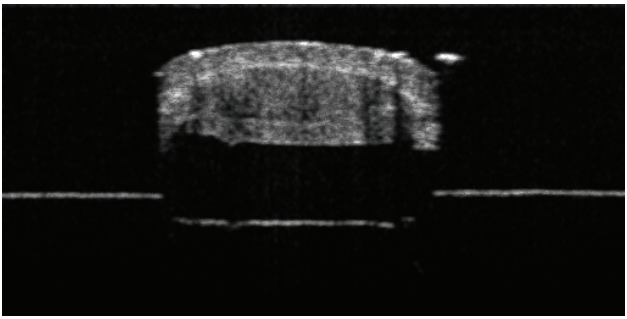

Fig.2. Structural image of the original frame

From this stack two consecutive scans 1024 × 512 pixels are chosen. To calculate their correlation they are read not in full, but divided into small pieces. The size of these pieces influences the quality of the result image. If it is too large, some of data of the small vessels might be lost. At the same time, if we make it too small, data can be at the noise level, and useful data can not be separated from it and be lost. Therefore, it was chosen as 8×8 pixels, as it was written in Enfield, Jonathan, Leahy, 2011. Correlation coefficient is calculated between the two pieces of these two frames. It becomes the first point of the correlation map. Then the sliding window, which chooses pieces, moves, and this operation repeats with the next two pieces and so up to the end of the width of the image. Then window is moved to the next string. And in this way over the whole image. This is how 2D correlation map is formed. To generate 3D OCT volumes, we need to repeat this algorithm for more than two frames.

The common problem of result images is the background noise. It has weak correlation and may seem to be useful data. It can be eliminated by masking the correlation image with a "structural mask", as it is shown in Fig.3. Thus, the threshold value is chosen, which is above the mean background value, under which all calculated coefficients take the value of 0 (Enfield, Jonathan, Leahy, 2011). After this mask is made there is much less noise in the result image.

Fig.3. Correlation mask, which help to eliminate the noise

Therefore, eliminating all this noise, result correlated image is received. It is shown in Fig.4.

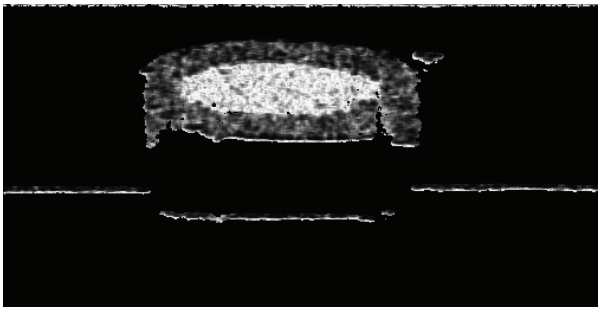

Fig.4. The result image, obtained by correlation analysis of initial image

After receiving this image, it is converted in binary string and written to binary file, from which it is possible to get a 3D image, which is shown in Fig.5.

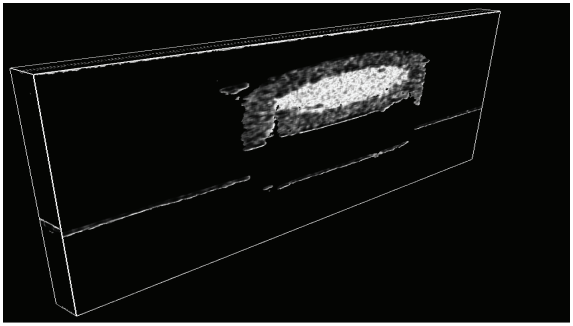

Fig.5. 3D image of the resulting correlated image

In this way, with the help of correlation method it is able to visualize areas with different dynamic states. The algorithm of this method is not complicated, but it provides a high resolution 3D images of biological tissues, which is independent of phase changes of the signals and has the ability to eliminate excess noise. All this is very helpful in medicine and can provide a powerful instrument for diagnosing and controlling diseases.

REFERENCES:

1. *Enfield J., Jonathan E., Leahy M.* In vivo imaging of the microcirculation of the volar forearm using correlation mapping optical coherence tomography (cmOCT) // Biomedical Optics Express. 2011.Vol. 2, No. 5. P. 1184–1193.
2. *Enfield J., Jonathan E., Leahy M.* Correlation mapping method for generating microcirculation morphology from optical coherence tomography (OCT) intensity images // J. Biophotonics.2011.Vol.4, No. 9, P. 583–587.
3. *Drexler W., Fujimoto J. G.* Optical Coherence Tomography. Technology and Applications. Springer.1326 p.
4. *Daly S. M., Leahy M. J.* 'Go with the flow': A review of methods and advancements in blood flow imaging // J. Biophotonics. 2012. P. 1–39
5. *Bonin T., Koch P., Huttmann G.* Comparison of fast swept source full-field OCT with conventional scanning OCT // SPIE-OSA.2011 Vol. 8091.

OLD PIPELINES` INSULATING COVER`S FEATURES AND ITS PROTECTIVE PROPERTIES

R.M. Karabalin

Zhangir Khan West Kazakhstan Agrarian-Technical University

Much attention is paid to the protection of underground pipelines against corrosion. Without it, underground pipelines fail during 5…10 years depending on properties of soil and existence of vagabond currents. Underground steel pipelines have double protection against corrosion: passive and active. The role of passive protection executes insulating covering, active – cathode potential. In case of the strong wear of insulating covering, active protection doesn't cope because of big losses of protective current on various defects of insulating covering. Therefore the role of insulating covering is doubly important.

Control of insulating covering condition is usually carried out by electrometric methods. However in interpretation of measurements results and subsequent calculations there are problems which we will consider in relation to

pipelines of gas-distribution systems (1). These pipelines have the following features which need to be considered in the analysis of their condition:

1. Practically all pipelines which have served 40 and more years and subjects to complex survey, are covered with bituminous insulation. Normative period of bituminous insulation exploitation is only 15…20 years. During 40 years, bituminous insulation strongly embrittles, fractures, exfoliates from the pipe surface, and almost completely loses protective properties.

2. Pipelines of gas supply system are exploited in settlements and industrial zones where surely there are stray currents from electrotransport and operating electric equipment. Stray currents break electrochemical protection, causing shift of potentials in the positive side. Thus some sections of the pipeline become anode in relation to the earth or other sections. If insulating covering is worn-out, at these sections strenuously there is a corrosion that quickly leads to formation of fistula and pipeline depressurization.

3. Pipelines of gas-distribution systems cross a set of roads, underground, terrestrial and air communications. It causes additional mechanical and electrical stresses that creates difficulties in case of service and diagnostics of pipelines.

4. Separate sections of the pipelines route very dynamically change: there are new plantings, constructions, fences, even new streets with houses and home structures; there are new roads and old are extended; beds of the rivers through which transfer pipelines change; there are new communications – underground and air. Some sections become unavailable to careful survey.

If insulating covering saved the protective properties throughout the pipeline, the above features wouldn't constitute danger. Unfortunately, insulating covering during 40 and more years of exploitation practically loses the protective properties. It expresses that all characteristics of covering (adhesion, transition resistance, mechanical properties, and electrical density) have very wide spacing, practically from zero, even within one bore pit. Dispersions of these parameters are at least twice more, than their mean values. Therefore results of measurements of insulating covering characteristics in local points at bore pit surveys, give nothing definite for the quality of insulating covering assessment. If calculate a residual resource of insulating covering on these values, we will receive any digits from zero and above.

It is possible to average certainly the measured values and to receive certain «average» values of a residual resource. But then it will be necessary to tell something about dispersion of a residual resource. Generally we will receive confusion: for one pipeline we will receive a set of accidental residual

resources. What their physical sense is and how to use these results in case of assessment of safety of one specific pipeline – it isn't known.

So, we returned to the initial question: how to diagnose insulating covering of the pipeline after the long exploitation? In our opinion, here it is impossible to use local characteristics of insulating covering. It is necessary to find such characteristics which describe protective properties of insulating covering on some finite section of the pipeline. Length of a section can be different depending on specific conditions, for example, 100 m or 1 km.

It is known that insulating covering shall execute two basic functions: most to hinder with access of ground water with its salts and ions to a pipe surface, to reduce to a minimum leakage of protective current from a pipe in soil (2). Access of ground water to a surface of metal and leakage of an electric current from a pipe in soil are interconnected and are described by the same mechanism – movement of molecules and ions from soil to a surface of metal and back. Therefore barrier properties of insulating covering is best of all characterized by transition resistance, not local, but integral for the selected section of the pipeline (length of 100 m or 1 km). Integral transition resistance of insulation actually incorporates all local characteristics of insulation, but isn't a random variable. Therefore there is no such concept as dispersion and dispersion. Integral transition resistance isn't mean value, and is something like the amount of a full range of random elements.

It is necessary to mark that for other characteristics of insulating covering (adhesion, mechanical properties, and electrical continuity) it is difficult to imagine integral values. Besides these characteristics describe technological properties of insulating covering, instead of protective. It is possible to imagine the coverings possessing very big adhesion, but not possessing any protective properties.

REFERENCES:

1. Building materials and devices / V. N. Osnovin, L. V. Shulyakov, Р-н-Д: Феникс, 2005. 443 p.
2. Modern building materials and technologies /U. N. Kazakov, U.E. vol. 2. – СПб.: ДЕАН, 2007. 176 p.

SPUTTERING OF ALUMINIUM NITRIDE THIN FILMS FOR *FBAR* AND *SAW* APPLICATIONS

R.N. Khanbekov

Saratov State University

Progress of modern technologies highly depends on the quality and the properties of materials they are based on. This problem especially concerns surface acoustic waves (SAW) and film bulk acoustic resonator (FBAR) devices which nowadays have to work within the GHz range. High hardness (11–16 GPa), wide band gap (6.0-6.2 eV), high electrical resistivity (10^9-10^{13} ohm*m), high thermal conductivity and acoustic wave velocity (Stan, Pasuk, Galca, Dinescu, 2010) make aluminium nitride quite interesting for a great range of applications, especially for microelectromechanical system (MEMS) and nanoelectromechanical system (NEMS) devices. For acquisition of AlN thin films different techniques can be used, such as molecular beam epitaxy (MBE), ion beam assisted deposition, chemical vapour deposition (CVD) (Assouar, El Hakiki, Elmazria, Alnot, Tiusan, 2004). In this work direct current (DC) and radio frequency (RF) magnetron sputtering of AlN films and their specifics are discussed.

Among a lot of different methods of physical vapour deposition (PVD) nowadays the magnetron sputtering is the easiest technique for obtaining the high quality AlN thin films. The whole sputtering station consists of a vacuum chamber, gas feeding system, vacuum pump, and a power supply. Inside the chamber there are a substrate and the magnetron which has its own water cooling system. The magnetron sputtering system on the Fig. 1 (Xiao-Hong Xu, Hai-Shun Wu, Cong-Jie Zhang, Zhi-Hao Jin, 2001) has a DC power supply, but RF power source also can be used.

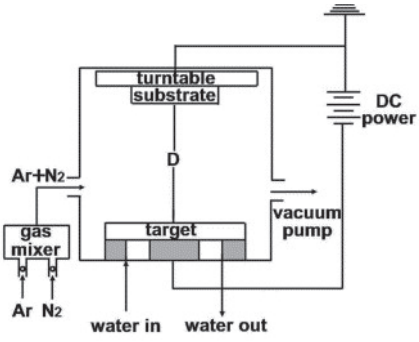

Fig. 1. Schematic drawing of the magnetron sputtering system with DC power supply

Target in the magnetron is a cathode. Electrons emitted from the cathode's surface are being retained by the magnetic field and circulate around the surface of the target (Fig. 2 (Gulbinski, 2008)). While moving they ionize the atoms of the inert gas

(Ar) and these ions hit the cathode making the atoms on the surface sputter and causing the secondary electrons emission. This collision cascade leads to a higher sputtering rate.

After this the sputtered atoms get onto the substrate forming the film on its surface.

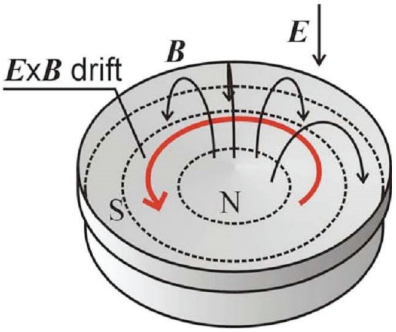

Fig. 2. Planar circular sputtering source

Aluminium nitride thin films can be obtained using RF or DC power source. Pure aluminium disk is used as the target, the gas that is being discharged into the chamber is Ar/№ $_2$ mixture with a variable proportion between the components. Deposition process is held at the working pressure of ~ 0.4 Pa, temperature of the substrate may vary from 300-400 K in case of no substrate holder heating, up to 673 K if the heating is on.

The main goal is to obtain the thin piezoelectric AlN film with the proper stoichiometry, polycrystalline structure, and c-axis orientation (Fig. 3 (Mishin, Marx, Sylvia, Lughi, Turner, and Clarke, 2003).

Fig. 3. TEM micrographs of high (left) and low (right) quality AlN films.

In this work AlN thin film (~300*10^{-9} m) was deposited onto the erbium-doped aluminium yttrium garnet (Er:YAG) substrate. The magnetron was connected to a RF power supply, gas pressure inside the chamber during the deposition process was 0,3 Pa. After the film was obtained its piezoelectric activity was examined, but our sample demonstrated no piezoelectric effect. In order to investigate the reason of the absence of the piezoelectric effect Auger-spectroscopy was applied. Results of the spectroscopy showed the presence of the oxygen in our sample (Fig. 4).

Presence of oxygen in the AlN film causes the amorphization of its crystal structure which leads to the absence of the piezoelectric effect. This means that in order to obtain the proper AlN thin films for SAW and FBAR devices the feeding gases must be highly pure.

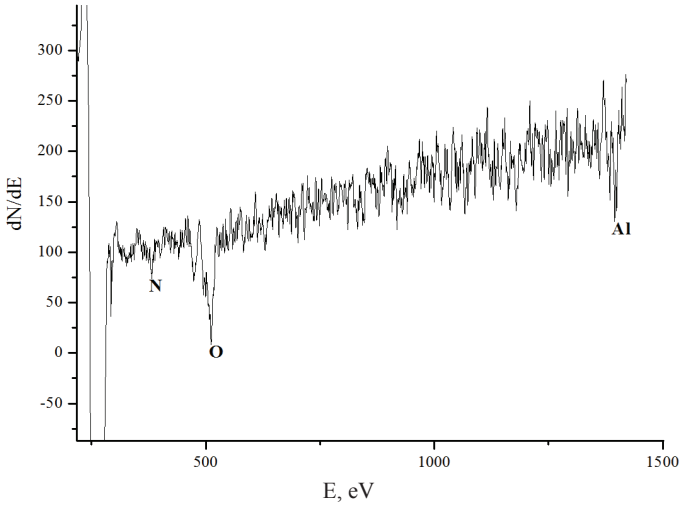

Fig. 4. Auger-spectre of the AlN film

A number of exceptional properties of aluminium nitride can make it in the near future an extremely widespread material for SAW and FBAR devices, optical sensors, and a lot of other applications. AlN films deposited by magnetron sputtering method represent a very high quality, even comparing with MBE deposited films, which can make the production of the devices less expensive and more technologically simple.

REFERENCES:

1. *Assouar M. B., El Hakiki M., Elmazria O., Alnot P., Tiusan C.*, "Synthesis and microstructural characterisation of reactive RF magnetron sputtering AlN films for surface acoustic wave filters". Diamond and Related Materials 13(2004)1111–1115.
2. *Gulbinski W.*, "Physical Vapour Deposition of Thin Film Coatings Part II Magnetron sputtering". European Summer School PPST 2008
3. *Mishin S., Marx D. R., Sylvia B., Lughi V., Turner K. L.*, and Clarke D. R., "Sputtered AlN Thin Films on Si and Electrodes for MEMS Resonators: Relationship Between Surface Quality Microstructure and Film Properties". 2003 IEEE Ultrasonics Symposium-2032.
4. *Stan G. E., Pasuk I., Galca A. C., Dinescu A.*, "Highly Textured (001) AlN Nanostructured Thin Films Synthesised By Reactive Magnetron Sputtering For SAW And FBAR Applications". Digest Journal of Nanomaterials and Biostructures Vol. 5, № 4, October-December 2010, p. 1041-1054
5. *Xiao-Hong Xu, Hai-Shun Wu, Cong-Jie Zhang, Zhi-Hao Jin*, "Morphological properties of AlN piezoelectric thin films deposited by DC reactive magnetron sputtering". Thin Solid Films. Volume 338. Issues 1–2. p. 62–67. Elsevier. 1 June 2001

ECOLOGICAL PROBLEMS OF THE URAL RIVER

L.V. Khon

Zhangir Khan West-Kazakhstan Agrarian-Technical University

The Ural River is a unique natural site and trans-boundary water artery of the Russian Federation and the Republic of Kazakhstan.

Ural River originates in the southern spurs of the Urals (Ural ridge – Tau) at an altitude 640 m above sea level. It crosses the territory of the Russian Federation, the West – Kazakhstan and Atyrau regions of Kazakhstan. [1]

The role and importance of the Ural River in the territory of Kazakhstan due to the following factors:

1. The Ural River is the **backbone** natural object of the West Kazakhstan and Atyrau regions.

2. Surface and ground water of the Ural River are the source of drinking water and water supply for the national economy of the West Kazakhstan and Atyrau regions, with the population over 1 million people.

3. The Ural River is the largest fresh water **fishery reservoir** in the West Kazakhstan and unique natural spawning sturgeon.

4. Ural river basin is intrazonal center of biodiversity in the West Kazakhstan, the source of animal and plant resources.

5. The Ural River is the only navigable waterway in Western Kazakhstan.

6. The valley and the Ural River is the natural reserve of rich biodiversity, a favorite vacation spot and the object of eco-tourism in the West Kazakhstan.

Environmental problems of the Ural River basin caused by natural and man-made factors. The primary causes of degradation of the Ural River are the natural processes of the channel's destruction, occurring as a result of the continuous flow of surface water. The negative consequences of this are:

– Siltation of the river channel and the formation of sills, resulting in shallowing of the river and the deterioration of its hydrological regime. As a result form reaches, bends, branches, oxbows etc.

– Coastal erosion in areas of bends and ground with a light texture. It threatens to exit the river from the bed and the flooding of large areas; [2]

In the Urals, these processes are exacerbated by stormy spring floods. Among the negative factors contributing to the silting of the river bed are also plain territory, slow-flowing, and slightly hilly terrain conditioning numerous zigzags bed. Therefore, the integrity and functionality of the river is not possible without the constant care for her.

Over the last few years the intensive floods on the Ural river made significant changes in channel processes in the area of the right bank near the village of Vladimirovka, where already hit 235 homes. There is a real threat of destruction of the roads of the national importance Uralsk – Atyrau and the bursting of the Ural's water into Kushum irrigation and watering system, with possible flooding of the five districts. In the flood zone may be 156 thousand people, 3 million hectares of agricultural land, 29 settlements. There will be a disruption of the cascade reservoirs of the Ural-Kushum system (Kirov, Bitikskoe, Dongulyukskoe, Pyatimarskoe). Next, the flow of water will move into the territory of Atyrau region and the Caspian Sea. The possible material and resource damage, the extent of the emergency will be in the nature of environmental catastrophe. In this connection, the work associated with the strengthening of the river Ural have an urgent nature. Bridge between the Urals and Kushum system is declining by 10-20 meters and now is less than 100 meters. [2]

In the last decade the problem of the pollution of the surface waters of the Ural River has declined. According to the state monitoring of the surface water of the Ural River, in 1992 water pollution index was 5.58, which corresponds to the category of «dirty» water. The peak of pollution was in 1996, when the WPI rose to 11.5 (the category of «very dirty»). Since 1998, water pollution dramatically reduced, and since then the Ural River surface water classified as «clean» and «moderately polluted».

But it should be noted that the main pollution of the river is in the neighboring territories of the Russian Federation and the Aktobe region of Kazakhstan (in r.Ilek).

The most polluted areas are the areas of the Ural River in Orsk and Orenburg.

Ilek river water is polluted by the compounds of fluorine, boron, hexavalent chromium. Water pollution of the Ilek river in the Aktobe region made dependent on the drainage filter sludge tanks and dumps of chemical plants. JSC «Aktobe plant of chromium compounds» continues river pollution.

The share of West Kazakhstan region in the pollution of the Ural River is negligible. It is the resets the clean-contaminated water of the Ural CHP and SCE «Oral Su Arnasy." People of many communities (including Uralsk), located on the banks of the river, pollute it by wastes of household and consumption.

With the rise and prospects for economic development in the basin of the Urals, the problem of water pollution remains, in connection with what it is necessary to create an intergovernmental coordination center for monitoring surface water of the Ural River.

The problems of the Ural River could be solved more quickly in the case of its inclusion in the list of water bodies of special national significance.

Water pollution is due to the penetration of harmful substances from the storage of waste as industrial as domestic nature, and from their burial ground. Also, the water is polluted by runoff from the production site, run-off from the fields of organic matter, fertilizers and plant protection products, seepage of contaminants from polluted surface waters and fields of filtration, oil wells, water intakes, etc.

The main water pollution is due to sewage discharge into the environment.

There are 6 major water users discharge waste water into the environment: KPO bv, LLP "Batis Su Arnasy» SCE «Aksayzhylukuat», JSC «Zhayykteploenergo», JSC «Condensate», Ural oil pipeline management and «KazTransOil».

Table 1

The volume of wastewater in the West Kazakhstan region

№	Designation	Categories of the discharges	2012г	2011г	+/-
1.	Industrial discharges, thouthand.m^3	Total, th.m^3	3738	5723	-1985
			3108	5065	-1957
		Volume-3B th.t.	5,6	4,9	+0,7
2.	Domestic waste water	Total, th.m^3	12001	11784	+217
		Volume 3B th.t.	3,4	2,6	+0,8
3.	Emergency and not legalized discharges	Total, th.м^3	0,8	5,1	-4,3
		Volume 3B th.t.	0,005	0,006	-0,001
4.	Discharges to the surface waters	Total, th.m^3	3108	5064	-1956
			3108	5064	-1956
		volume 3B th.t.	4,5	5,7	-1,2

As table 1 shows, in 2012, was produced 3738 thousand m3 of industrial discharges. Moreover, the majority of them, 3,108 thousand m3 are conditionally clean water, represents by the thermal waters of JSC «Zhayykteploenergo» and water LLP «Batis Su Arnasy» after the cleaning filters which are dumped in the Ural River.

The main part of the flows of Uralsk are domestic waste water, 12 001 thousand m3. It should be noted that industrial waste pollution is much higher than domestic wastewater, that proved by the index of the content of pollutants 5.6 tons to 3.4 tons

In the previous year, a significant part of the 5.1 thousand m3 were accidental and not legolized wastewater.

Compared with 2011, the volume of industrial discharges were reduced to 1985 thousand m3. This was due to the improvement of the sewerage systems of enterprises. Thus, in the JSC «condensate» was upgraded sewage treatment plants and sewage volumes decreased on 84%. Also, due to the reconstruction of the sewerage system and the commissioning of the modular plant for treatment of domestic sewage type BMOS SPN-50 «Sugar» owned to theUral oil pipeline management, reduced waste water discharge on 46.4%.

The volume of domestic waste water, on the contrary, increased on 217 thousand m3. In this regard, particular concern cause the fact that the technical condition of the constructions for waste water treatment in Uralsk PCG «Oral Su Arnasy» is in unsatisfactory condition, constructions are morally and physically obsolete, due to the significant deterioration and lack of proper care. Also transboundary pollution is influenced on the conditions of surface water.

On such a man-made background formed the qualitative composition of the main water artery of West Kazakhstan region, the Ural River and its tributaries and Chagan Derkul.

Table 2

The qualitative composition of the surface water of the Ural River

Index	OEL mg/l	The average annual concentration, mg/l		2011 y.		2012 y.	
		2011r.	2012r.	min	max	min	max
BOD5	3,0	1,87	1,79	1,20	3,20	1,0	3,79
Phenols	0,001	0,0014	0,0012	0,001	0,004	0,001	0,0014
Petroleum products	0,05	0,038	0,039	0,030	0,045	0,030	0,046
Ammonium salt	0,50	0,36	0,10	0,10	0,60	0,05	0,20
Nitrites	0,02	0,035	0,023	0,020	0,060	0,003	0,038
Chromium	0,02	0,04	0,036	0,01	0,07	0,01	0,06

Analysis of the annual average concentrations of pollutants by six components shown in Table 2, shows that in the surface waters of the Ural River in most qualitative indicators of pollution has reached or exceeds the thresholds.

So in 2012, the annual average concentration of phenol, nitrites, and hexavalent chromium exceed the maximum allowable concentration of fishery ponds and were in the range of 1–2 OEL. Oil content is also close to the threshold and at the level of 0.7-0.8 OEL. Relatively good position with the ammonium salt, and biological oxygen demand (BOD5). However, the sum-

mer low water, due to shortage of water and green water, biological oxygen demand consistently exceeds the OEL.

In 2012, a composite index of water pollution Ural River (WPI) was 1.27, which corresponds to 3-class quality, category – moderately polluted.Compared with 2011 concentration of BOD5, ammonium salt, phenol, nitrites and chromium slightly declined, except for petroleum products, the concentration of which remained practically at the same level.

Table 3

The qualitative composition of surface water of the Chagan river (right tributary of the Ural River)

Index	OEL mg/l	The average annual concentration, mg/l		2011 y.		2012 y.	
		2011r.	2012r.	min	max	min	max
BOD5	3,0	2,37	2,52	1,36	3,55	1,04	5,85
Phenols	0,001	0,0014	0,0013	0,001	0,0032	0,001	0,0018
Petroleum products	0,05	0,041	0,044	0,030	0,050	0,038	0,049
Ammonium salt	0,50	0,17	0,19	0,15	0,20	0,10	0,40
Nitrites	0,02	0,035	0,024	0,019	0,065	0,003	0,089
Chromium	0,02	0,01	0,01	0,01	0,01	0,01	0,01

Surface waters in the upper of the Chagan river formed in the Orenburg region in the middle and lower currents – in the West Kazakhstan region. And the whole catchment area is located in the area of agriculture. It influenced on the quality of its water.

In contrast to the surface water of the Ural River, water of the Chagan river characterized by low concentrations of hexavalent chromium, which are stable at 0.5 OEL. Annual average of the pollution by steel ingredients similar to the surface water of the Ural River. The exception is the biological oxygen demand, which is nearer to the threshold level and it is 0.7-0.8 OEL.

A comprehensive index of water pollution of the Chagan river (WPI) is 1.36, which corresponds to the 3-class quality, category – moderately polluted.

In recent years, in the drainage of the Chagan river rapidly develop oil and gas industry, and therefore the possible further deterioration of the quality of the surface water and groundwater. (Table III)

Surface water of the Derkul river fully formed on the territory of the West Kazakhstan region. Its catchment area is mainly in the agricultural land. River Derkul as river Chagan passes through many towns, in connection with what its waters are more exposed to organic pollution. considering the aridity, it en-

sures that the surface water of the Dercul river is is highly polluted by phenols, nitrites and BOD5.

Table 4

The qualitative composition of the surface water of the Derkul river (left tributary of the Ural River)

Index	OEL mg/l	The average annual concentration, mg/l		2011 y.		2012 y.	
		2011г.	2012г.	min	max	min	max
BOD5	3,0	2,91	2,75	2,2	3,52	1,30	4,65
Phenols	0,001	0,0020	0,0014	0,0011	0,009	0,0011	0,002
Petroleum products	0,05	0,037	0,041	0,030	0,047	0,031	0,047
Ammonium salt	0,50	0,20	0,27	0,10	0,25	0,10	0,80
Nitrites	0,02	0,031	0,020	0,022	0,055	0,005	0,051
Chromium	0,02	0,01	0,01	0,01	0,01	0,01	0,01

A comprehensive index of water pollution of the Derkul river (WPI) is 1.50, which corresponds to 3-class quality, category – moderately polluted.

But it should be noted that the major environmental problems of theUral River and, in general, all water bodies conected with the deterioration of the hydrological regime and the aridity of the last years. (Table 4)

REFERENCES:

1. *Chibilev A. A.* Ural basin: history, geography, ecology. – Ekaterinburg: UrO Ran, 2008.
2. *Sergaliev N. H.,. Kabdulov G. A, K. Ahmedenov,. Iskaliev D. ZH* Ural bed problems within West-Kazakhstan region. – Atyrau: Atyrau CSTI. -2012

SURVEY RADON-HELIUM USAGE RESULTS ON THE SOUTH-VJAZOVSKY LICENSE AREA

A.V. Kilyakov

Saratov State University

The territory under study is located in Chernojarovsky district of the Astrakhan region. The South-Vjazovsky license area is located in the southwest part of the Southwest-Caspian depression. This area is characterized by a complex geological structure because of active salt-dome tectonics.

The radon-helium survey was done in 2008 on the South-Vjazovsky license area Jurtovsky and Padinsky structures.

The basic difference of the used radon-helium survey method consists in the use soil gas radon, as detecting instrument of geodynamic zones and tectonic faults.

The method to conducting radon-helium survey consists in detecting gases concentration belonging to four groups. These groups are:

1. Hydrocarbon gases.
2. Radon, nitrogen, carbon dioxide, oxygen.
3. Helium and hydrogen.
4. Group by definition of background values. Analysis of gases from fourth group allows us to make judgment on what quantity of atmospheric nitrogen, carbon dioxide, oxygen present in the gaseous fluid.

As we know radon is a radioactive gas without color flavor and he the heaviest element in zero group of a periodic system, which is inert gas without stability and long-living isotopes.

All isotopes of radon are radioactive and quickly disintegrate the stable isotope has half-life 3,8 days. It constantly get to atmosphere from earth interior. It should be mentioned solubility of radon is 20 times more in natural gas than in water and it is eight times more in oil than in water (Филиппов, 2003).

Our research results in maps of a gases concentration distribution based on radon-helium survey. The drawn maps let to update the knowledge of geological structure of area under the study preferably the presence of tectonic faults with the help of the maps we can refine the data about oil and gas and a recommendations about the further exploration of studied area.

While we were conducting out studies on oil and gas deposit, it was stated that the geodynamic state of a depth is reflected near the daylight area in gas stream intensity index, which is discharged in atmosphere Earth, and is expressed in increased concentrations of radon, helium and methane concentration. Thus, tectonic faults and subvertical zones of a rock decompaction in geological section are fixed at 0,5–1,5m depths.

The petroleum deposit was revealed in 2008 year on Jurtovsky structure during formation tester Lower Triassic (induan stage). That year oil inflow was received from a well № 2 drilled on a crest of the structure from induan stage (Калинин, 2008).

184 short boreholes as the result of the analysis of physiographic and engineering-geological conditions on the South-Vjazovsky license area were drilled. They were up to 2 m deep and 80 boreholes were used for repeated measurements for further test.

During the study results on the Jurtovsky structure we measured radon concentration which ranged from 4,3* 10^3 Bk/m^3 to 190 *10^3 Bk/m^3 at mean 54,63* 10^3 Bk/m^3 (Fig. 1). Structure is marked by low soil gas radon concentration, surrounded by the tectonic faults distinguished by high concentration.

Sampling points with high radon concentration represent linear zones of northeast and southwest directions that indicate their correlation to tectonic faults. In areas of progressing salt-dome tectonics it often happens that tectonic faults are screen for hydrocarbon migration within lateral.

In some studies it is underlined that the fact that the majority of deposits in above-salt complex in the studied region were generated of hydrocarbon, which in its turn were generated by a deep-lying 4–6 km Carbon and Devonian source rock thick mass. The favorable conditions which are the generated traps, lithofacies characteristics of oil and gas bearing complexes, collector persistence, a hydro-geological situation and a number of other conditions coursed forming accumulation of oil and gas (Калинин, 2008).

On Jurtovsky structure above the tectonic faults radon concentration with high values which are from 100*10^3 and above Bk/m^3 are observed. On Padinsky structure not observed radon concentration with high values above tectonic faults were not observed, but the observable quantity exceeded the background values. Hydrocarbon trace have been detected in the holes drilled on Padinsky structure. It is possible to suppose that on Padinsky structure there had been a gaseous reservoir which dissolved in course of time. This conclusion is proved by the analogies with neighborhood deposits, which contain gaseous reservoirs. Padinsky structure is located hypsometrically above Jurtovsky.

On the block which is placed to the north of Jurtovsky structure low radon, methane and helium concentration were observed which indicates the hydrocarbon lack in this block (Fig. 1). It is confirmed that hole № 8 drilled on this block produced inflow of formation water without hydrocarbon.

One of the most promising for hydrocarbon accumulations new exploration is the western block on the South-Vjazovsky licence area. On this block we observed linear anomalies with high radon, methane, and helium concentration which correlate with tectonic faults (Fig. 1).

The western block of hydrocarbon bearing prospects are very high, as at this block high hydrocarbon gases concentration are observed. The increase of concentration from easier to heavier homologues of methane and high radon concentration over tectonic faults (10^5 Bk/m^3 and above) is detected.

The results of radon-helium survey on Jurtovsky structure agree with the earlier seismic works and with boring data, and update this data.

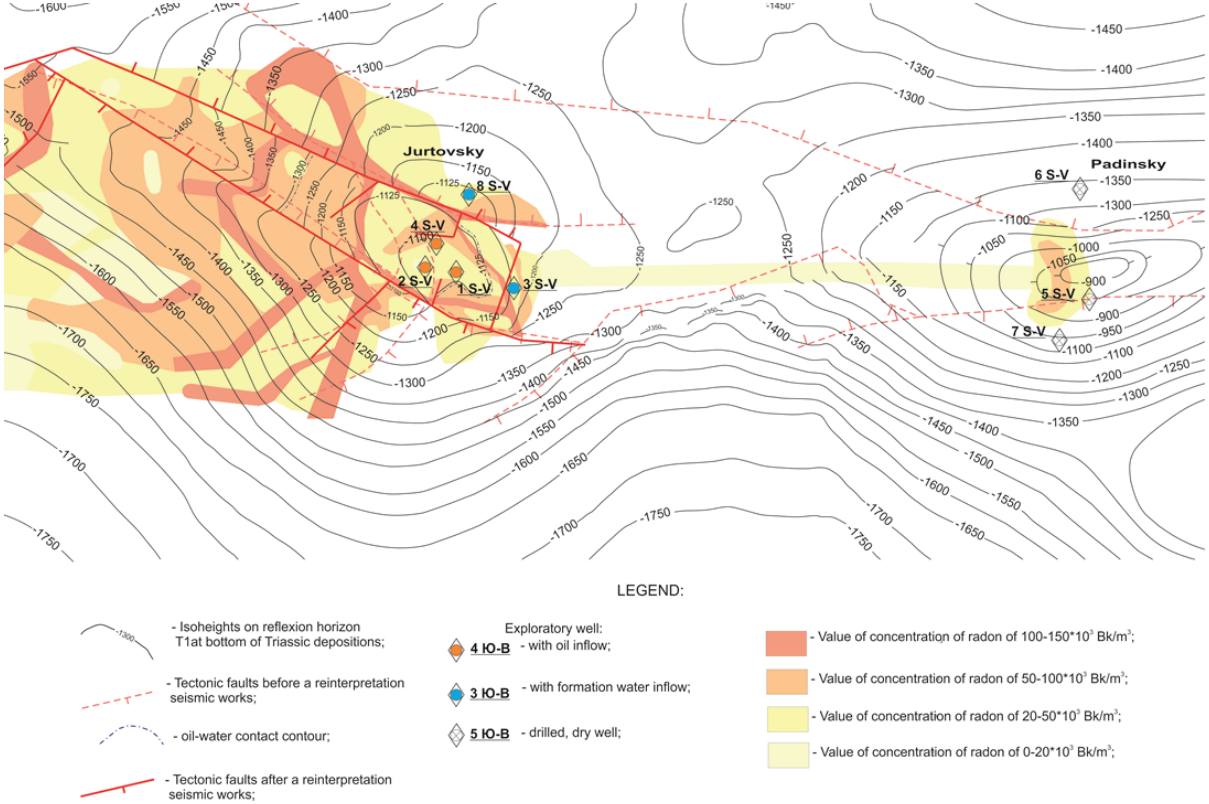

Fig. 1. The contour map on reflection horizon T_1. The radon concentration distribution in soil air.

After the reinterpretation of seismic works with consideration of radon-helium survey, tectonic faults locations have been updated and have coincide with radon-helium survey results.

Thus, according to the radon-helium survey results it is recommended to conduct a detailed MOGT 3-D seismic survey on the western block where supposed structural trap can be found.

Radon-helium survey can be used for oil and gas exploration, for mapping of tectonic faults, for field management and monitoring the well integrity and ecological observations.

REFERENCES:

1. *Филиппов В. П.* Применение индикаторного метода по радону для изучения нефтенасыщенных пористых сред. М.: ОАО «ВНИИОЭНГ». – 2003. 272 с.
2. *Калинин В. В.* Проект поисков залежей углеводородов и оценка их промышленной нефтегазоносности в надсолевых отложениях на выявленных и подготовленных структурах Южно-Вязовского лицензионного участка. Волгоград, 2008.

EXPLICIT MODELS FOR FLEXURAL EDGE WAVES PROPAGATION IN THIN SEMI-INFINITE ORTHOTROPIC PLATES

E.L. Kossovich

Saratov State University

It is well-known that flexural edge waves propagate not only in thin isotropic plates (Коненков, 1960), but also in anisotropic ones (Norris, 1994; Thompson et al, 2002; Zakharov and Becker, 2003). In order to study the laws of propagation of such waves one needs to extract their contribution into the whole dynamic response. All localized waves, including edge ones, are hidden in mathematical formulations of the original problems. Our approach to flexural edge waves relies on a recently developed one for surface waves. It is based on construction of the explicit models that describe the wave propagation. These models, highlighting the dual hyperbolic-elliptic nature of surface waves, have recently been created by Kaplunov and Kossovich (2004) for elastic and piezoelastic surface. They contain elliptic equations describing the decay in the interior away from the surface, and a hyperbolic equation at the surface corresponding to wave propagation. The models provide significant simplifications of the problems formulation. Development of similar

models for flexural edge waves seems not a trivial extension of the approach for surface waves, especially taking into account the dispersive nature of the latter. Therefore, the goal of the current work is to construct explicit models describing the flexural edge wave propagation in thin elastic plates made of orthotropic material.

We consider a semi-infinite plate, assuming that its middle plane occupies a space $-\infty < x < \infty$ and $0 \le y < \infty$. Within the framework of a classical Kirchhoff theory of plate bending, the equation of motion for a middle plane deflection w in case of an orthotropic plate takes following form

$$D_x \frac{\partial^4 w}{\partial x^4} + 2\left(D_1 + 2D_{xy}\right)\frac{\partial^4 w}{\partial x^2 \partial y^2} + D_y \frac{\partial^4 w}{\partial y^4} + 2\rho h \frac{\partial^2 w}{\partial t^2} = 0, \qquad (1)$$

where D_x, D_y, D_1 and D_{xy} are the bending stiffnesses, ρ is a density of plate material, $2h$ is the plate thickness, t – time coordinate.

The two types of boundary conditions are:

1)bending moment $M_0(x,t)$ at the plate edge

$$\begin{gathered} D_y \frac{\partial^2 w}{\partial y^2} + D_1 \frac{\partial^2 w}{\partial x^2} = -M_0(x,t), \\ D_y \frac{\partial^3 w}{\partial y^3} + \left(D_1 + 4D_{xy}\right)\frac{\partial^3 w}{\partial x^2 \partial y} = 0, \end{gathered} \qquad (2)$$

2)shear force $N_0(x,t)$ applied at the plate edge

$$\begin{gathered} D_y \frac{\partial^2 w}{\partial y^2} + D_1 \frac{\partial^2 w}{\partial x^2} = 0, \\ D_y \frac{\partial^3 w}{\partial y^3} + \left(D_1 + 4D_{xy}\right)\frac{\partial^3 w}{\partial x^2 \partial y} = -N_0(x,t). \end{gathered} \qquad (2)$$

After using the dimensionless parameters presented by equalities (3)

$$\begin{gathered} x = h\xi, y = h\eta, t = T\tau, w = hW^*, D_x = D\tilde{D}_x, \\ D_y = D\,\tilde{D}_y, D_1 = D\,\tilde{D}_1, D_{xy} = D\tilde{D}_{xy}, \end{gathered} \qquad (3)$$

where $D = \dfrac{D_x + D_y}{2}$ – is a typical bending stiffness, T – typical timescale; and applying Fourier and Laplace integral transforms to ξ – coordinate ($\xi \to ip$) and τ – coordinate , we come to the problems for the transformed analog of deflection $\hat{W}(\eta)$

In case of a bending moment applied at a plate edge, the exact solution takes following form

$$\hat{W}(\eta) = \frac{\hat{M}_0}{-is\lambda_0\sqrt{\hat{D}_v}} \frac{c^2}{c^4 - c_k^4} \frac{\Delta_1(c)\,\mathrm{e}^{\frac{\sqrt{-is\lambda_0\sqrt{\hat{D}_y}}}{c}\alpha_c\eta} + \Delta_2(c)\,\mathrm{e}^{\frac{\sqrt{-is\lambda_0\sqrt{\hat{D}_y}}}{c}\beta_c\eta}}{\Delta(c)}$$

where

$$\alpha_c = \frac{1}{\sqrt{\hat{D}_y}} \sqrt{\hat{D}_1 + 2\hat{D}_{xy} - \sqrt{\left(\hat{D}_1 + 2\hat{D}_{xy}\right)^2 - \hat{D}_x\hat{D}_y + c^4}},$$

$$\beta_c = \frac{1}{\sqrt{\hat{D}_y}} \sqrt{\hat{D}_1 + 2\hat{D}_{xy} + \sqrt{\left(\hat{D}_1 + 2\hat{D}_{xy}\right)^2 - \hat{D}_x\hat{D}_y + c^4}},$$

and also

$$\Delta_1(c) = -\left[2\hat{D}_{xy} - \sqrt{\left(\hat{D}_1 + 2\hat{D}_{xy}\right)^2 - \hat{D}_x\hat{D}_y + c^4}\right]\beta_c,$$

$$\Delta_2(c) = \left[2\hat{D}_{xy} + \sqrt{\left(\hat{D}_1 + 2\hat{D}_{xy}\right)^2 - \hat{D}_x\hat{D}_y + c^4}\right]\alpha_c$$

$$\Delta(c) = (\beta_c - \alpha_c)(c^4 - c_2^4),$$

$$X(c) = (\hat{D}_x\hat{D}_y - \hat{D}_1^2) - c^4 - 4\hat{D}_{xy}\sqrt{\hat{D}_x\hat{D}_y - c^4},$$

and c_k, c_2 are the roots of the equation which solution is the flexural edge wave speed coefficient. This equation was presented in Thompson et al (2002).

$$c_k = \left(\hat{D}_x\hat{D}_y - \left(\sqrt{\hat{D}_1^2 + 4\hat{D}_{xy}^2} - 2\hat{D}_{xy}\right)^2\right)^{\frac{1}{4}},$$

$$c_2 = \left(\hat{D}_x\hat{D}_y - \left(\sqrt{\hat{D}_1^2 + 4\hat{D}_{xy}^2} + 2\hat{D}_{xy}\right)^2\right)^{\frac{1}{4}}.$$

The root c_2 does not have any physical meaning, but c_k can be considered as a dimensionless constant wave speed coefficient.

In case of a shear force applied at a plate edge we come to a solution for the transformed rotational angle ($\frac{\partial w}{\partial y} = v \to \hat{V}$)

$$\hat{V}(\eta) = \frac{\hat{N}_0}{-is\lambda_0\sqrt{\hat{D}_y}} \frac{c^2}{c^4 - c_k^4} \frac{\Delta_3(c) e^{\frac{-\sqrt{-is\lambda_0\sqrt{\hat{D}_y}}}{c}\alpha_c\eta} + \Delta_4(c) e^{\frac{-\sqrt{-is\lambda_0\sqrt{\hat{D}_y}}}{c}\beta_c\eta}}{\Delta(c)} X(c), \quad (5)$$

where

$$\Delta_3(c) = -\left[2\hat{D}_{xy} + \sqrt{\left(\hat{D}_1 + 2\hat{D}_{xy}\right)^2 - \hat{D}_x\hat{D}_y + c^4}\right]\alpha_c,$$

$$\Delta_4(c) = \left[2\hat{D}_{xy} - \sqrt{\left(\hat{D}_1 + 2\hat{D}_{xy}\right)^2 - \hat{D}_x\hat{D}_y + c^4}\right]\beta_c.$$

Asymptotic analysis of solutions (5) and (6) (near the flexural edge wave poles $c = c_k$) allows to extract the contribution of this wave into the whole dynamic response. Also, on the basis of the asymptotic analysis we constructed the dual parabolic-elliptic models which explicitly depict the flexural edge wave contribution into the full deformation of the plate.

In case of applied bending moment the model consists of 1D parabolic equation which characterizes the wave propagation along the plate edge

$$\frac{c_k^{*4}}{D_y^2}\frac{\partial^4 w_e}{\partial x^4} + 2\frac{\rho h}{D_y}\frac{\partial^2 w_e}{\partial t^2} = Q_e^{(1)*}\frac{1}{D_y}\frac{\partial^2 M_0}{\partial x^2},$$

where $Q_e^{(1)*} = \frac{\Delta_1(c_k) + \Delta_2(c_k)}{\Delta(c_k)}$,

and 2D elliptic equation for the interior domain

$$\left(D_x\frac{c_k^{*4}}{D_y}\right)\frac{\partial^4 w_{in}}{\partial x^4} + 2\left(D_1 + 2D_{xy}\right)\frac{\partial^4 w_{in}}{\partial x^2 \partial y^2} + D_y\frac{\partial^4 w_{in}}{\partial y^4} = 0,$$

with boundary conditions

$$w_{in}(x, 0) = w_e(x),$$

$$D_y\frac{\partial^2 w_{in}}{\partial y^2} = -D_1\frac{\partial^2 w_e}{\partial x^2}.$$

In case of shear force applied at the plate edge the model has a similar form and is constructed for the rotational angle $v(x, y, t)$.

Let us now consider a point bending moment $M_0(x, t) = M_0\delta(x)e^{-i\omega t}$. It was established that the constructed models allow to not only find contribution of the flexural edge wave into the whole dynamic response, but also to vary it by adjusting the bending stiffness parameters. We found that taking $\hat{D}_x = \hat{D}_y = \hat{D}_{xy} = 1$, $\hat{D}_1 = 0.99$, the wave contribution shall be dominating as shown in Fig.1

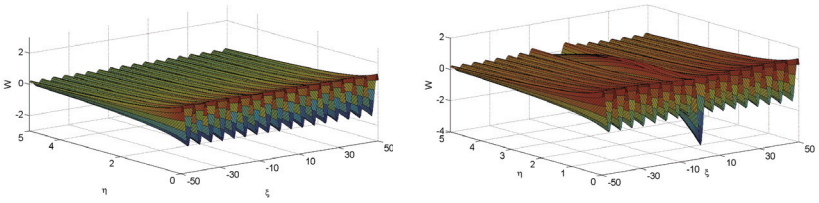

a *b*

Fig. 1. 3D profile of the parabolic-elliptic model (a) and exact solution (b)

Also, we may find such a material for which the edge wave contribution will be negligible. For example, it is $\hat{D}_x = \hat{D}_y = 1$, $\hat{D}_{xy} = 5$, $\hat{D}_1 = 0.5$. Results of calculation are presented in Fig.2.

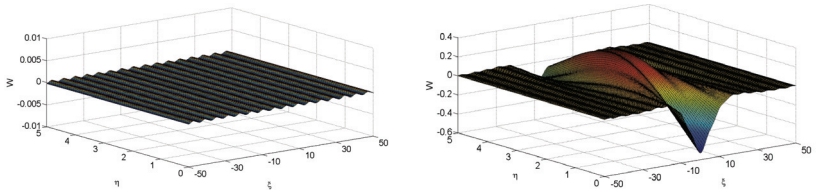

a *b*

Fig. 1 3D profile of the parabolic-elliptic model (a) and exact solution (b)

We have constructed explicit models which allow to extract the contribution of flexural edge wave propagating in thin semi-infinite orthotropic plate. It was shown that the aforementioned models also allow to vary this contribution by adjusting the parameters of plate bending stiffnesses.

REFERENCES:

1. *Коненков Ю. К.* Об изгибной волне «рэлеевского» типа // Акустический журнал. 1960. Т. 6. С. 124–126.
2. *Kaplunov Yu.D., Kossovich L. Yu.* Asymptotic model of {R} ayleigh waves in the far-field zone in an elastic Half-Plane // Doklady Physics. 2004. Vol. 49. № 4. P. 234–236.
3. *Norris~A.~N.* Flexural edge waves // Journal of Sound and Vibration. 1994. Vol. 171. P. 571–573.
4. *Thompson I., Abrahams I. D., Norris A. N.* On the existence of flexural edge waves on thin orthotropic plates // Journal of the Acoustical Society of America. 2002. Vol. 112. P. 1756–1765.
5. *Zakharov D. D., Becker W.* Rayleigh type bending waves in anisotropic media // Journal of Sound and Vibration. 2003. Vol. 261. P. 805-818.

DIMETHYL SULFOXIDE (DMSO) DIFFUSION IN SKIN TISSUE

M.D. Kozintseva

Saratov State University

The usage of DMSO increases the rate of absorption of some compounds through biological tissues, including skin; it can be used, for example, as a drug delivery system, because DMSO solution has low toxicity and increases penetration of tissues due to perforation of lipid's layer of the skin superficial layer. In this paper the diffusion coefficient of DMSO in the rat skin in vitro is estimated. The method is based on analysis of temporal dependence of the tissue collimated transmittance caused by partial replacement of interstitial fluid by the biocompatible immersion solution. Thus, we could achieve the optical clearing of the tissue due to DMSO diffusion into biological tissue, namely the tissue scattering properties modifications which were reduced during the experiment. A free diffusion model was used for a quantitative description of the process, assuming the diffusion coefficient as a constant in the whole volume of the sample. The value of DMSO diffusion coefficient was obtained, using the proposed model by fitting the experimental data.

The possibility of selective translucence of the superficial skin layers is very useful in developing functional imaging and therapeutic techniques. A potential benefit of the optical clearing is the improvement of laser therapeutic techniques that enable sufficient light penetration to a target embedded in tissue. Combination of optical clearing with laser radiation can reduce the laser fluences required for a therapeutic effect. However, in spite of numerous inves-

tigations dealing with transport of DMSO within biological tissue (Коваленко, Коваленко, Линник, 2009; Bui, McClure, Chang, Stoianovici, Hirshburg, Yeh, Choi, 2009) the problem of estimating the diffusion coefficient of the agent in skin has not been studied in details. Thus, goal of the study is to measure the diffusion coefficient of DMSO in skin.

The measurements of collimated transmittance have been performed using a commercially available spectrometer USB4000-Vis-NIR (Ocean Optics, USA) in the spectral range 400-1000 nm. The scheme of experimental setup for the measurements of collimated transmittance is presented on Fig. I. For this study, ten rat skin samples have been used. The samples have been obtained from autopsy and kept in saline during 24 hour until spectroscopic measurements at temperature 4–5°C. All measurements were performed at room temperature (about 20°C). The thickness of the samples was measured before the experiment and presented in Table I. 99.9% DMSO solution (SIGMA D8418, France) was used as a clearing agent. Refractive index of the solution is 1.476. It has been measured using Abbe refractometer at wavelength 589 nm.

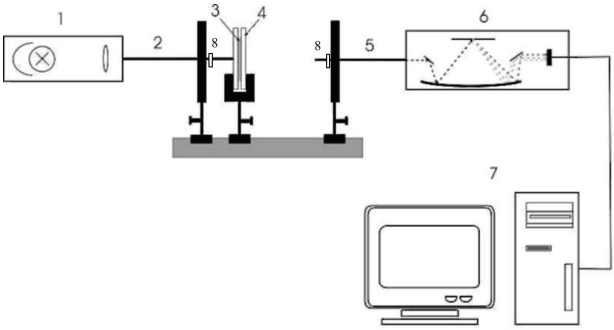

Fig. 1. The scheme of experimental setup for the measurements of collimated transmittance
1. The source of radiation (Halogen lamp HL 2000)
2. Delivering optical fiber (P400 1 UV VIS, Ocean Optics, USA)
3. Tissue sample
4. Glass cuvette with object plate
5. Receiving optical fiber (P400 1 UV VIS, Ocean Optics, USA)
6. Multichannel spectrometer (USB4000-Vis-NIR, Ocean Optics, USA)
7. PC (Personal Computer)
8. Collimators (74ACR, Ocean Optics, USA)

As it was mentioned, that the optical properties of biological tissues can be controlled effectively by using hyperosmotic immersion solution (Башкатов, 2002; Tuchin, 2007). In this case, the main mechanism is the optical clearing

of biological tissue can be described as the matching of refractive indices of scatteres (there are collagen fibers in skin) and the interstitial fluid. The optical clearing is a result of diffusion of the immersion solution into biological tissue.

With the penetration of the immersion solution into biological tissue, having a greater refractive index, than the refractive index of interstitial fluid of the tissue, we could see the decreasing of difference between the refractive indices of scatteres and the interstitial fluid (Башкатов, 2002). This process is described in detail in the paper.

We need to know the diffusion coefficient of the inserted liquid to construct mathematical models, describing the interaction of hyperosmotic immersion solution with the biological tissue.

The method of estimation of diffusion coefficient of hyperosmotic immersion solution in tissues is based on the measurement of time dependence of the collimated transmission of tissue, placed into clearing agent (Башкатов, Генина, Долотов, Правдин, Тучин, 2011).

In these experiments, the rat skin samples were used. The dermis of skin composes over 95% of the total skin thickness, so it follows, the optical properties of skin are determined by optical of skin dermis.

Diffusion of DMSO is described in the framework of free diffusion, and there were made certain assumptions about the transport process:

1) only concentration diffusion takes place; i.e., the flux of the chemical into tissue at the certain point within the tissue sample is proportional to the chemical concentration at this point;

2) the diffusion coefficient is constant over the entire sample volume;

3) penetration of a chemical into a tissue sample does not change the chemical concentration in the external volume;

4) the chemical does not interact with tissue components in the course of diffusion (Bashkatov, Genina, Tuchin, 2009).

Geometrically, the tissue sample can be represented as a plane-parallel plate of finite thickness, and boundary effects are neglected, because the area of the upper and lower surfaces of the plate is much greater, than the area of its sides.

Hence, we can solve one-dimensional diffusion equation:

$$\frac{\partial C(x,t)}{\partial t} = D\frac{\partial^2 C(x,t)}{\partial^2 x} \qquad (1)$$

where $C(x,t)$ is the concentration of DMSO within tissue sample, g/ml; D is the diffusion coefficient, cm^2/sec; x is a spatial coordinate, cm; t is the time of DMSO diffusion in skin, sec.

The key approach in characterization of transport of a chemical agent is that a set of boundary conditions defines the concentration profiles. Depending on the analytical solution used, tissue type, and the experimental setup, three kinds of initial and boundary conditions are most commonly used for studies of agent transport in tissues. All, however, are based on concentration *C (x, t)* as determined by Fick's second law.

The initial condition corresponds to the absence of an agent inside the tissue before the measurements, i.e.

$$C\,(x,0) = 0 \tag{2}$$

for all inner points of the tissue sample.

A tissue slab free of agent is immersed in solution with the agent concentration of C_0:

$$C\,(0,\,t) = C_0 \text{ and } \frac{\partial C(l,t)}{\partial x} = 0\,, \tag{3}$$

where l is the tissue sample thickness.

The solution of (1) with the initial (2) and the boundary (3) conditions has the form (Tuchin, Maksimova, Zimnyakov, 1997; Bashkatov, Genina, Tuchin, 2009):

$$C(x,t) = C_0(1 - \sum_{i=0}^{\infty} \frac{4}{\pi(2i+1)} \sin(\frac{(2i+1)\pi x}{l}) \exp(\frac{-(2i+1)^2 D\pi^2 t}{l^2}))\,, \tag{4}$$

The integral of (4) over x gives another physical quantity, average concentration as:

$$C\,(t) = C_0(1 - \frac{8}{\pi^2} \sum_{i=0}^{\infty} \frac{1}{(2i+1)^2} \exp(-(2i+1)^2 t\pi^2 \frac{D}{l^2}))\,, \tag{5}$$

where $C\,(t)$ is the volume-averaged concentration of an agent within tissue sample.

The scattering coefficient is described by equation (6):

$$\mu_s\,(t) = N\,\frac{\pi^2 a x^3}{8}(m^2-1)^2(1+\frac{2}{(m^2+1)^2})\,, \tag{6}$$

where N is the number of scatterers in unit volume; x is the diffraction parameter; m is the relative refraction index of scatterers; a is the radius of scatterers.

The dependence of the collimated transmittance of skin, that was placed in the hyperosmotic immersion solution, takes the form:

$$T \approx \exp(-(\mu_a + \mu_s(t))l), \quad (7)$$

where μ_a is the absorption coefficient of skin; μ_s is the scattering coefficient.

Equations (1) – (7) define the dependence of the transmittance coefficient of the concentration of the solution in the interstitial fluid in skin, what creates a direct problem. Inverse problem in this case is to restore the value of the diffusion coefficient on the temporal dependence of collimated transmittance. This problem is solved by minimizing the target function:

$$f(D) = \sum_{i=1}^{N} (T_c(D, t_i) - T_c^*(t_i))^2,$$

where N is the total number of data points obtained during the registration of temporal dependence of collimated transmittance with the fixed wavelength; T_c (D, t) is the calculated transmittance value, when the value of D is given; $T_c^*(t)$ is the experimentally measured transmittance value. (Bashkatov, Genina, Tuchin, 2009; Башкатов, Генина, Долотов, Правдин, Тучин, 2011).

The «complex» method was used to minimize the objective function (Банди, 1988). Iterative procedure was repeated until matching between the experimental and calculated data was gained.

Figures 2 and 3 show the spectra and temporal dependence of collimated transmission at different wavelengths, that characterise the optical properties of skin and their changes under the hyperosmotic immersion solution influence.

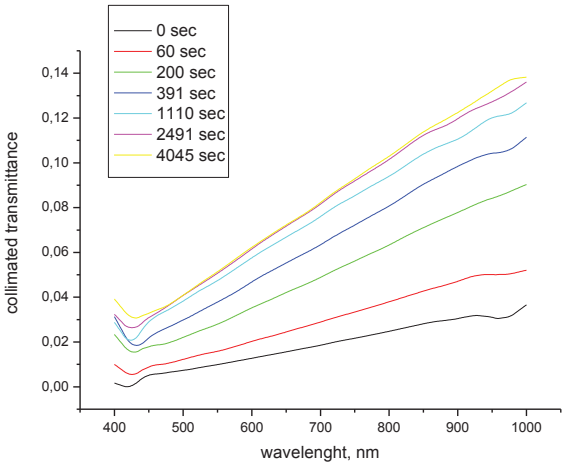

Fig. 2. The transmittance spectra of the rat skin measured concurrently with administration of DMSO solution at different time intervals.

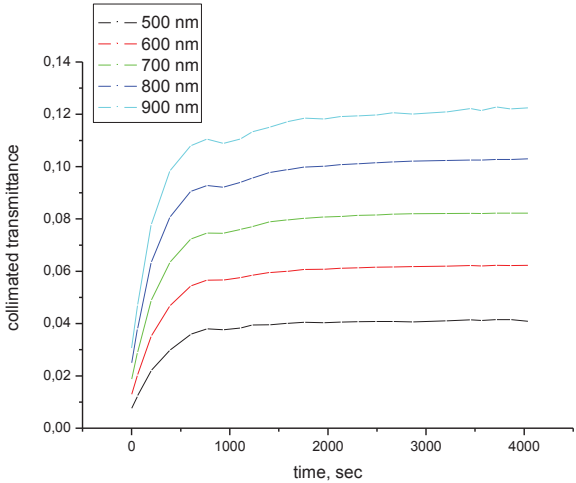

Fig. 3. The temporal dependence of collimated transmittance of rat skin measured at different wavelength concurrently with administration of DMSO solution.

Fig. 2 shows clearly, that the skin is a cloudy tissue at the initial time. During the DMSO diffusion into the skin, the interstitial fluid of sample was replaced by DMSO, and therefore, there is a process of reducing light scattering, and increasing of collimated transmission.

Fig. 3 shows the temporal dependence of collimated transmission of samples. The average value of the diffusion coefficient of DMSO molecules in the skin can be estimated, using the algorithm above. For every sample, the calculation was performed for four wavelengths (400, 600, 650 and 700 nm). Table I shows the average diffusion coefficient of DMSO molecules in skin.

Table I

DMSO diffusion coefficient in rat skin

Number of sample	Thickness, mm	Diffusion coefficient, cm^2/sec	Number of sample	Thickness, mm	Diffusion coefficient, cm^2/sec
1	0,63	$(3,99\pm0.21)\times10^{-6}$	6	0,88	$(1,28\pm2.87)\times10^{-6}$
2	0,87	$(9,98\pm0.68)\times10^{-6}$	7	1,33	$(7,13\pm0.72)\times10^{-6}$
3	0,51	$(7,13\pm2.24)\times10^{-7}$	8	0,41	$(2,59\pm1.50)\times10^{-6}$
4	0,32	$(1,89\pm1.78)\times10^{-6}$	9	0,87	$(1,84\pm0.28)\times10^{-6}$
5	0,56	$(7,94\pm0.63)\times10^{-6}$	10	0,47	$(4,06\pm0.04)\times10^{-6}$
Averaged diffusion coefficient $<D> = (4,78\pm3,045) \times 10^{-6}\ cm^2/sec$					

It was shown in the processing of our experimental data, that the diffusion coefficient of DMSO in skin is (4,78 ± 3,045) x10^{-6} cm^2/sec. Inasmuch as that diffusion coefficient increases with increasing temperature, it is expected, that the diffusion coefficients of DMSO in the skin in vivo will have a few large values, than in vitro experiments (Башкатов, Генина, Долотов, Правдин, Тучин, 2011; Тучин, Башкатов, Генина, Синичкин, Лакодина, 2001).

ACKNOWLEDGEMENTS:

Grant #224014 Network of Excellence for Biophotonics (PHOTONIC-S4LIFE) of the Seventh Framework Programme of Commission of the European Communities

REFERENCES:

1. *Банди Б.* Методы оптимизации. М.: Радио и связь, 1988. 128 с.
2. *Башкатов А. Н.* Управление оптическими свойствами биотканей при воздействии на них осмотически активными иммерсионными жидкостями / Дисс. канд. физ. – мат. наук, Саратов: СГУ, 2002, 198 с.
3. *Башкатов А. Н., Генина Э. А., Синичкин Ю. П., Кочубей В. И., Лакодина Н. А., Тучин В. В.* Определение коэффициента диффузии глюкозы в склере глаза человека // Биофизика, 2003, том 48, вып.2, стр. 309-313.
4. *Башкатов А. Н., Генина Э. А., Долотов Л. Е., Правдин А. Б., Тучин В. В.* Общий биофизический практикум. Биофотоника / Саратов: Изд-во Саратовского ун-та, 2011, 144 с.
5. *Бретшнайдер С.* Свойства газов и жидкостей. Л.:Химия, 1966. 536 с.
6. *Коваленко Г. В., Коваленко И. Ф., Линник Т. П.* Механизм транспорта ДМСО, глицерина и этиленгликоля через мембраны эритроцитов крысы и кролика (Институт проблем криобиологии и криомедицины НАН Украины (Харьков, Украина)): Вісник Харківського національного університету імені В. Н. Каразіна. Серія: біологія, Вип. 10, № 878, 2009р., с.109-116.
7. *Рид Р., Праусниц Дж., Шервуд Т.* Свойства газов и жидкостей. Л.: Химия, 1982. 592с.
8. Тучин В. В., Башкатов А. Н., Генина Э. А., Синичкин Ю. П., Лакодина Н. А. In vivo исследование динамики иммерсионного просветления кожи человека // Письма в ЖТФ, Т. 27, № 12, С. 10-14, 2001.
9. Bui A. K., McClure R. A., Chang J., Stoianovici Ch., Hirshburg J., Yeh A. T., Choi B., PhD Revisiting Optical Clearing With Dimethyl Sulfoxide (DMSO): Lasers in Surgery and Medicine 41:142–148, 2009.
10. *Bashkatov A. N., Genina E. A., Tuchin V. V.* Measurement of glucose diffusion coefficients in human tissues / Chapter 19 in: Handbook of Optical Sensing of Glucose in Biological Fluids and Tissues, Valery V. Tuchin (editor), Taylor & Francis Group LLC, CRC Press, 2009, pp. 587–621.
11. *Tuchin V. V., Maksimova I. L., Zimnyakov D. A., et al.,* "Light propagation in tissues with controlled optical properties," J. Biomed. Opt., vol. 2, 1997, pp. 401-417.
12. *Tuchin V. V.* Tissue Optics: Light Scattering Methods and Instruments for Medical Diagnosis, Bellingham, SPIE Press, 2007, 882 p.

REMUNERATION AS A DOMINANT FACTOR OF MOTIVATING EMPLOYEES IN RUSSIA

D.S. Kuzmin, S.V. Kuzmina

Saratov State University

Nowadays one of the most pressing issues in the activities of the leadership of almost every company is to provide the company with highly qualified staff that can develop in accordance with the needs of the company and the market. Personnel are a major competitive advantage of any company.

According to one of the most successful managers, the founder of the company SONY, A. Morita «No theory, program, or government policy can make the enterprise successful, this can make only people» (Морита, 2007).

To attract and, what is most important, to retain highly qualified employees in the company is possible only when they are properly motivated.

Motivation is one of the basic functions of management that is separated as an activity, which is the process of encouraging ourselves and others to activities aimed at achieving the goals of the organization (Дорофеева, 2011).

Motivation can be divided into two types: external and internal.

External motivation is a material motivation, aimed at meeting the needs of the so-called low-level (food, housing, etc.). Internal motivation is a moral motivation, aimed at meeting the needs of a higher level, of spiritual needs of a person (Аскаров, 2007).

In some theories of motivation, a dominant role is assigned to internal motivation. According to the «Theory Y» of American social psychologist D. McGregor employees tend to result, they are able to generate ideas, to accept responsibility and to direct their behavior to achieve the organization's goals. A «Theory Y» manager believes that, given the right conditions, most people will want to do work well. They believe that the satisfaction of doing a good job is a strong motivation.

The Goal Setting Theory of American psychologist Edwin Locke assumes that people in some degree perceive goals of the organization as their own and tend to achieve them.

Perhaps, after working for a long time in the company employees will take its goals as their own, but for new employees it will probably not be so. Getting a job people do not follow goals of the company, but their own.

The conception of Participatory management is based on the fact that if a person is interested in the activities of the organization, then he or she gets satisfaction from it, works more effective, better and more productive.

Now theories of motivation, in which the primary factor of motivation is economic needs of the employee (he or she may realize them with the help of material rewards), will be considered.

According to the «Theory X» of D. McGregor an employee tends to extract material profit and will do only that what will bring him or her the greatest economic benefit.

American psychologist A. Maslow in his «theory of the hierarchy of needs» argued that in the basis of the so-called hierarchy of needs, in the first place there are the physiological needs (needs for food, clothing), and in the second place there are the needs for security (the desire of people to be in a stable and safe condition: to have good housing, to be protected from diseases and other sufferings). These needs can be satisfied only with finances.

Moving from theory to practice, the opinion of the founder of the world's largest car manufactory H. Ford can be given. In his book «My Life and Work» he writes, «What good is industry if it be so unskillfully managed as not to return a living to everyone concerned? No question is more important than that of wages – most of the people of the country live on wages. The scale of their living – the rate of their wages – determines the prosperity of the country." (Ford).

Being a successful practitioner Henry Ford in the early XX century, made a "revolution» in the industry, putting forward and implementing the idea of a fair economic reward for employees. «We made the change not merely because we wanted to pay higher wages and thought we could pay them. We wanted to pay these wages so that the business would be on a lasting foundation. We were not distributing anything – we were building for the future. A low wage business is always insecure." (Ford). According to H. Ford the best incentive was cash compensation, because who lives well, he works well. The success of H. Ford fully confirms the soundness of his ideas.

We present the results of sociological studies conducted in Russia related to the problems of motivation.

According to the surveys by the Levada Center, to the question "If now you get a job, what factor would be the most important for you?" the answer "good salary» in 2000 85% of respondents chose, in 2012 – 81% (Общественное мнение, 2012). To the question «Which of the following statements about what work means for a person, is the most suitable for you personally?" option "Work – is primarily a source of livelihood» both in 2000 and in 2012 66% of

respondents chose (Общественное мнение, 2012). And to the question «What should be done first so that you work more and better?" the answer "pay more» in 1995 57% of respondents chose, and in 2010 – 72% (http://www.levada.ru/archive/otsenki-sotsialnykh-problem-i-zanyatosti/chto-nuzhno-bylo-sdelat-v-pervuyu-ochered-dlya-togo).

According to the survey conducted by WCIOM (Russian Public Opinion Research Center) in 2007 to the question «What do you think has the greatest impact on young people when they choose their future profession?" 52% of respondents chose the answer "Waiting for high incomes, wages in the chosen field of employment», the remaining options (prestige of the profession, career growth, personal ambition, etc.) scored from 1% to 10% (http://wciom.ru/zh/print_q.php?s_id=310&q_id=23992&date =07.10.2007).

From the analyzed opinion polls we can conclude that in contemporary Russia the main motivating factor is the incentives. Of course, the satisfaction of such needs as self-assertion, self-expression, social needs and others are necessary for the majority of workers in modern society. However, salaries and incentive payments have been and remain an important moment in the life of a working person. The youth of today, choosing their future profession, focuses generally on the material side. For most young people in the first place there is the satisfaction of material needs.

Generalizing the above, we can conclude that both material and moral motivation are important, but a dominant role should be assigned to financial incentives. Without moral motivation an employee can perform his or her duties, but without financial incentive practically no one will work. To support this idea we can quote H. Ford: «There is now a definite demand that the human side of business be elevated to a position of equal importance with the material side. And that is going to come about. It is just a question whether it is going to be brought about wisely-in a way that will conserve the material side which now sustains us, or unwisely and in such a way as shall take from us all the benefit of the work of the past years» (Ford).

REFERENCES:

1. *Аскаров Е.* Мотивация к качественному труду // Региональный еженедельник «Без проблем». 2007. № 45.
2. *Дорофеева Л. И.* Основы менеджмента. Саратов: Издательство Саратовского университета, 2011. 416 с.
3. *Морита А.* Сделано в Японии. Альпина Паблишер, 2007. 290 с.
4. Общественное мнение – 2012. М.: Левада-Центр, 2012. 232 с.
5. http://wciom.ru/zh/print_q.php?s_id=310&q_id=23992&date=07.10.2007.

6. http://www.levada.ru/archive/otsenki-sotsialnykh-problem-i-zanyatosti/chto-nuzhno-bylo-sdelat-v-pervuyu-ochered-dlya-togo.
7. *Ford H.* My Life and Work // http://www.gutenberg.org/cache/epub/7213/pg7213.html.

METHODOLOGY OF POLYMER FILAMENT MATERIAL PREPARATION FOR CLINICAL APPLICATIONS

G.P. Lyubun, N.O. Bessudnova

Saratov State University

INTRODUCTION:

In the present time the restoration or replacement of lost or damaged biological tissues and organs to ensure their normal functioning is a fundamental problem in modern reconstructive medicine and dentistry (F. F. Demarco, M. C. M. Conde, B. N. Cavalcanti and others, 2011). One of the most promising solutions to this problem is the development of the novel concepts and methodology of tissue engineering for synthesis of three-dimensional graft constructs that are equivalent to original organs and tissues in cellular composition, structure and function. This structural and functional compatibility can be achieved on the basis of ultra-thin polymer filament scaffold application.

The aim of the study is to compare different methods of polymer filament material preparation using scanning electron microscopy (SEM).

MATERIAL AND METHODS:

Polycaprolactone (PCL) (70000-80000 Mn, "Sigma –Aldrich") was used in the present research.

Preparation of Electrospinning Solution: PCL solution was prepared by dissolving 9.4% PCL in a solvent mixture of dichloromethane and *N,N*-dimethylformamide (77:23 weight ratio) followed by constant stirring at room temperature for 5 hours to obtain a homogeneous spinning solution (C. R. Reed, L. Han, A. Andrady and others,2009).

Electrospinning: To fabricate nanofiber non-woven material, an experimental setup was designed, the scheme of which is shown in Figure 1.

The apparatus was placed in a glass chamber. The polymer solution was placed in a 10-ml syringe attached to a pump on a horizontal mount. An electrical potential was applied to the needle using a high voltage power supply. A clean, grounded aluminum cylinder was used as a collector screen. The viscous polymer was injected through the syringe, across a voltage potential, produc-

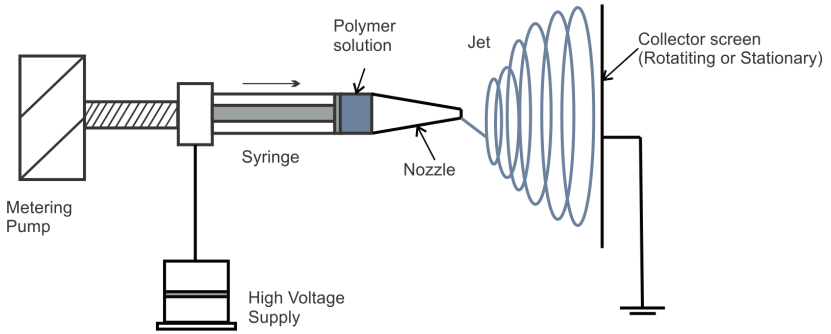

Fig. 1. Electrospinning apparatus.

ing a polymer jet that was directed toward a collector screen. Typical spinning parameters used in this study are listed in Table 1.

Table 1

Experimental parameters.

Solvent flow rate	0.5 ml/h
Voltage	17.6 kV
Working distance between the needle and collector screen	25.0 cm

Dehydration: Dehydration was performed in several ways using differently concentrated mixtures of ethanol/water, chemically pure acetone (Ralf Janda,1995) and sample exposure at high temperatures. High temperature influence on the stored specimens was studied using a dry-air sterilizer in different regimes. The samples of nanofiber non-woven material were exposed for 2 hours at temperatures, starting from 50ºC upto 59ºC.

SEM investigations: A scanning electron microscope Mira\\LMU, "Tescan" was selected to generate images of surface morphology of PCL samples. All images were produced in the regime of secondary electron detection. The samples were coated with gold in argon atmosphere to reduce sample charging.

RESULTS:

Influence of ethanol/water percentage that had been used in the process of sample dehydration did not show noticeable changes in surface morphology as shown in Fig. 2.

By the same token, the sample immersion into acetone for 20 minutes did not change surface morphology of nano-fiber filaments (see Fig. 3).

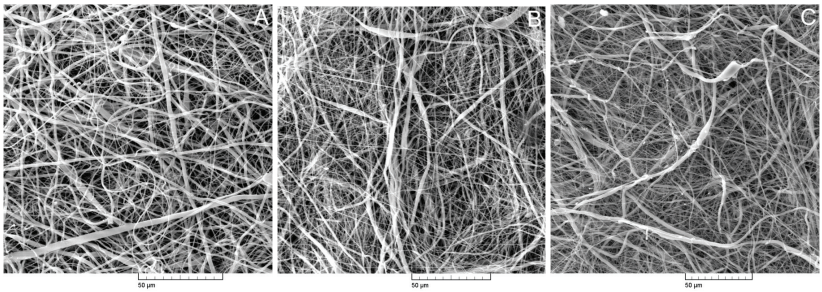

Fig. 2. SEM images of sample surface morphology at differently concentrated mixtures of ethanol/water; (A) –40%, (B) – 70%, (C) – 96%

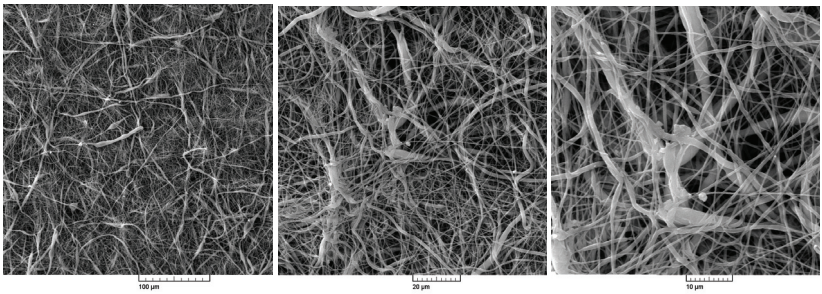

Fig. 3. SEM images of surface morphology of PCL immersed in acetone

Increase in temperature in the range of 55ºC to 58ºC resulted in the modification of the fiber structure, in particular, swirl fiber area formation. Further increase in temperature revealed fiber melting (see Fig. 4).

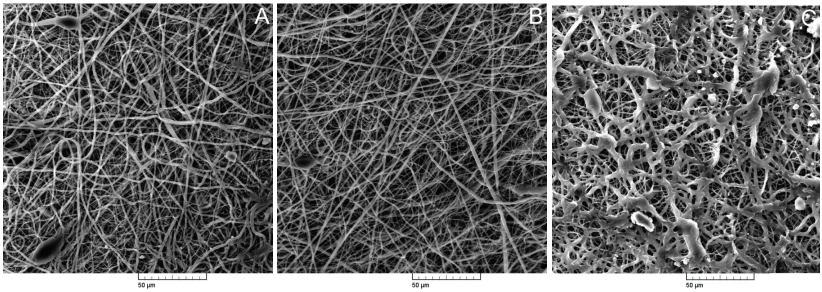

Fig. 4. SEM images of PCL surface morphology at different temperatures: (A) – 55ºC, (B) – 58ºC, (C) – 59ºC

CONCLUSION:

The treatment of fiber samples using chemically pure acetone and mixtures of ethanol/water has shown no significant changes in surface morphology of the samples. Consequently, ethanol could be applied as an agent for nanofilament scaffold sterilization without changes in their morphology before cell seeding.

The high temperature impact has resulted in the modification of the fiber structure. Nano-fibers are curving right round, crossing themselves. The observed phenomena of filament looping may be used to control the fiber structure and nanofibrous material porosity.

To sum it up, research findings point to the possibility to use a variety of methods in PCL scaffold preparation for further clinical research.

REFERENCES:

1. *F. F. Demarco, M. C. M. Conde, B. N. Cavalcanti, L. Casagrande, V. T. Sakai, J. E. Nör* Dental Pulp Tissue Engineering // Braz Dent J. 2011. Vol. 22, № 1. P. 3–14.
2. *R. Janda* Preparation of extracted natural human teeth for SEM investigations // Biomaterials. 1995. Vol. 16, № 3. P. 209 – 217.
3. *C. R. Reed, L. Han, A. Andrady, M. Caballero, M. C. Jack, J. B. Collins, S. C. Saba, E. G. Loboa, B. A. Cairns, J.A. van Aalst* Composite Tissue Engineering on Polycaprolactone Nanofiber Scaffolds // Annals of Plastic Surgery. 2009. Vol. 62, № 5. P. 505–512.

DEVELOPMENT OF OLIGOPOLISTIC MARKET IN RUSSIA

N.N. Mamedova

Saratov State University

The influence of oligopolistic market on the country's economy. Russian oligopolies. Perspectives of Russian oligopolistic market and measures to be taken to enhance its quality.

Currently, concentration of production has grown beyond branch-wise and regional limits, and developed into an aggregation whereby production output and financial assets centralize in hands of decreasing number of oligopolies. The economic power of oligopolists gets consolidated and their impact on the country development gradually rises. At the same time, they are the major sources of taxes, investments and economic growth. Economic security of Russia depends to a large extent on the financial stability of oligopolists.

The word “oligopoly” was derived from the Greek language and introduced into European vocabulary by the English humanist and statesman Thomas More (1478–1535) in his world-known novel “Utopia” published in 1516. An oligopoly is a type of market structure of imperfect competition in which very few firms dominate. Decision of each firm influences market situation and at the same time depends on decisions of other firms: making a decision a firm takes into consideration any possible reaction of other market participants. Interdependence of firms and forecasting the complexity of competitors’ actions are distinguishing features of oligopoly. In this connection oligopolistic prices change very rarely, i.e. there happen to be “sticky” prices which are beneficial for oligopolists. If there is a change of price, then all producers do it simultaneously, in one direction and by the same value.

Historically, Russian industry developed first of all as a large-scale industry. Such situation emerged as far back as in tsarist Russia, rapidly increased in Soviet economics due to the bias favorable to giant plants, and was inherited by modern Russia. Currently, competitive relations have been formed in several industries. At the same time, there are monopolized sectors and sectors with oligopolistic structure. Many contemporary Russian oligopolies act at the market as “heirs” of Soviet large enterprises which used to consist of the main plant and several co-operating or supporting plants. For modern Russia the concentration of property in hands of several principal “players” is a common phenomenon. Raw material industries, iron and nonferrous-metal industries have a distinctly oligopolistic character in Russia. Thus, more than 80% of industrial output of ferrous metallurgy of Russia is the share of 9 large companies: “YevrazHolding”, “Severstal”, “Novolipetsky Integrated Iron-and-steel Works”, “Magnitogorsk Integrated Iron-and-steel Works”, “Managing Company Metalloinvest”, “Mechel”, “Tube Iron and Steel Company”, “United Iron and Steel Company”, “Chelyabinsk Tube-rolling Mill Group”. In 2008 Russia ranked fourth in the world in steelmaking (72 million tones per year) (Fig.1).

Several oil companies produce oil, the largest of them as of 2007 were Public Corporation “Rosneft”, Public Corporation “Lukoil” and Public Corporation “TNK-VR” (Table 1).

The main sub-branches of chemical industry (fertilizer manufacturing and others) and machinery-producing industry (car manufacturing, aerospace industry and others) are oligopolized. Large enterprises, which definitely give tone to the market, form the basis of modern Russian economics. Thus, the car market in Russia is one of the vivid examples of oligopolies. The leaders of the branch are AvtoVAZ (545450 motor vehicles – 2010), KAMAZ (45189 mo-

tor vehicles – 2011) and GAZ (82000 motor vehicles, 11000 heavy vehicles "URAL", and more than 10000 buses – 2010).

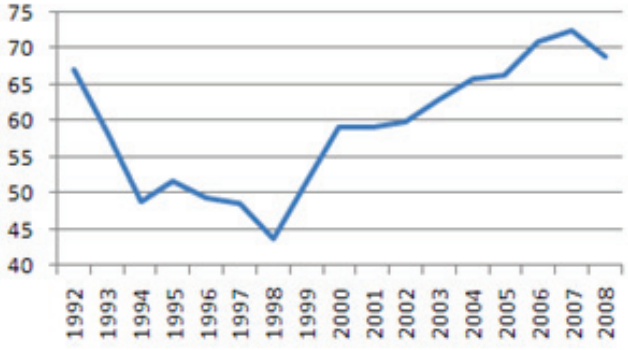

Fig. 1 "Steelmaking in Russia in 1992-2008", million tones.[1]

Table 1

"Petroleum industry of Russia"[2]

Oil company	Net profit, milliard dollars				
	2006	2007	4th quarter of 2007 – 3rd quarter of 2008	2009	2010
Rosneft	3,5	12,9	13,3	6,5	10,4
Lukoil	7,5	9,5	13,0	7,0	9,0
TNK-VR	6,4	5,7	8,3	5,2	5,8
Surgutneftegaz	2,8	3,5	6,3	3,7	-
Gazprom neft	3,7	4,1	5,9	3,0	3,1
Tatneft	1,1	1,7	1,9	1,7	1,5
Slavneft	1,2	0,7	0,5	0,1	-
Bashneneft	0,3	0,4	0,5	0,5	-
Total for TOP-8	26,5	38,5	49,7		

However, Russian oligopolists are rather weak compared with foreign companies with the similar turnover. The output per worker in the leading oil producing company "Lukoil" is 3.6 times lower than Brazilian Petrobras. The output capacity of Russian "Severstal" is 3.5 times less than the output capacity of Chinese Shanghai Baosteel Group Corporation, 4 times less than the output capacity of Brazilian Gerdau and more than 20 times less than the out-

[1] See: On the status and prospects of the steel industry in the Russian Federation// Website of Prime Minister of Russia 24th of July 2008.

[2] See: Petroleum industry of Russia (http://ru.wikipedia.org/).

put capacity of Japanese Nippon Steel. As for chemical industry, "Uralkaly" is 24 times less productive than Saudi company SABIC. The Russian leader of car manufacturing "AvtoVAZ" is 7 times inferior to the Indian car manufacturing corporation Mahindra&Mahindra.

In the near future, the turnout of rival products on the base of increase of technical level of production and adoption of novel and high technologies should be the main aim of innovative development of Russian oligopolies. As in the near future Russian economics will preserve the raw-material orientation, oligopolists should promptly develop raw-material field and key branches on the innovative basis. We should highlight some major development vectors of these spheres (coalmining, metallurgical, chemical and machinery-producing):

- adoption of modern cutting-edge technologies for coal and complex ores deep conversion;
- modernization of electric furnace steelmaking of iron and steel works; it will provide the output of products meeting the requirements of international standards;
- implementation of modern technologies for high-purity ferrosilicon brands production; it will enable the production of transformer and dynamo steel, steel wire cord;
- launching of new energy-efficient technologies.

There is no doubt that state support is necessary for preserving oligopolistic companies forming the major part of the Gross Domestic Product and the consolidated budget. At the same time, we should distinguish state interests and interests of oligopolistic structures. The above presented measures will help to save the largest oligopolistic companies of the country and avoid infringing national interests.

REFERENCES:

1. *Вечканов Г. С., Вечканова Г. Р.* Микроэкономика: Учебник. – СПб., 2008. 288 с.
2. *Гальперин В. М., Игнатьев С. М., Моргунов В. И.* Микроэкономика: Учебник. В 2-х т. – СПб., 2004. Т. 2. 486 с.
3. *Макконнелл К., Брю С.* Экономика. – М., 1993. 983 с.
4. АвтоВАЗ (http://www.autostat.ru/news/view/12871/).
5. Автомобильная промышленность России (http://www.minpromtorg.gov.ru/ministry/strategic/sectoral/10)
6. *Прокопов Б. И.* Влияние олигополистических структур на развитие национальной экономики (региональный аспект) // Проблемы современной экономики. 2009. № 1 (29). С. 40-43.

TRANSPORTATION OF OIL AND OIL PRODUCTS

A.I. Motyash

Zhangir Khan West-Kazakhstan Agrarian-Technical University

Oil – natural oily flammable liquid consisting of a complex mixture of hydrocarbons and other organic compounds. As a result of a chemical process – distillation, we have oil products – a mixture of hydrocarbons, and also individual chemical compounds, which include different types of fuel (petrol, diesel, kerosene, etc.), lubricants, electrical protection, solvents, petrochemical raw materials.

In the process of extraction, purification, delivery to refineries and processing, oil and its derivatives are a large number of stages, with the result that consumers are able to receive the necessary petroleum in necessary quantity.

With increasing of oil production in the oil fields, increasing the volume of its transportation, improved delivery methods. For a long time it was done very primitive way, with the caravan. Wooden barrels and skins filled with oil or kerosene, loaded on wagons and thus brought to the place. Or on the water – in oak, and later steel drums. This method of transportation was very expensive, the cost of oil was too high.

At present, for non-piped transportation of oil and oil products use all kinds of trucks. Oil, gas and their derivatives are highly toxic, explosive and flammable substances, because of their packaging, transportation and storage are regulated by specific standards. In particular, well-defined types of containers approved for storage and transportation of petroleum products, the methods of the pouring, the methods of marking and safety in transportation. Transport and packaging in compliance to the rules – a prerequisite for obtaining a permit for transportation of petroleum products. So for different types of fuel and other light petroleum products allow the carriage in drums and cans with the maximum volume of pouring 95% of the total capacity. For «viscous» oil products – oils, lubricants, bitumen, allowed the use of polymer and glass containers, no limit on the amount required. Some viscous oil products – such as bitumen – may require heating in the draining, other substances – the facilities in the form of lower drain devices or insulating protective layer. Because virtually every oil product have specialized containers, rail and road tank which fully complies with safety and practicality.

Each mode of transportation has its own advantages and disadvantages. The fastest way to the air is very expensive, require special security meas-

ures, because this method of delivery are rare – in cases of emergency or inability to deliver fuel by other means. For example, for military purposes, or in cases of actual inaccessible of terrain for the other, except for air transport modes.

In the more extent is common the railway. Geography of railway oil transportation from places of extraction to refineries, to storage or to consumers, is tied to the so-called oil and gas basins. Despite the convenience of railway transportation of oil products over long distances, the oil products – such as gasoline, diesel fuel or liquefied gas – is optimal to deliver by truck to a short distance to the place of selling. Transportation of fuel in this manner significantly increases its value in use. Profitability of trucking is limited the distance of 300-400 kilometers, which determines their local character – from the depot to the station and back.

The cheapest and most environmentally friendly way to transport oil are pipelines. Oil in them is moving at a speed of 3 m / s under the influence of pressure difference created by the pumping stations. They are placed at intervals of 70-150 kilometers, depending on the road relief. At a distance of 10-30 kilometers in pipes placed bolts, which able to block off some parts in the accident. The inner diameter of the pipe, usually ranges from 100 to 1400 mm. They are made from high-plastic steel, capable of withstanding thermal, mechanical and chemical effects. Gradually take on more and more popular pipelines made of reinforced plastic. They do not corrode and have a virtually unlimited service life.

Oil pipelines are underground and surface. Both types have their advantages. Onshore pipelines easier to build and maintain. In the event of an accident is much easier to detect and repair damage to the pipe, held above the ground. At the same time, underground pipelines are less affected by changes in weather conditions, which is especially important for Kazakhstan, where the difference between winter and summer temperatures in some regions, has no analogues in the world. Pipes can be made and on the bottom of the sea, but because it is technically difficult and expensive, large spaces oil intersect with tankers, but offshore pipelines often used for oil transportation within a single oil-producing complex.

There are three types of pipelines. The field data pipelines, as the name implies, connects well with the objects in the field. Interfield lead from one field to another, to the main pipeline, or just far located the industrial facility, located outside the initial oil production complex. The main oil pipelines are laid to deliver oil from the fields to the handling and to the places of consumption, to which, inter alia, include tank farms, oil terminals, refineries. Since the

application of pipeline cost effective and they work in any weather and at any time of year, it is a means of oil transporting is really indispensable.

Nevertheless, the bulk of international oil traffic is carried tankers. Convenient transport for oil and fuel transportation are the sea and river tankers. River oil transportation, compared with railway, reduce costs by 10-15%, and by 40% in comparison with the car.

Small tonnage tankers used for special purposes – including to transport bitumen; tankers of general-purpose which having deadweight (total weight of goods, which vessel can takes) at 16 500-24 999 tons, used for the transport the oil products; middle tonnage tankers (25 000-44 999 tons) – for deliver oil and it's products. Large tonnage tankers are considered more than 45, 000 tons, and they account for a greater burden on the transportation of oil by sea. For oil transportation by river arteries using barges deadweight 2000 – 5000 tons.

Oil and petroleum products are loaded into tankers from the shore and unloading is performed by using ships pumps and pipes, that constructed along the deck. However supertankers deadweight of more than 250,000 tons, as a rule, simply cannot enter the port, when fully loading. They are filled from sea platforms and unloading, pumping the liquid contents to smaller tankers.

Today over 4,000 tankers are float the seas and oceans of the world. Most of them are owned by independent shipping companies. Oil corporations conclude the treaty with them, getting right to the using of the vessel.

Conditions of safe transportation of oil products.

To date, the producers of container for oil products are produced a wide range of rail and road tankers, metal and polymeric containers of different sizes. Cans produced by volume from 5 to 50 liters, barrels from 48 to 250 liters. The most widely used metal containers, but in recent years have increasingly used containers created from advanced polymer materials. Modernization of material and technical base carriers of oil products, using of modern materials for manufacture of container, the improvement of safety rules – it's a prerequisite of the successful development of the industry. But despite the constant tightening of security, transportation of oil products is damaging to the environment. Representatives of international environmental protection organizations believe that the measures taken to date to protect the environment from oil pollution is not enough. Especially dangerous sea and river tankers. Therefore necessary measures such as the removal from service of obsolete and single hull vessels, the development of a clear plan to eliminate oil contamination.

High security requirements forcing the carrying oil companies to modernize material and technical base. The introduction of new modern models

of tanks, containers, equipped with control systems of pressure, temperature, humidity and other parameters require large material investments. That is why in conditions of market, large companies are competitive, if they work on a full cycle. This means that the company itself produces, processes, stores and transports the oil products.

Oil and gas industry is fast becoming an extremely high-tech manufacturing. Although stands out a group of countries, where the observance of environmental norms are often overlooked, in the whole production and transportation of petroleum products are safer. The growth rate of consumption, the discovery of new oil and gas directly lead to the improvement of existing and creation of new forms of transport.

REFERENCES:

1. *Vasil'ev G. G., Korobkov G. E., Korshak A. A.* Pipeline transport of oil.
2. *Konnova G. V.* Equipment of transportation and storage of oil and gas.
3. *Aliev R. A., Beloysov V. D., Nemudrov A. G.* Pipeline transportation of oil and gas.
4. *Vilkovan A. I., Venculis L. S., Zaicev V. M., Filatov V. D.* Modern methods and means of dealing with oil spills.

MALWARE SPREADING IN THE DIRECT CONNECT NETWORK BY THE ENGLISH-SPEAKING COUNTRIES

M.I. Piunov

SARATOV STATE UNIVERSITY

Among the crimes in the computer information area unlawful acts connected with the malware spreading in peer-to-peer (P2P) networks have become more common. P2P networks have been threatening computer users after P2P-Worms were developed. Worm files had names attractive for users and located themselves among other harmless files. Moreover, the total quantity of those P2P-Worms among other harmless files was small. By 2010 the number of infections through P2P networks had been placed second after the attacks through Internet browsers (Гостев, 2010). Recently hackers have used P2P networks more intensively to spread different Trojans. Special nodes, called Trojan nodes, contain thousands of different malware. Such nodes have become the most widespread in one of the most popular P2P networks in the CIS, which is based on the Direct Connect technology.

Our research was conducted with the help of a specially created program, called *Direct Connect Network Scanner*, known as *Easy DC++ Scanner* (Юрин И. Ю., Пиунов М. И., 2012). 1435 Trojan nodes with different names were detected within the period from the 4th of November 2012 to the 25th of February 2013. It was found that these nodes spread more then 29 620 900 different files which are malware or contain malware with the total volume more then 16Tb.

We calculated that more than a quarter of nodes (27%) are located in such English-speaking countries as the United States, the United Kingdom, Canada, Australia, New Zealand. The leaders among them are the United States and the United Kingdom – 53% and 35% of distributors correspondingly. These countries spread a third of all malware in the Russian-speaking segment of the Direct Connect network. We estimated that 51% of these files are spread as RAR or ZIP archives. The size of the malware samples varies quite widely: from 5Kb to 10Mb. In most cases RAR or ZIP archives have size of 250Kb – 1Mb, while executable files have the size of 100-250Kb or 0.5-1Mb.

Our research showed that in order to attract attention and deceive search engines these files are always given names familiar to users and even have appropriate icons, for example:

– films such as *Clash of the Titans, Faster, Jane Eyre*;

– operating systems such as *Windows XP SP3, Windows Server 2008 R2 Black Edition x64, Windows Se7en XP Black Edition (2010)*;

– software such as *Microsoft Office 2010 Professional Plus, Adobe Photoshop CS5 Extended 12.0, Adobe Captivate 5.0*;

– music such as *Rihanna – Discography, 50 Cent – Gettin Money, ABBA – Greatest Hits*;

– games such as *Gran Turismo 4, Gears of War, Assassins Creed II*;

– books such as *C and C++ ebooks, E-Books for Delhi University Under Graduate Students in Computers.*

To generate a large number of spreading files different methods are used. The easiest way is renaming. However, the files obtained in this way do not differ from each other by size and the Tiger Tree Hash (TTH). To generate files different by TTH and by size random length bytes sequences are appended to their overlay. Sometimes the files can be archived with outside files.

It was shown that in 51% of cases antivirus was unable to detect harmful files from Trojans nodes. Most of these files were created with the use of code encryption, MSIL or AutoIt technology, which causes difficulties for the analysis. From time to time the files on Trojan nodes are replaced to avoid their banning. The files found during our research belong to the following catego-

ries according to Kaspersky Laboratory classification: Backdoor, HackTool, Trojan, Trojan-Downloader, Trojan-Dropper, Trojan-FakeAV, Trojan-Ransom, Virus, Worm. We found that the greatest numbers of files are from the following families:

– Backdoor.Win32.DarkKomet – 20% of files;
– Trojan.Win32.Llac – 13% of files;
– Trojan-Ransom.Win32.Foreign – 9% of files;
– Trojan-Downloader.Win32.Bagle – 6% of files;
– Trojan.Win32.Jorik – 5% of files.

Most of this Trojans have a destructive impact on computers or aim to force people pay money. For example, Trojan.Win32.Jorik has been created to attack a Russian on-line bank system; Backdoor.Win32.SpyAll is a Trojan-Banker which steals confidential information from banks, financial institutions and payment systems (Backdoor.Win32.SpyAll.a, 2010).

Types of threats which are being spread by some English-speaking countries are given in Table 1, where the threats are grouped according to the country-distributor and their occurrence. The table shows, that different countries spread different malware.

Table 1

Threats by English-speaking countries

Country-distributor	Types of threats	Occurrence (%)
United States	Backdoor.Win32.DarkKomet	30
	Trojan.Win32.Llac	9
	Trojan-Downloader.Win32.Bagle	7
	Backdoor.Win32.SpyAll	5
	Trojan-Ransom.Win32.Foreign	4
	Trojan-Downloader.Win32.Kuluoz	3
	Worm.Win32.VBNA	3
	Worm.Win32.Bybz	3
United Kingdom	Trojan-Ransom.Win32.Foreign	18
	Backdoor.Win32.DarkKomet	16
	Trojan.Win32.Llac	10
	Trojan.Win32.Jorik	10
	Worm.Win32.VBNA	5

End table 1

Country-distributor	Types of threats	Occurrence (%)
Canada	Backdoor.Win32.VB	18
	Trojan-Downloader.Win32.Andromeda	18
	Trojan.Win32.Jorik	9
	Trojan-FakeAV.Win32.Windef	9
	Virus.Win32.Sality	9
Australia	Trojan.Win32.Llac	75
	Backdoor.Win32.DarkKomet	25

Thus, our research showed that the problem of malware spreading in Direct Connect Network has always been of the greatest importance. The greatest number of the Trojan nodes and files which are being spread by them demonstrates insufficiency of present countermeasures. During our study, we detected and analyzed files unknown to modern antivirus programs. One more problem is imperfection of antivirus detection algorithms. On the one hand, distributors try to attract users, using techniques of social engineering, and on the other hand they try to bypass antivirus protection.

REFERENCES:

1. *Юрин И. Ю., Пиунов М. И.* Выявление троянских узлов в пиринговой сети Direct Connect // Криминалистические чтения, посвященные памяти заслуженного юриста Республики Беларусь, доктора юридических наук, профессора Г. И. Грамовича: материалы Междунар. науч. – практ. конф. / Под ред. В. Б. Шабанова [и др.]. Минск: Акад. МВД, 2012. С. 378–379;
2. *Гостев А.* Kaspersky Security Bulletin 2010. Развитие угроз в 2010 году [on-line resource]. – URL: http://www.securelist.com/ru/analysis/208050677/Kaspersky_Security_Bulletin_2010_Razvitie_ugroz_v_2010_godu (request date: 30.01.13);
3. Backdoor.Win32.SpyAll.a // SecureList [on-line resource]. – URL: http://www.securelist.com/en/descriptions/7966625/Backdoor.Win32.SpyAll.a (request date: 10.02.13).

BEER-LAMBER LAW IN PHOTONIC CRYSTALS SPECTROSCOPIC STUDY

A.S. Plastun, A.I. Konukhov

Saratov State University

Non-Dispersing Infrared Spectroscopy (NDIR) is widely used for gas and liquid media detection (Wei-Cheng Lai, 2011). Photonic crystals with defect of periodical structure can be used as optical filter for NDIR-spectroscopy. Due to the long effective length of the radiation propagation in photonic crystal fiber (PCF) sensor sensitivity can be improved (Yu. S. Skibina, 2011). But integral transmittance coefficient of the PCF can widely vary from its value, predicted by Beer-Lamber Law. This law is used for transparent media transmittance calculation and is used in transparent media spectroscopy. But in case of PCF this law cannot be properly applied due to the geometry of the fiber. Light passes through core of the fiber and cladding. Then different beams begin to interfere with each other, so light, passed through such structure can be considered as a superposition of different beams. In such situation Beer-Lamber Law cannot be applied to whole structure, only for modes of the central core. This situation exists due to the modal properties of the PCF. For guided modes of the PCF effective propagation length can exceed fiber length (Sneider, 1987).

In our work PCF transmission was calculated by using biortiogonal modes field decomposition. Equations for PCF modes (Joannopulos J.D, 2008).

$$\begin{aligned}\nabla_{\perp}^2 H_x + k_0^2 n^2(x,y) H_x + \frac{\partial \ln n^2}{\partial y}\left(\frac{\partial H_x}{\partial y} - \frac{\partial H_y}{\partial x}\right) = \beta^2 H_x(x,y),\\ \nabla_{\perp}^2 H_y + k_0^2 n^2(x,y) H_y + \frac{\partial \ln n^2}{\partial x}\left(\frac{\partial H_y}{\partial x} - \frac{\partial H_x}{\partial y}\right) = \beta^2 H_y(x,y)\end{aligned} \quad (1)$$

where H_x, H_y – transverse components of magnetic field vector, n refractive index, β – mode propagation constant (tangential component of the wave vector), $n\ (x,y)$ –complex refractive index. The values H_x, H_y, n^2, $\ln n^2$ are expanded in Fourier series. The result is a matrix form eigenfunctions and eigenvalues problem of β^2 value. Then we introduce right and left eigtnvectors.

$$\begin{aligned}\mathbf{M} \cdot \vec{r}_i &= \beta^2 r_i\\ \vec{v}_j \cdot \mathbf{M} &= \beta^2 \vec{v}_j\end{aligned} \quad (2)$$

where $\mathbf{r}_l$,$\mathbf{r}_r$ _ right and left vectors, containing Fourier components of H_x, H_y fields. **V** and **r** vectors are biortogonal, which allows us to expand inner field of the PCF using biortogonal conditions.

On fig. 1 PCF characteristics and supercell shape are shown.

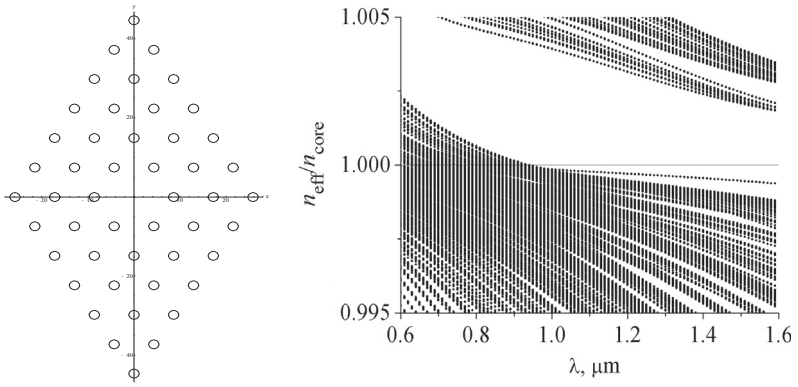

a *b*

Fig.1. (a) Cross section of the PCF. (б) effective refractive index $n_{eff}=\beta/k$ depending on the wavelength λ, n_{core} – refractive index of the core

For the PCF transmittance calculation Gaussian beam expansion in eigenvectors **r** (2) (PCF modes) was used. Fig.2 shows Pointnig vector cross distribution after Gaussian beam propagation through 1 meter length PCF.

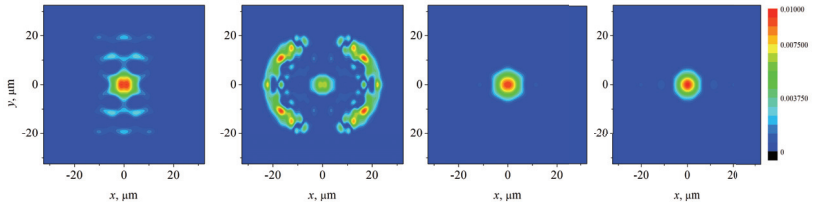

Fig.2. Different wavelength intensity profiles. Left to right– 0,67 μm, 0,82, μm, 1,3 μm, 1,55 μm. Input field is flat wavefront Gaussian beam with constriction radius ω_0 = 8 μm.

The used method can be applied for fiber transmission (Fig. 3). In photonic crystal bandgap area λ> 1,1 μm. PCF transmission coefficient approaches the core transmission coefficient. This situation occurs due to the excitation of the core fundamental mode. The proposed method calculates the transmission of a single-mode and multimode PCF with the vector nature of the guided

modes field consideration. In practical application, this method of calculating PCF modes and light propagation can be used in spectroscopy applications and gas or liquid media sensors development. In this case it is used for media cell designing.

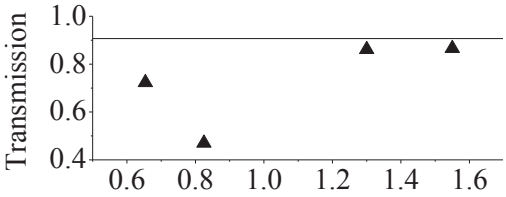

Fig. 3. Transmission coefficient for 1 meter lenth glass (solid line) and 1 meter length PCF (form ig.1) – triangles.

REFERENCES:

1. Photonic crystal slot waveguide absorption spectrometer for on-chip nearinfrared spectroscopy of xylene in water, Wei-Cheng Lai et. al., Appl. Phys. Lett. 98, 023304 (2011);
2. *Снайдер А., Лав Д.* Теория оптических волноводов. М.: Радио и связь, 1987
3. *Joannopulos J. D.* et. al., Photonic Crystals. Molding the Flow of Ligh, Princeton Univ. Press, 2008, 305.
4. *Yu. S. Skibina et al*., Photonic crystal fibres in biomedical investigations, *Quantum Electronics* 41 (4) 284 – 301 (2011)

THE AMOUNT OF FLAVONOIDS IN STONECROPS (*SEDUM MAXIMUM* (L.) HOFFM.) AND PURPLE STONECROP (*SEDUM TELEPHIUM* L.)

V.O. Plastun, N.A. Durnova

Saratov State Medical University

INRODUCTION:

Medical plants based preparations are increasing their importancy in modern medicine. In this case, both finding new medical plants and development of active components receiving are actual and important goals. We chose two species of stonecrop (*Sedum telephium* L. and *Sedum maximum* (L.) Hoffm.) as our subjects of research. These plants have wide spectrum of

biological effects: tonic, wound healing, antioxidant etc. (Бабенко В. С. 1964, Запрометов М. Н. 1993, Кит С. М., Годун В. М. 1964). Main active components of the stonecrop are flavonoids (Краснов Е. А., Саратиков А. С., Суров Ю. П., 1979).

Main goal of our work was determining percentage of flavonoids amount in different parts of the plant. Materials and methods. Shredded stems with leaves, buds and flowers were used as a research plant material. During the development of the extraction procedure of flavonoids from stonecrop herb we studied the effect of different technological parameters on the flavonoids output: the concentration of the extractant, the ratio of raw materials and extractive solvent and the extraction time. Ethanol was used as an extractant. The main criterion for selection was the flavonoids amount in terms of rutin and of dry raw materials.

Flavonoids concentration determination in the obtained extract is determined spectrophotometrically using a complexation reaction with aluminum chloride. RSO routine was used as a measurement standard. Optimal method of extracting flavonoids from purple stonecrops has been described more detailed previously (Пластун В. О., Дурнова Н. А., 2011).

RESULTS AND DISCUSSION:

We compared the content of flavonoids in different parts of the large and purple stonecrop using our developed techniques.

The results of the research are presented in the Table 1.

Table 1

The amount of flavonoids in different parts of large and purple stonecrops

Specimen	Plant part	Flavonoid amount, %
Large stonecrop	inflorescences	2,97
	leaves	2,21
	stems	2,07
Purple stonecrop	inflorescences	3,55
	leaves	1,53
	stems	0,63

According to the study, the average amount of flavonoids in the large stonecrop is 2.4%, while in purple stonecrop – only 1.9%. Nevertheless, the distribution of flavonoids in various organs of these two types stonecrops is not the samey. In purple stonecrop the main amount of flavonoids is concentrated

in inflorescences and makes 3.55%, the difference between the content of the flavonoids in inflorescences and stems of the purple stonecrop is more than 5 times. Flavonoids in large stonecrop are distributed uniformly in overground part. The maximum amount of flavonoids in large stonecrop is also found in the inflorescences (2.93%), but it is slightly higher than the minimum amount (1.5 times).

CONCLUSIONS:

The amount of flavonoids in the large stonecrop is 2.4%, in purple stonecrop – 1.9%. The bulk of the purple stonecrop flavonoids is concentrated in the inflorescences, and in the large stonecrop they are distributed uniformly over the overground part.

Stonecrop species have wide spectrum of medical use due to the high amount of flavonoids and other biological active compounds. The extracts obtained by this method, can be used in further analysis of their biological activity as well as for quality assessment of medicinal plant materials.

REFERENCES:

1. *Бабенко В. С.* Новые источники лекарственного сырья для получения тканевых препаратов // Изучение и использование растительных ресурсов СССР. – Л., 1964. С. 311–314.
2. *Запрометов М. Н.* Фенольные соединения. – М.: Наука, 1993. 270 с.
3. *Кит С. М., Годун В. М.* Изучение антимикробных свойств некоторых растений // Фитонциды в народном хозяйстве. – К., 1964. С. 16–129.
4. *Краснов Е. А., Саратиков А. С., Суров Ю. П.* Растения семейства толстянковые. – Томск, 1979. 208 с.
5. *Пластун В. О., Дурнова Н. А.* Методика экстракции флавоноидов очитка пурпурного *Sedum telephium* L. // Традиции и инновации фармацевтической науки и практики / Материалы Всероссийской научно-практической конференции с международным участием, посвященной 45-летию фармацевтического факультета КГМУ, 2011, С. 330-332.

ANALYSIS OF ELECTRONIC STRUCTURE OF SEVERAL AROMATIC MONOKETONES

M.V. Pozharov

Saratov State University

INTRODUCTION:

Today, lanthanides and their compounds find many application in various fields of science and technology such as metal glass (Yu H. B., Yu P., Bai H.Y, 2008) and ceramic material enhancement (Qiu Guanming, Li Xikun, Qiu Tai et al, 2007) and toluene nitration catalysis (Parac-Vogt T. N., Deleersnyder K. and Binnemans K, 2004). However, one of their most prominent uses is luminescent material production. For the past decade, synthesis and study of luminescent characteristics of lanthanide organic compounds remains a relevant problem (Freidzon A. Ya, Scherbinin A. V., Bagaturyants A. A., Alfimov M. V., 2011; Hao Liang, Fang Xie, 2009; Tsaryuk V., Zhuravlev K., Zolin V. et al., 2006; Juan-Fen Wang, Fan-Tao Meng, Su-Ling Xu et al., 2011).

As almost all lanthanides (except for lanthanum) have 4f-electrons which are screened by 5s-electrons, their luminescence spectra consists of several thin spectral bands unique for each lanthanide ion. However, f-f electron transfers in pure ions are parity-forbidden and, thus, have low intensity. But if lanthanide ion is coupled with organic ligands included into host material of organic light-emitting diode (OLED), f-f electron transfers become enabled due to disruption of ligand field symmetry and vibronic coupling effect (Freidzon A. Ya, Scherbinin A. V., Bagaturyants A. A., Alfimov M. V., 2011). In these compounds, intensity of central ion radiation can be boosted by non-radiative energy transfers from host material to ligands and then from ligands to the lanthanide. Both neutral molecules i.e. 1,10-phenantroline or 2,2'-bipyridyne (Freidzon A. Ya, Scherbinin A. V., Bagaturyants A. A., Alfimov M. V., 2011; Hao Liang, Fang Xie, 2009) and organic acid anions (Tsaryuk V., Zhuravlev K., Zolin V. et al., 2006; Juan-Fen Wang, Fan-Tao Meng, Su-Ling Xu et al., 2011) can be used as such ligands.

Aromatic monoketones (chalcones) are yet another group of substances that can be potentially used as electron donor ligands due to possible electron excess located on carbonyl oxygen. However, there is no theoritical or experimental research data concerning lanthanide-chalcone complex compounds. Theoritical study of geometry and electron structure of chalcone molecules can give an approximation of their potential electron-donor properties and

choose a substance most appropriate for luminescent lanthanide complex production.

Thus, we decided to study electron structure of several chalcones that were previously synthesized by scientists of Chair of Organic and Bioorganic Chemitsry. For convenience sake, the studied compounds can be divided in two groups: dibenzilidenecyclohexanone and its substituted compounds and 4-phenyl-3-buten-2-one and its substituted compounds. These compounds were chosen because their methods of synthesis has been thoroughly studied and can be produced with relatively high yield.

RESEARCH METHOD:

Geometry of studied compounds was calculated with the help of *Gamess Firefly v.7.1* (a quantum chemical software complex) with using B3PW91 potential and UHF-SBKJC basis set which can be used to optimize structure of molecules containing the rare earth metal atom (Freidzon A. Ya, Scherbinin A. V., Bagaturyants A. A., Alfimov M. V., 2011). Electron structure of studied compound was calculated by NBO module included in *Gamess Firefly v.7.1.* Structure of studied compounds is shown on Fig. 1.

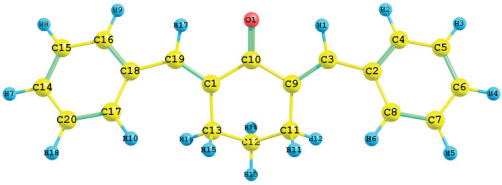

a

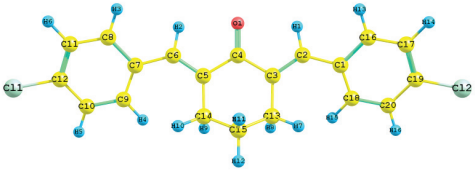

b

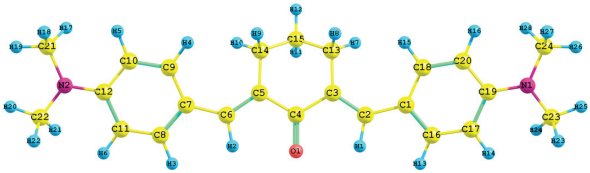

c

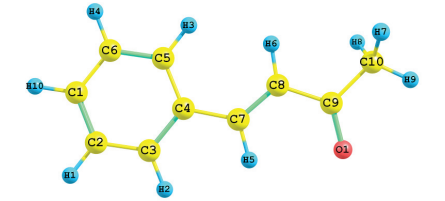

d

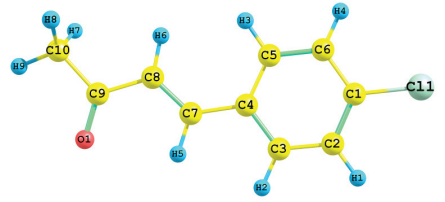

e

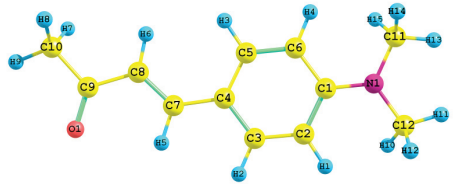

f

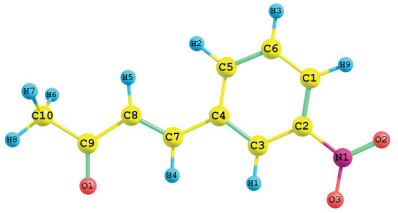

g

Fig. 1. Structure of studied compounds (a – 2,6-dibenzilidenecyclohexanone, b – 2,6-di (4-chlorobenzilidene) cyclohexanone, c -2,6-di (4-dimethylaminobenzilidene) cyclohexanone, d – 4-phenyl-3-butene-2-one, e – 4-(4-chlorophenyl)-3-butene-2-one, f – 4-(4-dimethylamino-phenyl)-3-butene-2-one, g – 4-(3-nitrophenyl)- butene-2-one

RESULTS AND DISCUSSION:

According to calculated data, dibenzilidenecyclohexanone and its substituted compounds have non-planar structure, i.e. benzene rings of benzilidene fragments deviate from cyclohexanone ring by 28–29° while carbon atoms C_{12} (Fig. 1a) and C_{15} (Fig. 1b) form a “chair conformation” (planar angle = 63–

64°). Electron density is mostly concentrated on oxygen which is supported by high negative charge value and general direction of dipole moment (shown as blue arrow on structure diagram). Addition of chlorine to benzilidene fragments leads to decrease of negative charge and dipole moment values and increase of C=O bond length. In the case of dimethylamino-substituent addition, C=O bond length also increases but negative charge and dipole moment increase as well (Table 1).

Table 1

Relevant parameters of geometry and electron structure of dibenzilidenecyclohexanone and its substituted compounds

Compounds	l (C=O_1), Å	μ, D	q (O_1)	E (LUMO), eV
2,5-dibenzilidene-cyclohexanone	1,241	3,32	-0,626	-2,51
2,5-di (4-chlorobenzilidene)-cyclohexanone	1,273	2,35	-0,609	-2,68
2,5-di (4-dimethylaminobenzilidene)-cyclohexanone	1,279	4,08	-0,650	-1,85

Unlike the previous group of chalcone, 4-phenyl-3-buten-2-one and its substituted compounds have mostly planar structure. The only deviations from it are caused by sp^3 hybridization of methyl groups. NBO analysis of these compounds have shown that in all cases electron density is concentrated on carbonyl oxygen (O_1) and carbon (C_{10}) vicinal to carbonyl carbon (C_9). Introduction of various substituents to benzene ring has almost effect on C_{10} atom charge and leads to slight changes of O_1 atom charge and decrease of C_1=O_9 bond. However, it should be noted that addition of substituent group significantly affected value and direction of dipole moments of the aforementioned compounds (Table 2).

Molecular donor-acceptor capabilities can be characterized by electron energy of lowest unoccupied molecular orbital (LUMO) (Костюков В. В., Мухина Ю. В., Евстигнеев М. П., 2009).. If E (LUMO) > 0, then electron presence on this orbital is energetically unfavorable and electron transferred to such orbital as a results of molecule excitation will try to leave it. Thus, molecules with E (LUMO) > 0 will act as electron acceptors. By contrast, if E (LUMO) < 0, then a "foreign" electron transferred to LUMO will remain there as it is energetically favorable, thus, such molecules will act as electron donors. As we could see from Tables 1 and 2, all studied compounds excluding 4-phenyl-3-buten-2-one can act as electron donor ligands while 4-(3-nitrophenyl)-3-buten-2-one has the best electron donor capacity

Table 2

Relevant parameters of geometry and electron structure of 4-phenyl-3-buten-2-one and its substitued compounds

Compounds	l (C_1=O_9), Å	q (O_1)	q (C_{10})	μ, D	E (LUMO), eV
4-phenyl-3-buten-2-one	1,265	-0,597	-0,663	3,95	-0,09
4-(4-chlorophenyl)-3-buten-2-one	1,234	-0,584	-0,663	2,39	-2,44
4-(3-nitrophenyl)-3-buten-2-one	1,233	-0,575	-0,664	6,26	-3,24
4-(4-dimethylaminophenyl)-3-buten-2-one	1,237	-0,602	-0,662	6,95	-1,74

CONCLUSION:

According to calculation data, 4-(3-nitrophenyl)-3-buten-2-one is the best choice for electron donor ligand as evidenced by lowest LUMO energy, high dipole moment, excess of electrons on both of nitro group oxygen atoms (O_2 and O_3) as well as narrowly located atoms O_1 and C_{10}.

2,5-dibenzilidenecyclohexanone, 2,5-di (4-chlorobenzilidene) cyclohexanone and 4-(4-chlorophenyl)-3-buten-2-one can also act as good electron donor ligands.

ACKNOWLEDGEMENTS:

The author thanks Zacharova T. V. and Mushtakova S. P. for their helpful advice.

REFERENCES:

1. *Костюков В. В., Мухина Ю. В., Евстигнеев М. П.* Методические указания к выполнению лабораторных работ по дисциплине «Моделирование биофизических систем /Севастополь: Изд-во СевНТУ, 2009. – 48 с.
2. *Freidzon A. Ya, Scherbinin A. V., Bagaturyants A. A., Alfimov M. V*. Ab Initio Study of Phosphorescent Emitters Based on Rare-Earth Complexes with Organic Ligands for Organic Electroluminescent Devices // The Journal of Physical Chemistry. A – 2011. Vol. 115. Issue 8. P. 4565–4573
3. *Hao Liang, Fang Xie* Optical investigation of Sm (III)-β-diketonate complexes with different neutral ligands // Spectrochimica Acta Part A: Molecular and Biomolecular Spectroscopy – 2009. Vol. 73, Issue 2, P. 309-312
4. *Juan-Fen Wang, Fan-Tao Meng, Su-Ling Xu et al.* Preparation, luminescence and thermal properties of lanthanide complexes with 2-chloro-4-fluorobenzoic acid // Thermochimica Acta – 2011. Vol. 521. Issues 1–2. P. 2–9
5. *Parac-Vogt T. N., Deleersnyder K. and Binnemans K.* Lanthanide (III) complexes of aromatic sulfonic acids as catalysts for the nitration of toluene// Journal of Alloys and Compounds – 2004, Volume 374, Issues 1–2, P. 46–49

6. *Qiu Guanming, Li Xikun, Qiu Tai et al* Application of Rare Earths in Advanced Ceramic Materials // Journal of rare earths – 2007, Vol.25, P.281
7. *Tsaryuk V., Zhuravlev K., Zolin V. et al.* Regulation of excitation and luminescence efficiencies of europium and terbium benzoates and 8-oxyquinolinates by modification of ligands // Journal of Photochemistry and Photobiology A: Chemistry – 2006, Volume 177, Issues 2–3, 314–323
8. *Yu H. B., Yu P., Bai H. Y.* Lutetium and thulium based rare earth bulk metallic glasses // Journal of Non-Crystalline Solids – 2008, Issue 354, P. 4539–4542
9. NBO 5.G. E. D. Glendening, J. K. Badenhoop, A. E. Reed, J. E. Carpenter, J. A. Bohmann, C. M. Morales, and F. Weinhold (Theoretical Chemistry Institute, University of Wisconsin, Madison, WI, 2004); http://www.chem.wisc.edu/~nbo5)

EVOLVING ROLE OF STANDARDS IN TRANSPORTATION SYSTEM

N.E. Savelyeva

Zhangir Khan West Kazakhstan Agrarian-Technical University

"If you think of standardization as the best that you know today, but which is to be improved tomorrow; you get somewhere."
Henry Ford (1863–1947)

Standards are critical to achieving a satisfactory transportation infrastructure (both vehicle and roadway) and have shaped the direction of the transportation industry since its inception. The purposes for standards remain much the same as they have been for close to a century, but the level at which they are specified and the organizations involved in their development have changed. Government mandating of standards is increasingly being replaced by governmental support of industry-developed standards. The globalization of the transportation industry has also affected the outlook on standards, and thereby our approach to their development and enforcement. The standards process, content, and outlook continue to evolve as the transportation industry and traveler needs demand.

Standards have always played an important role in the design of both in-vehicle and infrastructure transportation systems. The agreement upon basic standards supported the development of a national railway system utilizing a common gauge, and thereby seamless cross-country transportation of passengers and freight.

The reliance upon standards is based upon several needs. There is a significant need for compatibility among transportation systems, whether that is

as simple as standardized rail shape, size, and width of separation, or as challenging as a single frequency, transmission protocol, and message structure for radiofrequency automatic vehicle identification tags utilized for electronic toll collection.

The second need for standards is to assure quality in transportation products and systems. For many years, the best examples of this were the standards highway departments used in specifying paving material, paints, and structural supports. As vehicle quality has become a more critical competitive factor, the use of quality standards has become equally pervasive inside the vehicle as it is in the transportation infrastructure. Over the last several years, the automotive industry has developed its own version of the widely applied ISO 9000 process quality certification, QS 9000, to assure that the goods incorporated into the vehicle (from passenger car to class 8 heavy vehicle) meet at least a minimal acceptable standard for product quality.

The third driving force supporting standards is the need for safety. Although many vehicle safety standards have arrived in the form of regulations, safety standards have also been critical in transportation infrastructure, with examples such as breakaway signposts, guardrail placement and configuration, work zone safety procedures, and defined illumination levels on heavily traveled roadways.

As transportation systems become more complex (and less directly measurable, such as with the software in an engine control unit), the nature of standards continues to change to fit the new requirements, the new types of systems (containing more electronics and software), and the interagency and international environment in which they must operate. Where an early standard may have dealt with a physical interface (or may have only defined performance, leaving the methodology up to the manufacturer), more recent transportation standards work at a more detailed level, and require more specific measures within the transportation product or system.

The standards process in the emerging field of Intelligent Transportation Systems (ITS) is an example of the state of transportation standards development today. The first ITS standards emerged in a hybrid situation: in-vehicle standards, but for use in government-owned vehicles.

The Intelligent Transportation Systems (ITS) Standards program has teamed with standards development organizations and public agencies to accelerate the development of open, non-proprietary communications interface standards to support ITS application development and deployment. Intelligent Transport Systems (ITS) include telematics and all types of communications in vehicles, between vehicles (e.g. car-to-car), and between vehicles and fixed

locations (e.g. car-to-infrastructure). However, ITS are not restricted to Road Transport – they also include the use of information and communication technologies (ICT) for rail, water and air transport, including navigation systems.

In general, the various types of ITS rely on radio services for communication and use specialized technologies. (Fig. 1 Various types of ITS)

Fig. 1. Various types of ITS.

These standards define how ITS systems and components interconnect and exchange information to deliver ITS services within a multimodal transportation network. The consistent and widespread use of ITS standards will permit data and information sharing among public agencies and private organizations, fostering an environment of information sharing and interoperability. Most standards are voluntary, consensus-based, and open:

1. Voluntary, meaning their use is not mandated by law.

2. Consensus-based, meaning that a published standard has attained general agreement through cooperation and compromise in a process that is inclusive of all interested parties.

3. Open, meaning that they are not proprietary and are available for anyone to use.

The use of standards encourages industry growth by minimizing development costs, increasing compatibility and interoperability. Currently nearly 100 standards have been developed under this program. In table I you can see some of these standards.

Table I

Standards of ITS

Name of standards	Description
1. ITE ATC API – Application Programming Interface (API) Standard for the Advanced Transportation Controller (ATC)	An advanced transportation controller (ATC) software application program interfaces (APIs) that support ITS data flows and standards enabling the deployment of ITS functions. The APIs provide a template for API programming for specific functionality associated with equipment and market packages defined by the National ITS Architecture.
2. ITE ATC Controller 5.2 – Advanced Transportation Controller (ATC)	Standard for advanced transportation controller (ATC) devices to support ITS data flows and standards that enable deployment of ITS. Capable of operating in the ATC cabinet and using the ATC application program interfaces.
3. APTA TCIP-S-001 3.0.0 – Standard for Transit Communications Interface Profiles	This standard allows for TCIP components to exchange information using standardized mechanisms. Data will be exchanged among transit devices, systems and subsystems. The standard covers the following business areas: Scheduling, Passenger Information, Incident Management, TCIP Tool Support, Onboard Systems, Control Center, Fare Collection, Spatial Representation, Common Public Transport and Transit Signal Priority.
4. NTCIP 1101 – Simple Transportation Management Framework (STMF)	A set of rules and protocols for organizing, describing and exchanging transportation management information between transportation management applications and transportation equipment such that they interoperate with each other.
5. NTCIP 2201 – Transportation Transport Profile	This standard defines a bandwidth efficient transport profile that is a combination of standards to transmit data when the subject devices are directly connected to the central controller or computer and do not require network services.

Harmonization of international standards and architecture around the vehicle platform is a process through which various stakeholders, vehicle and equipment manufacturers, standards organizations, and governments work together to agree on common standards.

ITS have been faced with the need for several overarching standards. The standards have typically addressed areas utilized both inside the vehicle and by the transportation infrastructure. Standards for identifying «where I am» have the particular importance and have been more formally referred to as spatial database reference standards. Consistent with the need to promote development and innovation within the industry, the focus has been on a common standard for transfer of the information, rather than for how it is used within a system. Thus, multiple developers and manufacturers can use their own for-

mats within their devices, but can exchange information through a common format.

The need (and demand) for standards in transportation continues to exist, perhaps at its greatest level ever. While the traveler no longer faces the confusion of differing road sign shapes, sizes, messages, and placement as he/she motors from one state to the next, the new challenges of electronic map database compatibility (for the same motorist's onboard vehicle navigation system) create a demand for appropriate standards. Both traditional transportation standards-setting bodies and new standards organizations are involved in their development. Government performs in multiple roles, often as facilitator rather than regulator. Standards are influenced by the need for global competitiveness. The role of standards in transportation continues to be an important one, with new and intelligent ways being applied to achieve the overarching goals of moving people and goods across the nation and around the world.

REFERENCES:

1. *Battalov S.* Standardization, certification and metrology. St. Petersburg university named after G. V. Plehanov, St.Petersburg, 2003
2. *Shlenskaya T. V., Chicheva-Philatova L. V., Antonova I. A.* Standardization of transportation system. "MGUTU", Moscow, 2004
3. *Khrustaleva L. V.* Transportation system. The practice. "KNORUS", Moscow, 2011
4. *Lific I. M.* Standardization and certification. "Urait", Moscow, 2009
5. *Dailidko A. A., Urchenko U. A.* Standards of transport. "Logos", Kiev, 2000

PHASE VELOCITY OF SPACE-CHARGE WAVES IN N-INN SEMICONDUCTOR STRUCTURES

O.S. Senatov, S.A. Sergeev

Saratov State University

The best known functional device of the space charge waves (SCW) in semiconductors is the thin-film traveling wave amplifier on n-GaAs (the Dyn, Matareza, 1972; Kumabe, Kanbe, 1985). Distinctive feature of such devices is the broadbandness which not always can be considered as the useful property. The new design of a frequency transformer of millimetric range was offered for realization of the frequency-selective modes (Mikhaylov, Sergeyev, Goryachev, 2000; Mikhaylov, Sergeyev, Ignatyev, 1999). Its work is based on SCW parametrical interaction in negative differential conduction (NDC)

semiconductors.The offered design contains an output element in a form of the interdigital transducer (IT) for coupling with electrodynamic system. The parameters of transducer should be designed to filter out parasitic spectral components and keep the useful ones thus making the output part of converter frequency selective. To define the finger step in transducer it is necessary to know precisely the phase speed of SCW of a signal that should be filtered.

Theoretical calculation of the frequency profile of SCW phase speed in n-GaAs, n-InP and n-GaN was presented in (Mikhaylov, Sergeyev, 1998; Mikhaylov, Sergeyev, 2009; Sergeyev, Mikhaylov, 2009). It was shown that the phase speed of SCW can significantly differ from the electron drift velocity. The dispersion equation was obtained and SCW propagation constant $\gamma = \alpha + i\beta$ was found by means of known one-dimensional model (Carroll, 1972) from Poisson and continuity equations. Phase speed of SCW at the known γ can be calculated as:

$$v_{ph} = \omega / \beta$$

Dependences of phase speed of SCW on frequency was calculated as described in (1). The numerical values of parameters and sizes typical for n-InN were used: relative capacitivity $\varepsilon = 14$; for an electric field strength $E_0 = 90$ kV/cm: electron drift velocity $v_0 = 3 \cdot 10^7$ cm/s, electron diffusion constant $D = 50$ cm^2/s (Starikov et. al., 2005; Farahmand et. al., 2001; O'Leary et. al., 1998; Wu, 2009). Data on the frequency profile of differential mobility of electrons μ_d for n-InN in the field $E_0 = 90$ kV/cm were used from reference (Starikov et. al., 2005).

Dependencies of phase speed of SCW v_{ph} from frequency $f = \omega / 2\pi$ for indium nitride are presented in figure 1. The electron concentration in the semiconductor was used as parameter in calculations, with values $n_0 = 10^{14}$ cm^{-3} (a curve with number 4) $5 \cdot 10^{14}$ cm^{-3} (3) и 10^{15} cm^{-3} (2,1). Dependence of v_{ph} versus f for $D = 100$ cm^2/s and $n_0 = 5 \cdot 10^{14}$ cm^{-3} was given for comparison (curve 5).

All dependences shown were obtained taking into account the frequency dispersion of differential mobility of electrons. The exception was made for a curve 1 calculated for the same parameters as a curve 2 but with $\mu_d = \text{const} = -0{,}0343$ m^2/Vs. The horizontal dotted straight line notes values of charge drift velocity $v_0 = 3 \cdot 10^7$ cm/s.

From the presented dependencies it is evident that the phase speed of SCW can be different from the drift speed for the electrons. Thus at frequencies below the boundary frequency of amplified SCW f_c (Mikhaylov, 1999)

phase speed of SCW v_{ph} is less than the electrons drift velocity v_0, and for frequencies $f > f_c$ phase speed becomes greater than v_0. The analysis shows that difference of phase speed of SCW from v_0 is due to the diffusion influence: diffusion slows down growing SCW and accelerates the fading ones. The difference of v_{ph} and v_0 increases with growth of an electron concentration n_0 and, in particular for frequencies, smaller f_c can reach 1% for n-InN.

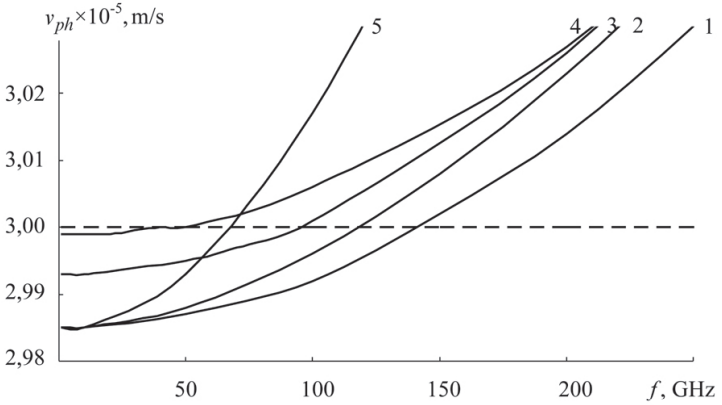

Fig. 1. Dependences of phase speed of WSC v_{ph} on frequency $f = \omega / 2\pi$.

It also can be noted that the distinction between v_{ph} and v_0 becomes even more evident with increase of D (curves 3 and 5) and taking into account the frequency dispersion of electron differential mobility (curves 1 and 2).

The results obtained in this work should be considered for the calculation of geometrical sizes of the coupling elements for the transformation of electromagnetic signals into SCW and back. It becomes especially important for developing the functional devices of SCW for short-wave part of the microwave range that intended for functioning in the frequency transformation mode and which demands creation of frequency-selective coupling elements.

REFERENCES:

1. *Дин Р., Матарезе Р.* Новый тип СВЧ-транзистора – усилитель бегущей волны на n-GaAs // ТИИЭР. 1972. Т. 60, № 12. С. 23–43.
2. *Кэррол Дж.* СВЧ-генераторы на горячих электронах. М.: Мир, 1972. 382 с.
3. *Михайлов А. И., Сергеев С. А.* Фазовая скорость волн пространственного заряда в полупроводниках с отрицательной дифференциальной проводимостью // Вопросы прикладной физики. Саратов: Изд-во Сарат. ун-та, 1998. Вып. 4. С. 75–76.

4. *Михайлов А. И., Сергеев С. А.* Влияние концентрации электронов в пленке арсенида галлия на граничную частоту усиления волн пространственного заряда в тонкопленочных полупроводниковых структурах // Письма в ЖТФ. 1999. Т. 25, Вып. 4. С. 85 – 90.
5. Патент 2138116 РФ, МКИ H 03 D 7/00, 7/12, H 01 L 27/095. Преобразователь частоты СВЧ диапазона / А. И. Михайлов, С. А. Сергеев, Ю. М. Игнатьев (РФ). № 98116381/09, Опубл. 20.09.99. Бюл. № 26.
6. *Михайлов А. И., Сергеев С. А., Горячев А. А.* Интегральный преобразователь частоты миллиметрового диапазона длин волн на волнах пространственного заряда в полупроводниках с отрицательной дифференциальной проводимостью // Изв. ВУЗов. Радиоэлектроника. 2000. Т. 43, № 2. С. 16–24.
7. *Михайлов А. И., Сергеев С. А.* Фазовая скорость волн пространственного заряда в полупроводниковых структурах на основе n-GaAs, n-InP и n-GaN // Вопросы прикладной физики: Межвуз. науч. сб. Саратов: Изд-во Сарат. ун-та, 2009. Вып. 16. С. 38–39.
8. *Сергеев С. А., Михайлов А. И., Сергеева Б. В.* Фазовая скорость волн пространственного заряда в полупроводниковых структурах на основе n-InP / Физика и технические приложения волновых процессов: материалы докл. VIII Международ. науч. – технич. конф.: Приложение к журналу «Физика волновых процессов и радиотехнические системы». СПб.: Политехника, 2009. С. 132–133.
9. Monte Carlo Simulation of Electron Transport in the III-Nitride Wurtzite Phase Materials System: Binaries and Ternaries // M. Farahmand, C. Garetto, E. Belloti etc. // IEEE Transaction on Electron Devices. 2001. Vol. 48, № 3. P. 535–542.
10. *Kumabe K., Kanbe H.* GaAs travelling-wave amplifier // Int. J. Electronics. 1985. Vol. 58. P. 587–611.
11. Electron transport in wurtzite indium nitride // S.K. O'Leary, B. E. Foutz, M. S. Shur etc. // J. Appl. Phys. 1998. Vol. 83, № . 2. P. 826–829.
12. Monte Carlo calculations of hot-electron transport and diffusion noise in GaN and InN / E. Starikov, P. Shiktorov, V. Gružinskis etc. //Semicond. Sci. Technol. 2005. Vol. 20. P. 279–285.
13. Monte Carlo calculations of static and dynamic electron transport in nitrides // E. Starikov, P. Shiktorov, V. Gruinskis etc. // J. Appl. Phys. 2005. Vol. 98. P. 083701(1–7).
14. *Wu J.* When group-III nitrides go infrared: New properties and perspectives // J. of Appl. Phys. 2009. Vol. 106. P. 011101 (1–28).

FORMATION OF ORDERED MULTILAYER STRUCTURES BASED ON ORGANIC MATERIALS FOR ITS APPLICATION IN PHOTOVOLTAIC CONVERTERS

A.S. Sergeeva

Saratov State University

At the present time energy supply is the basis of any production functioning and therefore of the entire human civilization. Different technological advances have become an integral part of people's live, but they are possible only with sufficient and affordable energy. The question of using alternative energy sources becomes more topical because world demand for electrical energy constantly grows. Solar energy is an unlimited source; it is converted into electricity using photovoltaic converters (PC). Now used in practice solar cells based on inorganic semiconductor materials, crystalline and amorphous silicon occupy about 85% of the market. But such devices are expensive due to difficult production technology, resulting in silicon crystalline solar cells (SC) are not widespread.

Innovative solutions in the area of photovoltaic cells recently attracted attention of researchers. The SC device allows using a wide range of materials. Organic compounds have several advantages e.g. low cost, easy processing technologies, lightness and flexibility of materials, environmental safety. Therefore, researchers attend to organic materials in solar cells fabrication (Troshin, Lubovskaya, Rasumov, 2008). The compounds of fullerenes (n-type) and polymers (p-type) are one of the best materials for organic PC with surround heterojunction. Thin-film dye-sensitized cells (such as phthalocyanine dyes) are another promising development (Chickneyan, Briseno, 2003; Mutolo, Mayo, Rand, 2006).

In addition to the used materials variation, modern researches develop of creative PC designs that improve energy conversion efficiency. The future of solar industry consists in using of nanotechnology approaches and occurs on the way of material layers improving. Different PC constructions, such as spherical solar cells, structures based on "core/shell" microparticles, nanowire arrays or photonic crystals, plasmon-resonant structures were developed.

One report describes the photosensitive fibers production from the macroscopic structured preforms (rods with 33 mm in diameter and 20 cm in length) containing variously located semiconducting, metallic and insulating components (Bayindir, Abouraddy, Shapira, 2006). The fabrication of

nanostructured fibers occurs by thermal drawing (drawing in a viscous state at high temperature). Thus it was obtained cheap, flexible, kilometer-long ordered nanophotonic devices.

Another article presents the SC design which consist of vertically oriented zinc oxide nanowire arrays (n-type ZnO) surrounded by a film of copper oxide nanoparticles (p-type Cu_2O). It's possible to fabricate a device with a relatively thick light absorpted layer (for effective photon absorption) and a small distance between wires (for a short exciton diffusion) to maximize the efficiency of structure (Uthirakumar, 2011).

Spherical solar microcells have a light-receiving surface covering whole sphere that allows using sunlight coming from all directions (Minemoto, Takakura, Hamakawa, 2006; Taira, 2007). Cells consist of silicon formed into spheres with p-n-junctions on the entire surface. Microspheres have a diameter about 1 mm (up to 2 mm); it increases the ratio of surface area to volume and therefore efficiency improvement. The application of anti-reflection coating (CdS-film) allows rise of photocurrent by 16% - to 27.6 mA/cm^2, and the conversion efficiency - up to 11%. Small spherical cell size allows also the fabrication of modules in various forms, as well transparent and flexible modules.

It was offered another new method for the light absorption in thin-film SC, which metallic nanostructures supporting the surface plasmons is used (Atwater, Polman, 2010). It becomes possible to create the optically thick, but very physically thin photovoltaic absorber layer. Thus it was produced the thin layer at 10-100 nm with broad light adsorption.

Zhou1 D. and Biswas R. create a texture with a two-dimensional photonic crystal on the back (bottom) metal plate of the cell, which scatters light inside the active absorbing layer and increases the path length of solar photons. The photovoltaic cell configuration contains a 2-D diffraction photonic-crystal grating between the absorbing layer and distributing Bragg reflectors (DBR), can absorb photons effectively, and increasing the efficiency of the cell (Zhou1, Biswas, 2008).

In the next work obtaining of "nanodomes" solar cells were carried by Zhu and coauthors (Zhu, Hsu, Yu, 2010). Effective reflection decreasing and absorption increasing over a wide spectral range were observed for these devices. Amorphous silicon layer with 280 nm thickness can absorb 94% of the light at 400-800 nm wavelength. It is significantly higher than 65% absorption of a flat film. Almost full absorption allows to become very high short-circuit current ~ 17.5 mA/cm^2, and energy efficiency ~ 5.9% (25% higher than of a flat film).

A review and analysis of modern research in the field of photovoltaics allow us to conclude that the modification of solar cell surface by nanostructured materials, which improves their efficiency, is promising direction. Recent scientific developments in this area contain also organic materials (instead inorganic) because they enable to reduce the cost of PC and simplify the production process. In this regard, we are developing models of structured photoactive layers based on organic materials and its creation methods during some years. Different technologies of organized films formation are considered in this paper.

The formation and investigation of "core/shell" microparticles and multilayer structures were conducted at Saratov State University. The synthesis of spherical silica nanoparticles was carried out at Saratov State Technical University by using the sol-gel method.

Materials: Poly(sodium 4-styrenesulfonate) (PSS, 70–100 kDa), poly(allylamine hydrochloride) (PAH, 70 kDa), poly(diallyldimethylammonium chloride) (PDADMAC, 35 wt.%, 200–350 kDa), copper phthalocyanine (CuPc), iron phthalocyanine (FePc), calcium chloride ($CaCl_2$), sodium carbonate dehydrate ($NaCO_3$), tetraethoxysilane (TEOS) , propanol, ethanol, ammonium hydroxide, acetic acid. All chemicals were used without further purification. All solutions were prepared in deionized water.

Calcium Carbonate Microparticle Preparation: Calcium carbonate ($CaCO_3$) particles were fabricated as follows. $CaCl_2$ and Na_2CO_3 solutions (0.33 M) were mixed under vigorous stirring leading to the precipitation of $CaCO_3$ particles. The size of $CaCO_3$ particles was controlled by the duration of the steering cycle; in the current experiments in the range of 2 to 8 μm was chosen. Subsequently three centrifugation and washing steps with pure water were performed in order to remove the un-reacted components.

"Core-Shell" Structure Fabrication: Multilayer microparticles were fabricated as follows. The $CaCO_3$ microparticles were coated using the LbL assembly technique (Decher, 1997). The first layer was made by adsorption of positively charged PAH from 2 mg·mL^{-1} solution in 0.5 M NaCl. The dispersion was continuously shaken during 15 min followed by three centrifugation/washing steps with deionized water. The second layer was prepared by absorption of negatively charged phthalocyanine dye (MPc) from 0.25-1 mg·mL^{-1} water solution (15 min of shaking) followed again by three centrifugation/washing steps. This procedure was repeated N times to deposit N bi-layers on the surface of $CaCO_3$ microparticles. Thus, were obtained "core/shell" microparticles with $CaCO_3$ cores and $(PAH/MPc)_N$ shell structure. Number N of monolayers in shells structure is 4, 6, 8, 10, 12, 16, 20 and 30.

Methods: AFM images of structures were recorded with an Integra Spectra microscope (NTMDT, Saratov, Russia) in the tapping mode. AFM data analysis was performed using the Gwyddion software.

Optical microscopy images were obtained in bright field transmission mode with an Olympus IX71 microscope (part of INTEGRA Spectra setup). For imaging and laser irradiation a 100x/0.90 M Plan FL N objective was used. Optical images were captured from the video signal of the microscope camera.

For Raman spectroscopy analysis and imaging an Integra Spectra Setup (NTMDT, Saratov, Russia) was used. A helium–neon laser (wavelength 632.8 nm, max. power on sample 25 mW) and a solid state CW laser (wavelength 473 nm, maximum power on sample 35 mW) were used for irradiation.

SEM investigations were performed with a Quanta 200 FEG FEI scanning electron microscope operated at an acceleration voltage of 7-30 kV. For sample preparation, a drop of the sample solution was placed onto a silicon wafer, dried in air, and sputtered with gold.

The Zeta-potential of suspensions was measured by a Zetasizer Nano-Z (Malvern Instruments Ltd, Saratov, Russia).

A spectrophotometer "Lambda 950" (with pure water as the reference) was used for investigation of UV, vis absorption spectra of structures and supernatants.

The experimental work is divided into some stages, at each of them ordered structures obtained by using specific techniques.

At the **first stage** it was formed organized structures from multilayer "core-shell" microparticles on glass substrates modified with different charged polyelectrolytes. Firstly it was obtained all needed solutions. Then "core/shell" microparticles with $CaCO_3$ cores and $(PAH/MPc)_N$ shell structure were formed.

Water suspensions of "core/shell" microparticles were investigated by optical microscopy and scanning electron microscopy. The particles have a spherical shape and diameter about 2 μm. During microparticles formation supernatants were selected. Its adsorption spectra were measured by spectrophotometer "Lambda 950". A lot of dye molecules remained in supernatant because high concentration phthalocyanine solutions were used during adsorption of shell layers. It was obtained distinct spectra of supernatants: there are all three characteristic for phthalocyanines peaks (at wavelengths ~ 340nm, ~ 620nm and 690nm). Exactly these last two peaks in the visible range are used by researchers in photoelectronics.

The Raman scattering spectra (RS) of "core/shell" structures were received to confirm the presence of adsorbed substances. By the presence

of phthalocyanine characteristic peaks we can prove its existence in shell structures (Fig. 1). Characteristic peaks of the blue (green) phthalocyanine dye series (1/cm): 681 (684), 1339 (1060), 1450 (1387), 1503 (1527).

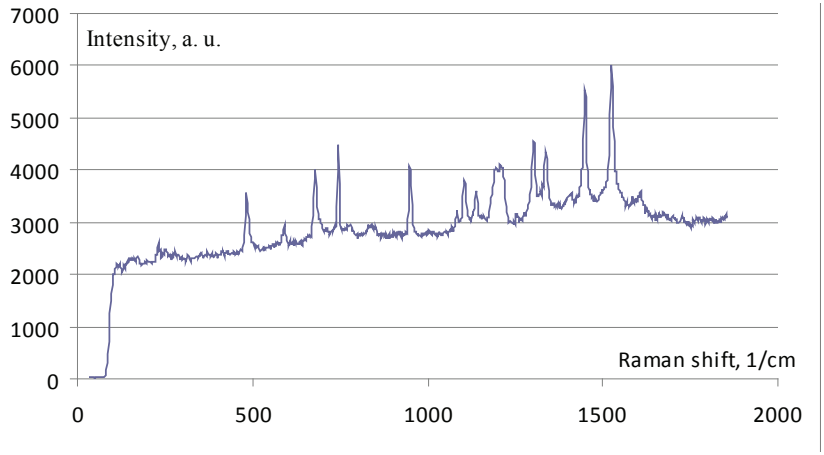

Fig. 1 □aman spectrum of □core/shell□ structures (CaC_3 core □ (□□/□□c)$_{10}$ shell)

□ large amount of □core/shell□structures (with $CaC□_3$ core and (□□□/Cu□c)$_5$, (□□□/Fe□c)$_5$ shell) were produced speci□cally. □hen □core/shell□par□ticles were deposited on glass surfaces and drying during 8 hours. □article layers were removed from substrates and annealed on the setup □□□□□500 □20.10 □uild 36□. □emperature is increased up to 400□C, and simultaneous□ly the change in mass of dry microcapsules was measured. □he annealing of structures is carried out to phthalocyanine compounds photosensiti□ation(the transition from □□to active □□phase occurs at high temperature) (□enthilarasu, □ahn, □oo□□young□ee,2007). □aman spectra of □core/shell□structures (with $CaC□_3$ core and (□□□/Cu□c)$_5$, (□□□/Fe□c)$_5$ shell) were obtained before and after annealing. □pectrum analysis (intensity, peak position) allows to con□clude about the presence of adsorbed substances (dyes), and con□rms a transi□tion to photoactive phthalocyanine phase.

Finally, the organi□ed assemblies of the obtained □core/shell□particles were formed on the surface of substrates modi□ed with different charged polyelectrolytes. □ surface of glass substrates was cleaned and covered with polyelectrolyte solutions. □ome glasses were covered with a □□□ solution, other with a □□□. □hus, the glass surface was positively charged in the □rst case and negatively charged in the second case. □ubstrates were drying dur□

ing 1-2 hours. 100 µl suspension of "core/shell" structures (with $CaCO_3$ core and $(PAH/MPc)_5$ shell) were deposited on these glasses and drying. The multilayer microparticles have negative charge on its surface (due to phthalocyanine charge). Drops of the suspension do not spread on substrates with PAH and keep the form of a hemisphere. A drop of suspension was spreading on other substrates having PSS on glasses. It was forming a thin layer because negatively charged microparticles slid on similarly charged surface. Thus spherical "core/shell" microparticles with negative charge must form monomolecular structured film on glasses with the same charged surface. But it is not so in fact. We received organized film only on certain areas. And there was monomolecular but randomly oriented layer on other space (with agglomerates of "core/shell" particles). This disorder occurs probably due to the fact that electrostatic forces were too small.

Samples preparation for electrical measurements was carried out. Two types of conductive substrates were produced. The layer of microparticles was deposited between top and bottom contacts. It was attempted to measure current-voltage characteristics. Formed film structures were appeared too uneven, so that it was not possible to measure the electrical characteristics. Currents were either very small (the sensitivity of the measuring device was not enough to its distinction) or samples were shorted out. Thus it is necessary to achieve a high packing density of formed films to carry out the electrical measurements. Then another technology for obtaining an ordered structure was proposed, it described in the second stage.

At the **second stage** glass substrates were modified by SiO_2 nanospheres (100-300 nm in diameter). Deposition of SiO_2 coatings onto glasses was carried out by immersion the substrates in synthesized silica sols and pulling from colloidal solutions at a controlled rate (100 ± 5 mm/min). Oppositely charged MPc and PEI (polyethyleneimine) layers were applied on top of silica spheres coating by using the LbL assembly technique (Decher, 1997) (Fig. 2). Structures like glass/SiO_2/$(PEI/MPc)_n$ (n=1..7) were obtained. It was received more intense, vivid color of multilayer structures with increasing applied coatings number.

Structures were investigated by AFM, ellipsometry. The relief uniformity and the thickness of coatings were explored. Fig. III shows the AFM image of obtained structure, thickness is approximately 500 nm. The Raman scattering spectra of structures were received. Analysis of these spectra concludes that all substances were adsorbed because there are peaks typical for deposited materials on the graphs. Formed structures have been more uniform than films produced in the previous 1st stage.

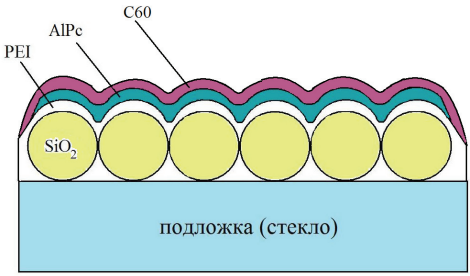

Fig. 2 A schematic model of the structure SiO_2/PEI/AlPc/C_{60} (only first layers are illustrated)

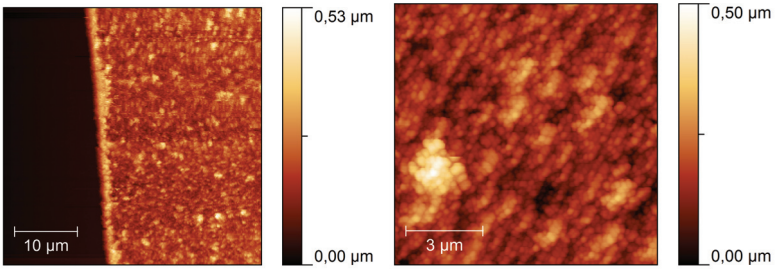

Fig. 3 AFM-images of structure SiO_2/$(PEI/AlPc)_n$

At the **third stage** organized structures were formed using Langmuir-Blodgett technique. The monolayer of "core/shell" structures (with $CaCO_3$ core and $(PAH/MPc)_n$ shell) was formed on the interface and compressed to the close-packed state (it is reached at the specific area per one particle is 44 $Å^2$). Monolayer on the water surface can be seen with naked eye due to phthalocyanine dye in the shell. At this stage may be obtained the most uniform and close-packed structures.

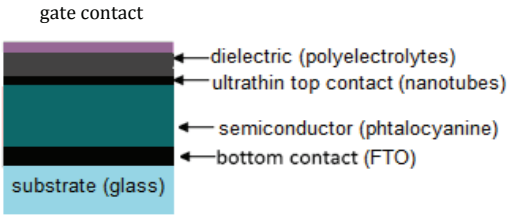

Fig. 4. Schematic illustration of photoconductive structure «substrate / bottom contact / semiconductor / ultrathin contact / gate dielectric / gate contact (supposedly used materials are displayed in parentheses)

At **forth stage** the design of a hybrid photoelectric converter based on structured materials was developed (Fig. 4). It is a multilayer thin film structure using one conductivity type organic semiconductor. Lower part of the construction (bottom contact, semiconductor, thin top contact) is a working part. The light should fall vertically on top of the structure. The gate contact and dielectric are transparent layers. The creation of such structure is caused the following factors, which allow improving the electrical characteristics (Regan, Byrnes, Gannett, Ergen, Vazquez-Mena, Wang, Zettl, 2012). The voltage is externally applied to a gate to invert a region of semiconductor – it is field-effect "doping" of semiconductor. A thin insulating layer is used to block the recombination current.

It was formed a bottom part of illustrated design (substrate/bottom contact (FTO)/semiconductor layer $(MPc/PAH)_n$, where n=10, 20, 30). Formation of thin film structure on solid substrates occurs using the LbL method on setup "Polyion-1M". Formed multilayer structures were investigated by AFM, SEM, optical microscopy, Raman scattering spectroscopy. Organic materials are well adsorbed on substrates with a conductive coating (FTO), so that the resulting multilayer coatings are orderly. But a detailed study of the entire surface of coatings allowed seeing the presence of areas with irregular structure. This is probably due to defects in the substrate itself (such as microcracks), therefore the multilayer coating is uneven. Such microdefects can negatively influence on the conductivity and other properties of thin-film coatings. Therefore it is necessary to use higher-quality substrates or modify existing ones before fabricating photoelectric converter structure.

Innovative solutions in the area of photovoltaic cells recently attracted attention of researchers. This work is another step in this field. Here the nano- and microstructured thin-film coatings are presented, which can be used as a photoactive layers. The dyes of phthalocyanine series are promising for use as p-type conductivity semiconductor in photoconductive devices. The using of presented materials helps to reduce the cost of solar energy. Presented film formation methods allow to obtain multilayer ordered structures easily and without significant production costs.

Author thanks to Stanislav Viktorovich Eskin, graduate student of Chemistry Chair, Y.A. Gagarin Saratov State Technical University, for providing materials and conducting of experiments on synthesis spherical silica cores technology.

REFERENCES:

1. *Troshin P.A., Lubovskaya R.N., Rasumov V.F.* Organic Solar Cells: structure, materials, critical parameters and development prospects // Russian nanotechnologies. 2008. T. 3, № 5-6. C. 56-77. (in Russian)
2. *Atwater H., Polman A*. Plasmonics for improved photovoltaic devices // Nature materials. V. 9. 2010. P. 205-213.
3. *Bayindir M., Abouraddy A.F., Shapira O. et al.* Kilometer-Long Ordered Nanophotonic Devices by Preform-to-Fiber Fabrication // IEEE Journal of selected topics in quantum electronics. 2006. V. 12, №. 6. P. 1202-1213.
4. *Chickneyan Z.S., Briseno A.L. et. al.* Polyelectrolyte-Mediated Assembly of Copper Phthalocyanine Tetrasulfonate Multilayers and the Subsequent Production of Nanoparticulate Copper Oxide Thin Films // J. Nanosci. Nanotech. 2003. V. 4. P. 1-7.
5. *Decher G.* / Science. 1997. V. 277. P. 1232.
6. *Minemoto T., Takakura H., Hamakawa Y.* Chemical bath deposition for the fabrication of antireflective coating of spherical silicon solar cells / Solar Energy Materials & Solar Cells. 2006. V. 90. P. 3576-3582.
7. *Mutolo K.L., Mayo E.I., Rand B.P. et. al.* Enhanced Open-Circuit Voltage in Subphthalocyanine/C60 Organic Photovoltaic Cells // J. Am. Chem. Soc. 2006. V. 128. P. 8108.
8. *Regan W., Byrnes S., Gannett W., Ergen O., Vazquez-Mena O., Wang F, Zettl A.* Screening-Engineered Field-Effect Solar Cells // Nano Letters. 2012. V. 12. P. 4300−4304.
9. *Senthilarasu S., Hahn Y. B., Soo-Hyoung Lee* Structural analysis of zinc phthalocyanine (ZnPc): thin films: X-ray diffraction study // JOURNAL OF APPLIED PHYSICS. 2007. V. 102. P. 043512.
10. *Taira K.* Sphelar Cells Save on Silicon, Capture Light From All Paths // JEI, Dempa Publications. 2007. P. 26-27.
11. *Uthirakumar A.P.* Fabrication of ZnO Based Dye Sensitized Solar Cells // Solar Cells Dye-Sensitized Devices. 2011. P. 435-456.
12. *Zhou1 D., Biswas R.* Photonic crystal enhanced light-trapping in thin film solar cells // Journal of Applied Physics. 2008. V. 103, № 9 P. 093102.
13. *Zhu J., Hsu C.M., Yu Z. et al.* Nanodome Solar Cells with Efficient Light Management and Self-Cleaning // Nano Lett. 2010. V. 6, № 9. P. 1979-1984.

THE INFLUENCE OF NONIONIC SURFACTANT ON PHOTOMETRIC DETERMINATION OF "PHOTOSENSE"

D.D. Shamankov[1], E.I. Selifonova[1], R.K. Chernova[1], D.A. Gorin[1], E.A. Lukyanets[2]

[1] Saratov State University

[2] State Research Center of Organic Intermediates and Dyes "NIOPIC", Moscow

Metallophthalocyanines are widely used in many industries. Chemically stable phthalocyanine dyes are photo-and semiconductors, oxidation catalysts (Rosenthal, Ben-Hur, 1989). Metallocomplexes of phthalocyanines have been used as an electrode-active component in the membrane of ion-selective electrodes (Шведене, Лейзерович, Косталындина, Коваль, Плетнев, 2000). In the last decade, there is an increased interest in the use of phthalocyanines as photosensitizers for photodynamic therapy of cancer (Кортава, 2008). This is due to the fact that the photosensitizers have a great therapeutic potential. At present, the «Photosense» are widely used as a photosensitizer. The "Photosense" is a mixture of sodium salts of sulfonated aluminum phthalocyanine.

The absorption spectrum of an aqueous solution of the drug «Photosense» contains several bands characteristic of all metallophthalocyanines (Зиминов, Рамш, Спиридонов, Юрре, Бутхузи, Туриев, 2009). As follows from Fig. 1 the band at 679 nm, responsible for the color of the compound has the greatest intensity. Therefore, the wavelength of 679 nm was selected as an analytical during the photometric measurements.

Several features of «Photosense» are essential obstacles for realization photometric technique of its determination. They are: high hygroscopicity not allowing to sample the substance; not complete solubility in water; the existence of poorly-filtered fine insoluble particles in the solutions under photometry; the sensitivity to light and the corresponding instability of aqueous solutions in certain conditions.

The present study is devoted to our development of a photometric technique for "Photosense" analysis in view of the above complicating circumstances.

Thermogravimetric studies were performed in air at derivatograph «Paulik – Paulik – Erdei – OD – 103", weighed sample – 100 mg, heating rate 10 ^{0}C/min in the temperature range 20-900 ^{0}C (thermocouple Pt-Pt / Rh), the standard – calcined aluminium oxide.

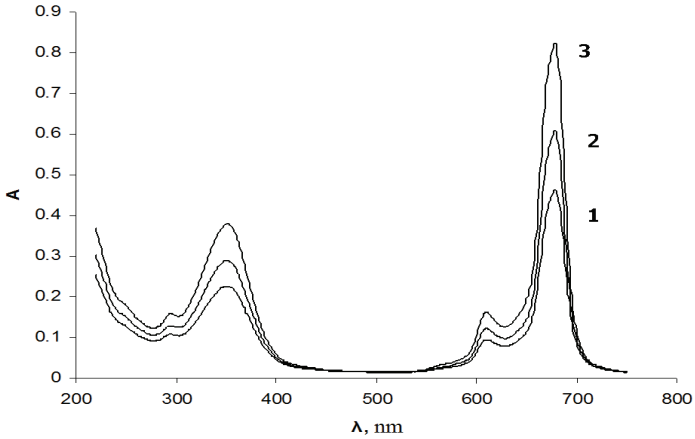

Fig.1. Electronic absorption spectrums of water solutions of «Photosense»: 1 – 0,05 mg/25ml, 2 – 0,07 mg/25ml, 3 – 0,10 mg/25ml

Thermogravimetric studies in a nitrogen atmosphere were performed at thermogravimetric analyzer series TGAQ500 with FTIR Nicolet 6700 in the temperature range of 20-920 ^{0}C with a heating rate of 10 ^{0}C/min.

The absorption spectrums were taken off the spectrophotometer «Shimadzu UV-2550».

Registration of the optical density of the solutions were perfomed on the photo colorimeter 3-01-»ZOM3» at a wavelength of 679 nm.

We carried out thermogravimetric studies of "Photosense" in an air medium and in the nitrogen atmosphere. As follows from Fig. 2, the hygroscopic drug contains 18–19% of water, which was removed within 80–180°C. The anhydrous "Photosense" is stable at 250°C (air).

Thermogravimetry data allows to get the exact content of anhydrous «Photosense» mass at 250^{0}C. In the future we used the dehydrated substance for the preparation of solutions and setting up calibration plots.

The volume of the solvent (deionized water), the time of dissolution, and the water temperature have been established to be important factors at dissolution of the substance in water, which influence the completeness of dissolution. At the ratio of the mass of sample: the volume of water is less than 1:10, there exist very fine and almost insoluble particles of the preparation in solution, detected when filtering the solution.

The data presented in Table. 1 shows that the addition of OP-10 to an aqueous solution of the «Photosense» increases its solubility, as evidenced by

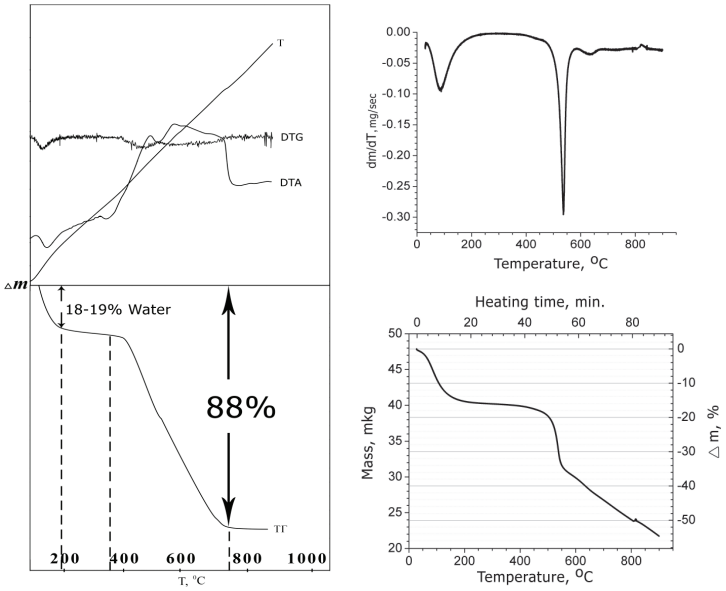

Fig.2. Thermograms of "Photosense": (a) – air, (b) – nitrogen atmosphere

the increase in the optical density (A). Obtained and analyzed calibration plots A-C for series of solutions of the drug in the presence and absence of the OP-10 (Fig.3).

Table1

Some parameters of points of calibration plots of "Photosense"

C, %	In absence OP-10		In presence OP-10	
	$E^{1\%}$, sm	A	$E^{1\%}$, sm	A
2,0 x10^{-4}	2195	0,439	2570	0,514
2,9 x10^{-4}	2117	0,614	2417	0,701
4,4 x10^{-4}	2043	0,899	2309	1,016
5,8 x10^{-4}	2063	1,197	2286	1,326
7,0 x10^{-4}	2037	1,426	2241	1,569

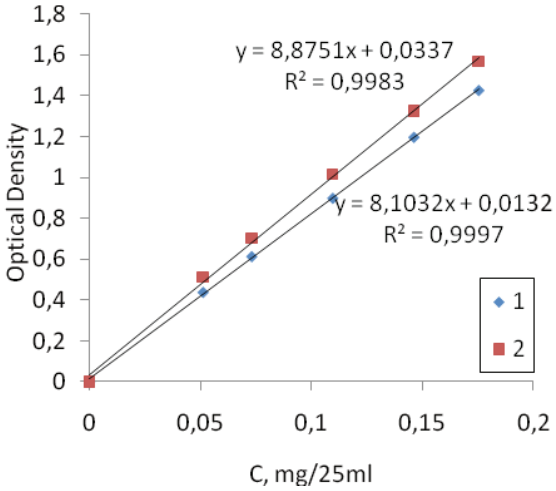

Fig. 4. Calibration plots of "Photosense":
1 – in absence OP-10; 2- in presence OP-10.

It should be noted that heating promotes solubility. As Table. 2, after 30 minutes of heating at 74^0C optical density remains practically constant.

As in the presence of sunlight optical density of the solution decreases significantly, studies were carried out without any direct sunlight.

Table 3

Changes of optical density of a solution of the «Photosense» in presence of OP-10 (without heating and after heating)

Time, min	A (Without heating)	A (With heating, 74^0C)
0	0,880	0,886
10	0,883	0,981
20	0,886	0,999
30	0,888	1,001
60	0,895	-
90	0,900	-
120	0,904	-
150	0,906	-

Thus, this study found an increase in the solubility of the drug «Photosense» in deionized water in the presence of nonionic surfactant OP-10. We obtained and analyzed calibration plots A-C for series of solutions of the drug in the presence and absence of the OP-10. A water content (18–19%) in the substance was installed. We also describe a method of preparation of anhydrous fixed "Photosense" mass by thermogravimetric technique.

REFERENCES:

1. *Зиминов А. В., Рамш С. М., Спиридонов И. Г., Юрре Т. А., Бутхузи Т. Г., Туриев А. М.* Синтез и исследование физико-химических свойств комплексов фталоцианинов с d- и f-элементами // Вестн. Санкт-Петербургского Ун-та Сер. 4. 2009. Вып. 4. С. 94-108.
2. *Кортава М. А.* Липосомальная форма фотосенса для фотодинамической терапии опухолей. Автореф. дис. … к-та биол. наук. М. Рос. онк. н. Центр им. Н. М. Блохина РАМН, 2008. 25 с.
3. *Шведене Н. В., Лейзерович Н. Н., Косталындина Е. В., Коваль Я. Н., Плетнев И. В.* Фталоцианат алюминия как активный компонент мембранного ионселективного электрода, обратимого к салицилату // Вестн. Моск. Ун-та. Сер. 2. Химия. 2000. Т.41. № 1. С. 34–36.
4. *Rosenthal. I.; Ben-Hur. E.* In Phthalocyanines. Properties and Applications; Leznoff, C. C., Lever, A. B., Eds.; VCH Publishers: New York, 1989; 393 p.

CLOUD POINT EXTRACTION AND SPECTROPHOTOMETRY DETERMINATION OF BRILLIANT BLUE IN A DRINK «POWERADE»

N.B. Shestopalova, R.K. Chernova, D.V. Zhukova, M.V. Rahmanina

Saratov State University

Synthetic food dyes are used to make, enhance or restore the color of food. Low sensitivity to the conditions of technological processing and storage, high resistance to acids and alkalis makes their widespread use in the food and pharmaceutical industries. The excess of the value of acceptable daily intake of synthetic food dyes can be dangerous to humans. In this regard, the content in food is strictly rationed. The main difficulty in the determination of food dyes in food products is the need to remove them from the complex matrix.

Extraction with organic solvents, inefficient and environmentally dangerous. Extraction of the point cloud (cloud point extraction, CPE) using non-ionic surfactants (nonionic surfactant) is an environmentally friendly alternative to conventional extraction.

The advantages of this method include the achievement of high rates of concentration when using small sample volumes and the ability to extract both hydrophobic and hydrophilic substrates. Simple and rapid method, good compatibility with the physical – chemical methods of analysis makes micellar extraction is one of the promising methods for the separation and concentration.

Micellar extraction is based on the phase separation of aqueous solutions of nonionic surfactant cloud point temperature, and the formation of two phases: the surfactant and water saturated with surfactant concentrations close to the CMC. For the purpose of extraction and concentration of analytes using rich phase surfactants. Important for the purposes of analysis, have physical and chemical characteristics of the resulting surfactant-rich phase: viscosity, density, speed of formation and volume, optical transparency in the UV and visible regions of the spectrum, there is no interaction with the analyte.

Currently as extraction increasingly using polyoxyethylene alkylphenols. The solubility of these compounds in the water due to the formation of hydrogen bonds between water molecules, the oxygen atoms of the polyoxyethylene chain and the end of the polar hydroxyl groups. When heated aqueous solutions of nonionic surfactant is a destruction of these connections. At a certain temperature, the solution becomes cloudy and stratified. Compact and high viscosity of the micellar phase can easily separate the aqueous phase by decantation.

Now for the micellar extraction is used not only individual nonionic surfactant, but also their mixtures as well as different compositions with other materials (polymers, polyelectrolytes, organic compounds, etc.). Our use of the technical preparation OP-10 is not an individual chemical compound, it should be seen as a mixture of polymer homologues as varied length alkyl and oxyethylene chains, the degree of unsaturation, etc. However, this has little effect on the physical and chemical characteristics of the phase separation and the use of OP-10 for the CPE.

For the extraction of organic compounds following factors significantly affect the extraction of analytes from a variety of environments: pH, concentration of nonionic surfactant, electrolyte additives, temperature.

This work was to study the effect of acidity, concentration of nonionic surfactant and dye brilliant blue on the parameters of a cloud point extraction phases OP-10, spectrophotometric determination of the dye in the energy drink «Powerade» Pre-extracting it at the point cloud.

In this work we used industrial food coloring brilliant blue (E133), manufactured by «FOODCO» (Purity 70%), sodium sulfate (analytical grade), polyoxyethylene alkylphenol OP-10 with an average ethoxylation degree of 10-12

(Purity 80%). Working solutions were prepared by dissolving the exact portions in distilled water. Acidity supports the addition of the required amounts of 0.1 M NaOH and HCl.

The absorption spectra of solutions were measured with a spectrophotometer Shimadzu UV – 1800. Acidity of the medium was measured using a pH meter-mV 150-MP.

Micellar extraction of dye was carried out by the following procedure. Aqueous solutions of OP-10 (10%), containing all the necessary components were placed in dimensional tubes of 10 ml, fixed on a tripod, was immersed in a heat-resistant glass with water and heated to 90°C at a rate of 1,0°C per minute at a constant stirring. The temperature was monitored with a thermometer immersed directly in the water bath. When the temperature opacities (T_c) showed characteristic opalescence solutions. Further heating leads to separation into two phases (T_s). The distribution of dye was monitored spectrophotometrically by measuring the light absorption of aqueous solutions before and after the phase separation, and the micellar phase after dilution. Based on the data expected a recovery (R,%) and distribution coefficients (D) dyes.

The cloud point of water 1-10% solutions of OP-10 is in the range of

85-90ºC and decreases with increasing concentration of nonionic surfactant. Adding electrolytes in this range of concentrations almost always leads to a decrease in the cloud point. The largest decrease in the cloud point was observed for sulfates of alkali metals (Р. К. Чернова, Н. Б. Шестопалова, Л. М. Козлова, 2012). Therefore, as a supplement we selected 0.2M sodium sulfate, which lowers the cloud point to 66°C, increases the viscosity of the micellar phase, and has the effect of salting. Changing the pH of the solution in a wide range does not affect the phase separation of aqueous solutions of OP-10.

We studied the micellar extraction in the presence of 0.2 M Na_2SO_4 triphenylmethane dye brilliant blue:

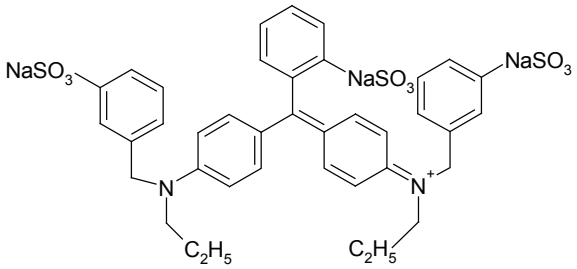

The absorption spectra of aqueous solutions of the dye and the aqueous and micellar phases in a neutral (pH = 7) are shown in Figure 1. The absorption maxima of aqueous solution E133 – λmax = 629 nm, in 10% OP-10 – λmax = 634 nm. Electronic spectra are identical, indicating that finding dye molecules in various phases in one form. Introduction to the system (OP-10)-H_2O-Na_2SO_4 dye E133 has no effect on the cloud point and the amount of the phases.

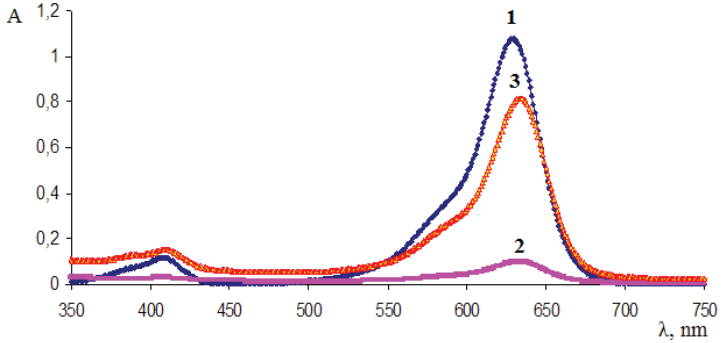

Fig. 1. The absorption spectra of the dye E 133.
1 - initial aqueous solution, 2- after the extraction of the aqueous phase and 3-phase micellar solution. C (E133) = 10 mg/l, C (OP-10) = 10%, C (Na_2SO4) = 0,2 M.

According to (2), the calculated degree of recovery (R,%) and the distribution coefficient (D), as well as the optimized extraction conditions for E133.

Effect of pH of the medium was studied in the pH range 1–13 at the dye concentration of 5 mg / l and the addition of 0.1 M NaOH and HCl. Found that the extraction efficiency E133 remains almost constant in the pH range 4-10 (Fig. 2). Optimal for the extraction was selected pH range 6–8.

Found that the extract E133 depends on the concentration of OP-10 in the initial solution. Increase in the concentration of nonionic surfactant in the range of 1 to 10% leads to an increase in the degree of extraction of dye micellar phases to 97% for the dye concentration of 1 mg / l. (Fig. 3). The increase in the generation of micellar phase with increasing concentration of OP-10 also increases the value of the distribution coefficient of dyes.

Extraction parameters depend on the concentration of the dye in the initial solution (Table 1). With the reduction of the content of E133, an increase of values R,%, and D. When the dye concentration of 1 mg / L, he is almost completely recovered in the micellar phase (R 95%).

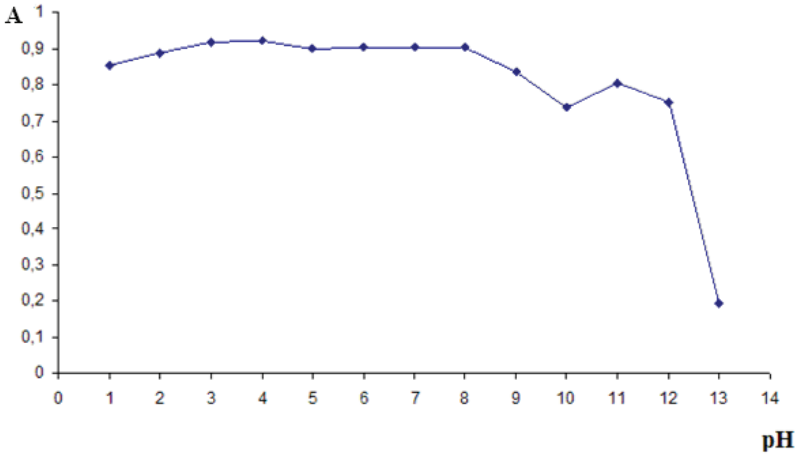

Fig. 2. Dependence of the optical density of the solution of the micellar phase of E133 pH. λ max = 634 nm, C (E133) = 5 mg / l.

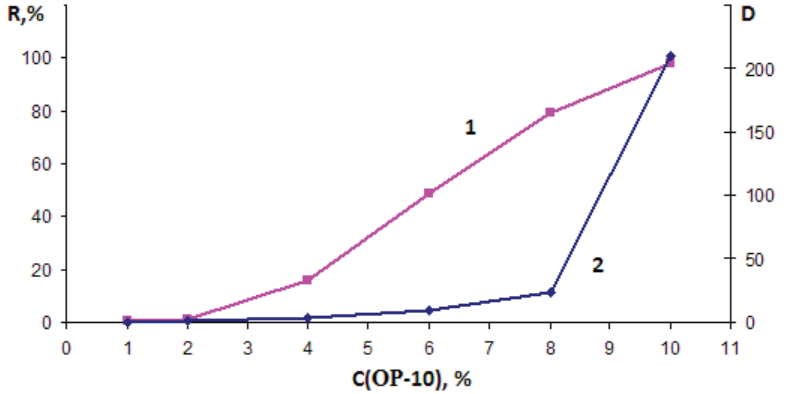

Fig. 3.Depending on the degree of extraction (1) and the distribution coefficient (2) E 133 on the concentration of OP-10. C (E 133) = 1 mg / L, C (Na_2SO_4) = 0,2 M.

The studied system is applied to the extraction-photometric determination of E133 in the energy drink «POWERED» a phase of OP-10 at Cloud. Direct spectrophotometric determination of E133 in the drink is not possible due to its optical opacity.

Table 1

Quantitative characteristics of the micellar extraction E133.

C (OP-10),%	D			R,%		
	10 mg/l	5 mg/l	1 mg/l	10 mg/l	5 mg/l	1 mg/l
1	3,114	0,314	0,24	3,05	0,316	0,31
2	1,122	1,063	0,59	2.24	2.12	1,19
4	2,89	2,56	3,77	8,2	7,34	15,58
6	4,5	3,24	8,52	22,32	14,57	48,63
8	5,64	5,91	23,80	47,88	33,95	79,49
10	8,95	10,32	209,2	63,03	66,28	97,89

Determination of the dye was performed by the following procedure. For this, 1 ml of the drink, 5 ml of a 10% solution of the OP-10, 2 ml of 1 M Na_2SO_4 solution was placed in a graduated test tube and the solution volume was adjusted with distilled water to a total volume of 10 ml. The resulting solution was heated in a water bath to the cloud point and held for 5 minutes to complete phase separation. After cooling, the aqueous phase was separated by decantation. Micellar phase was diluted with distilled water to a total volume of 5 ml and measured the absorbance of the solution at λmax = 634 nm. Dye content was found from the calibration curve. As a result, determining the content of the dye in the energy drink «Powered» is 16,2 ± 1,7 mg / kg, not to exceed the permissible content of this dye in soft drinks (ODC – 10-100 mg / kg).

Thus, we have established the ability to extract the point cloud phases OP-10 dye E133. Extraction in the surfactant-rich phase does not change the state of the dye. Determined by the degree of extraction and distribution ratio of dye at varying acidity, concentration of nonionic surfactant and dye. Optimal conditions for the extraction-photometric determination of E133 in soft drinks.The technique of extraction-photometric determination of dye E133 in the energy drink «POWERED». The results are compared with the recommended regulations, dye content is less than the estimated maximum concentration in soft drinks.

REFERENCES:

1. *Р. К. Чернова, Н. Б. Шестопалова, Л. М. Козлова* Некоторые аспекты влияния электролитов на фазовое разделение и «cloud point» экстракцию азорубина в системе (ОП-10)-H_2O // Известия Саратовского университета. Серия Химия. Биология. Экология. – 2012. – Т.12. вып.4. С. 11–16.
2. Основы аналитической химии / Под ред. акад. РАН Золотова Ю. А. М.: Высшая школа, 1996. –384с.

THE EFFECT OF SODIUM SULFATE ON THE PHYSICAL AND CHEMICAL PARAMETERS OF THE CLOUD POINT EXTRACTION OF SUNSET YELLOW

N. B. Shestopalova, R. K. Chernova, M. E. Tokareva

Saratov State University

Phase separation in systems of non-ionic surfactant - H_2O - salt has important practical significance and of interest to experts of different profiles. In analytical practice surfactant-rich micellar phase, which is formed at the point cloud is used for separation and concentration of inorganic substances and organic nature. (*Кущевская Н.Ф., Горбачевский* А.Н., *Дорощук* В.А., *Куличенко С.А., 2008*). For the system (OP-10) - H_2O cloud point is 90 º C, the temperature stable phase separation of about 100 º C. At said temperature range of organic analytes extraction becomes impossible due to their decomposition. In this regard, relevant search terms the phase separation of micellar solutions of non-ionic surfactant at a lower temperature. At the same time micellar phase, used for analytical concentration must meet several requirements: the compact localization, sufficient viscosity, small volume, optical transparency.

The purpose of this study was to investigate the possibility of obtaining rich phase OP-10 and suitable for the concentration at room temperature (20 - 25 º C) with sodium sulfate. Evaluation of the possibility of extraction of dye yellow "sunset" from aqueous solutions and determine the parameters of the micellar extraction.

The choice of salt caused the greatest impact on lowering the cloud point in systems with non-ionic surfactants (*Чернова Р.К.*, *Шестопалова Н.Б.*, *Козлова Л.М.*, 2012) and its own preliminary studies.

In this work we used industrial food dye yellow «sunset» (E 110), manufactured by «FOODCO» (purity 70%), sodium sulfate (analytical grade), polyoxyethylene alkylphenol OP-10 with an average oxyethylation degree of 10 -12 (purity 80%). Working solutions were prepared by dissolving the exact weighed portions in distilled water.

The absorption spectra of solutions were measured with a spectrophotometer Shimadzu UV - 1800.

Cloud point extraction of the dye in the system (OP-10)-Na_2SO_4-H_2O performed by the following procedure. Placed in a test tube weighed portion salt was added 0,1-1,0 ml of the dye solution concentration of 0,1 g / l and diluted to volume with distilled water to 5 ml, stirring to dissolve the salt. In this

tube was added the appropriate volume of the initial 20% solution of OP-10 and adjusted total volume distilled water to 10 ml. Observed turbidity of the solution. Thoroughly mixed and placed in a glass with water at 25 ° C for 30 minutes to complete phase separation. Noted the volume and characteristics of the micellar phase.

The aqueous phase was separated by using a needle with the syringe. Micellar phase was diluted with distilled water up to 5 ml and measured the light absorption of water solutions before and after the phase separation and the micellar phase after dilution. Based on these data we calculated the degree of extraction (R) and the distribution coefficients (D) dye.

Phase separation of aqueous 10% solution of OP-10 is at a temperature of about 90 º C. Adding sodium sulfate (0,2 M) lowers the cloud point to 66 º C. Further growth of Na_2SO_4 concentration reduces the temperature limit of the exfoliation in the system, but the phase formed is delocalized in the entire volume, and phase separation is difficult.

Found optimal concentration ratio of the OP-10 and salt, at which the formation of two liquid phases, and the compact phase enriched OP-10 with a lower density, is located in the upper part of the solution. Phase separation observed in the concentration range of OP-10 from 1 to 10% and salt content of 6 to 9%. In this case, the lower the concentration of OP-10, the greater the quantity of salt needed for phase separation system. The increase in ionic strength leads to a "salting out effect" that favors dehydration polyoxyethylene layer micelles OP-10, the more compact packaging thereof and as a consequence, decrease the cloud point to room temperature.

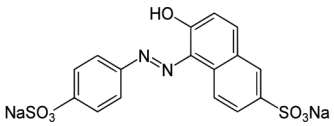

We investigated extraction capabilities of the system (OP-10)-Na_2SO_4-H_2O at 25 ° C to extract the azo dye yellow "sunset":

In micellar extraction is important to consider the possible interactions between the extractant, analyte and the injected salt. Were obtained absorption spectra of an aqueous solution of dye and solutions aqueous and micellar phases in a neutral environment (pH = 7). Forms of electronic spectra of dye in solutions OP-10 are identical (λ_{max} = 483 nm), which indicates the finding of the dye molecules in various phases in identical form (Fig. 1).

Concentration of the initial solution of non-ionic surfactant affects on the parameters extraction. We found that when the dye concentration of 10 mg / l

of extracting it from the aqueous solution most effectively 10% solution of the OP-10. The distribution coefficient is about 56, and degree of extraction above 96%. (Table 1).

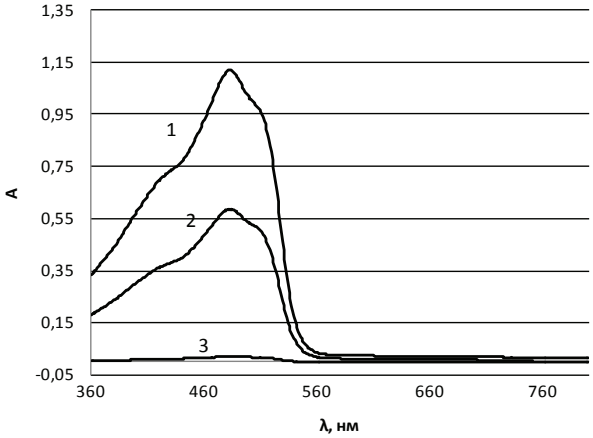

Fig.1. The absorption spectra of the dye E110. 1 - micellar solution phase, 2 - the initial dye solution 3 - aqueous phase after extraction. C (E110) = $2{,}2 \cdot 10^{-5}$ mol / l, C (OP-10) = 10%, m (Na_2SO_4) = 0,82 g

Table 1

Parameters extraction E110 at varying concentrations of OP-10.

C(ОП-10), %	D	Sr, %	R, %	Sr, %
5	67,46 ± 10,70	6,4	94,39 ± 0,87	0,37
10	55,77 ± 11,37	8,0	97,65 ± 1,49	0,60

Introduction to the system electrolyte additives not only helps to reduce the cloud point, but also improves the parameters of extraction by salting out effect. So the cloud point extraction (66 °C) E110 in the presence of 0,2 M Na_2SO_4 solution allows to extract up to 86% of dye.

Adding electrolyte increases dehydration polyoxyethylene of chains and promotes growth of the micelles in solution. This leads to an increase in the concentration of the analyte in the micellar phase and most complete extraction of the phase separation.

We have studied the effect of different concentrations of Na_2SO_4 on degree of extraction E110 ($2{,}2 \cdot 10^{-5}$ mol / l), the concentration of the solution OP-10 - 10%. Turbidity of solutions was observed when adding 0,80 g of crys-

talline Na_2SO_4 to 10 ml of 10% solution of the OP-10. Increase in mass additives to 0,86 g does not affect the physical and chemical parameters of the exfoliation. The volume ratio of the aqueous and micellar phases is preserved. However, with increasing salt concentration from 0,80 to 0,86 g increases the distribution coefficient and degree of extraction of dye E 110 (Fig. 2).

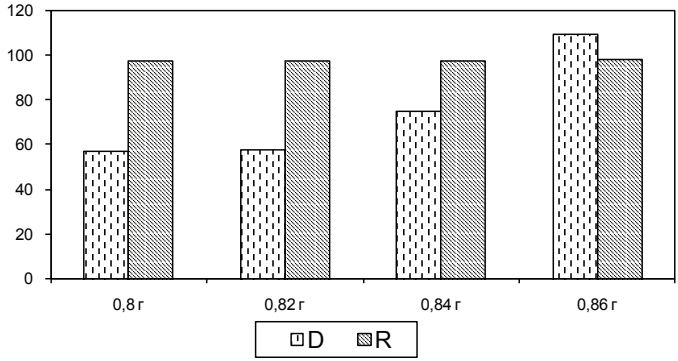

Fig.2. The influence of the mass of Na_2SO_4 on the distribution coefficient (D) and the degree of extraction (R,%) in the phase of the dye E110 OP-10 at 25 ° C.
C (OP-10) = 10%, C (E110) = $2,2 \cdot 10^{-5}$ mol / l.

As seen from the data, with increasing mass of salt increases degree of extraction and distribution coefficient. Almost complete extract of dye E110 from aqueous solutions (R > 98%) achieved by adding 0,86 g Na_2SO_4 to 10 ml of a solution containing 10% OP-10.

We investigated the possibility of extracting the point cloud of food dye yellow "sunset" in the temperature range 20-25 ° C in the system (OP-10) - Na_2SO_4-H_2O. The optimal extraction conditions (C (OP-10) - 10%, m (Na_2SO_4) - 0,86 g, volume - 10 ml), under which the distribution coefficient and the degree of extraction is 109,6 and 98,6%, respectively.

REFERENCES:

1. *Кущевская Н.Ф., Горбачевский А.Н., Дорощук В.А., Куличенко С.А.* Мицеллярно-экстракционное концентрирование микрокомпонентов фазами неионных ПАВ при температуре помутнения // Химия и технология воды. – 2008.- Т.30. № 5. С. 521-543.
2. *Чернова Р.К., Шестопалова Н.Б., Козлова Л.М.* Некоторые аспекты влияния электролитов на фазовое разделение и «cloud point» экстракцию азорубина в системе (ОП-10)-H_2O // Известия Саратовского университета. Серия Химия. Биология. Экология. – 2012. – Т.12. вып.4. С.11-16.

SYNTHESIS OF COPPER-CONTAINING BIOCIDAL NONWOVENS BASED ON POLYVINYL ALCOHOL

E.M. Soldatenko, S. Yu. Doronin, R.K. Chernova, Yu.E. Sal'kovsky, D.A. Bokova

Saratov State University

Nowadays, searching for new antibacterial drugs alternative to antibiotics is one of the most urgent tasks (Egorova E. M., Revina A.A, Rostovshchikova T. N., Kisileva O.I, 2001). Copper compounds have antibacterial properties, and their antimicrobial properties can be amplified by reducing the size of copper particles (10–100 nm). Materials with copper nanoparticles can acquire new functional features. Copper nanoparticles can be used in medicine: in antibacterial coatings of biomedical devices, antimicrobial packaging, to fight wound infections and skin diseases (Antonov S. F., Paramonov B. A., Dobritsa V. P., Ribalchenko O. V., Shliakov A. M., 2008). The application of copper nanoparticles on medical dressings is a way of obtaining new materials with antibacterial properties. Studying the influence of various matrices on the nanoparticles attached to them is also of interest.

This work presents our results of producing nanoscale copper particles by chemical means and fixing them on a matrix of nonwoven polymer composites.

Explored were variants of obtaining copper nanoparticles at varying the nature and concentration of the reducing agent ($NaBH_4$, $C_6H_8O_6$), the concentration of copper acetate, as well as pH and in the presence of a surfactant.

It has been spectrophotometrically found that copper particles of larger sizes are formed in the system $[(CH_3COO)_2Cu]$: $[NaBH_4]$ at low concentrations of the reducing agent. However, in these conditions, they are rapidly oxidized due to the lack of the reducing agent in the reaction system. This agent is hydrolyzed at a high rate at these concentrations. At higher concentrations of the reducing agent, smaller nanocopper particles are formed, which eventually aggregate and are oxidized, but their lifetime increases (an excess of $NaBH_4$).

When ascorbic acid is used as a reducing agent, copper reduction effectively proceeds even at its low concentrations (Obraztsova I. I., Simenyuk G. Yu., Eremenko N.K, 2006.). In the first minutes of the reaction, a copper–ascorbic acid complex is formed, which undergoes some redox process with the formation of ultrafine copper and the oxidation products of ascorbic acid. The 1.5 excess of ascorbic acid is the optimum molar ratio of $[(CH_3COO)_2Cu]$:

[$C_6H_8O_6$], as evidenced by the optical density growth within the range of 450–650 nm (Fig. 1). In this case, the stability of copper nanoparticles to oxidation is higher in comparison with the particles obtained by borohydride reduction. For further production of composite materials, a system of obtaining copper nanoparticles with ascorbic acid was used.

Previously, we studied the antimicrobial activity of ultrafine copper powder samples with respect to the clinical strain of Staphylococcus aureus with the laboratory code number 92 (Doronin S. Yu., Chernova R. K., Alipov V. V., Beloliptseva G. M., Lebedev M. S., Shapoval O. G.). For these purposes, a copper powder suspension (2 mg / ml) in physiological solution of sodium chloride was used for getting working concentrations of 1,000, 100, 10, and 1 μg / ml, respectively. The microbial load was 3×10^4 microbes / ml (McFarland turbidity standard). The results obtained showed that the copper nanoparticles exhibited biological activity at concentrations above 10 μg / ml.

Nonwoven fabrics were produced on a laboratory device for nanofiber material electrospinning Nanospider NSLAB 200S (Elmarco s.r.o., Czech Republic). Fig. 2 shows electron micrographs of the original nonwoven material based on poly (vinyl alcohol) and of the copper-containing nonwoven material. One can see that the average fiber diameter of the material is in the range of 100–500 nm (Fig. 2a).

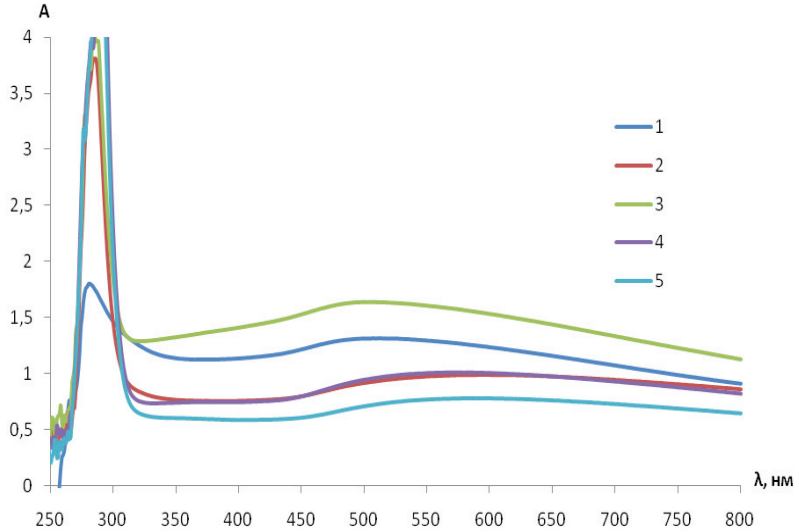

Fig. 1. Electronic absorption spectra of the Cu $(CH_3COO)_2$ – $C_6H_8O_6$ system. *c* (Cu^{2+}) = 1.4 mM, *c* ($C_6H_8O_6$): 1– 0.7, 2–1.4, 3–2.1, 4–2.8, 5–4.2 mM. Response time is 40 min.

The copper content was within 4.5–13%, and the particle size was in a range of 50–200 nm. The photographs were obtained on an electron microscope MIRA 2 LMU (Tescan s.r.o., Czech Republic) in the mode of dispersion analysis.

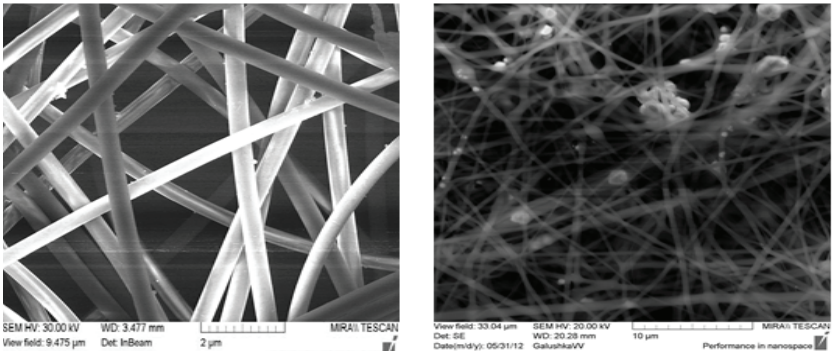

Fig. 2. Photomicrographs of our nonwoven material based on poly (vinyl alcohol) (*a*) and that with embedded ultrafine copper particles obtained by reduction of copper acetate with ascorbic acid (*b*).

Thus, this study can be considered as a way of producing antibacterial materials for medical or other purposes.

REFERENCES:

1. *Egorova E. M., Revina A.A, Rostovshchikova T. N., Kisileva O. I.* Bactericidal and catalytic properties of stable metal nanoparticles in reverse micelles. // Bulletin of Moscow University. Series 2, Chemistry, 2001. – Vol. 42. – № 5. – P. 332–338.
2. *Antonov S. F., Paramonov B. A., Dobritsa V. P., Ribalchenko O. V., Shliakov A. M.* Biocompatible compounds containing silver nano-clusters useful for treating burns and ulcers: study of safety and bioactivities и др. // Materials of the Fifth International Conference on Science and Business: Science and Training for Biosafety. 2008. Vol 1. P. 134–135.
3. *Obraztsova I. I., Simenyuk G. Yu., Eremenko N. K.* Preparation of ultradisperse copper powders by reduction of copper salts with L-ascorbic acid and electrically conducting formulations based on these powders // Russian Journal of Applied Chemistry. 2006. Vol. 79. № 5. P. 707-710.
4. *Doronin S. Yu., Chernova R. K., Alipov V. V., Beloliptseva G. M., Lebedev M. S., Shapoval O. G.* Synthesis and bactericidal properties of the ultradisperse powder of copper. // Proceedings of Saratov University. Chemistry. Biology. Ecology. 2011. Vol.11. № 1. P.18–22.

WEBSITE AS AN INSTRUMENT OF INFORMATION MANAGEMENT

V.A. Solovyova

Saratov State University

The importance of information management is growing every day. Development of civilized countries is aimed towards formation of the information society – a society in which the majority of workers are engaged in production, collection, storage, processing and use of information, particularly in its highest form – the form of knowledge.

In connection with this, it is evident that effective management is needed at all stages of the life cycle of information. The efficiency of this management may be said to determine the ownership of technological innovation to a considerable extent.

The companies should use a competitive advantage – powerful and effective information system allowing to create, accumulate and use operational and full information. «A good management information system will only reap the benefits if the companies gain insight to better align strategies and identify critical relationships and gaps along four key company dimensions – people, process, culture and infrastructure» (1). The inattention to quality and efficiency of information systems causes loss of positions.

Nowadays the Internet is one of the most important sources of information. The companies begin to use its sources more and more. Global information network has penetrated almost in every aspect of human life and business. A new system of global commerce is compiled over the Internet and unites sellers, buyers and brokers in a trading community. The Internet can be seen as a new «environment of the information society».

The growing popularity of the Internet is due to the fact that the use of this technology can be implemented almost in all business processes via electronic form to buy and sell products and services, to invest, to get information, to enter into agreements, etc. This point of the Internet is associated with an avalanche development of e-commerce.

The Cisco's investigation revealed that one of three students and young professionals consider the Internet an important and original essential for recourses like air, water, food and crib.

The Cisco Connected World Technology Report also demonstrated that more than a half of the respondents in the research can't live without the In-

ternet and see it as «an inherent part of their lives» – in some cases even more important than cars, dating and parties (2).

There are various kinds of information on internet sites, portals, blogs, etc. We are going to speak about websites.

A website is a collection of web pages, images, videos or other digital resources that are addressed with a common domain name or IP address on an Internet Protocol network (3). The main features of every site are:

– web page;

– logical link between the pages;

– overall design;

– the existence of cross-references.

Today a website is the face of a company or organization. It is also a simple way to provide information to all interested parties. Website is an important part of company's image. "Personally, I think institution's website is a reflection of the organization," says Terry Calhoun, director of media relations at the Society for College and University Planning (4).

Website can be useful for the department of the University since it is the main resource from which anyone can get the needed information at any time, from any location. For example:

– school leavers and their parents will be able to get the information they need;

– all students can receive relevant information;

– students enrolled in a similar profession may find the information they need, or transfer, or reach to postgraduates supervision;

– work within the department can be reorganized and improved;

– interested parties receive the latest news;

– well designed website can be a cause for pride.

To make the website competitive continuous improvements are needed. There is a great variety of quality tools for these purposes, for example seven basic tools of quality.

A brainstorming session with representatives of the 471 group was held to identify the needs and desires of the students on department's website filling. Its results are shown on the Ishikawa diagram (Fig. 1).

We delimited the items we have on the website of Nano- and Biomedical Technology Department, the most potential and interesting items that we can implement on the site and some unrealistic items. Then we interviewed the lecturers and several groups of students about the most potential and interesting items.

Students mostly chose the variants «Reviews of graduates about the possibilities of employment with received specialty» (more than 85%) and «Information about the curriculum " (near 80%).

The majority of lecturers chose the variants "Reviews of graduates about the possibilities of employment with received specialty» (near 90%, «Information about the curriculum " (more than 80%), "Inverse links with lecturers» (nearly 70% while only 30 percent of students chose this variant).

It is important to take into consideration both opinions of students and lecturers and to implement chosen items. As a result the site will be more informative, convenient, effective and usable.

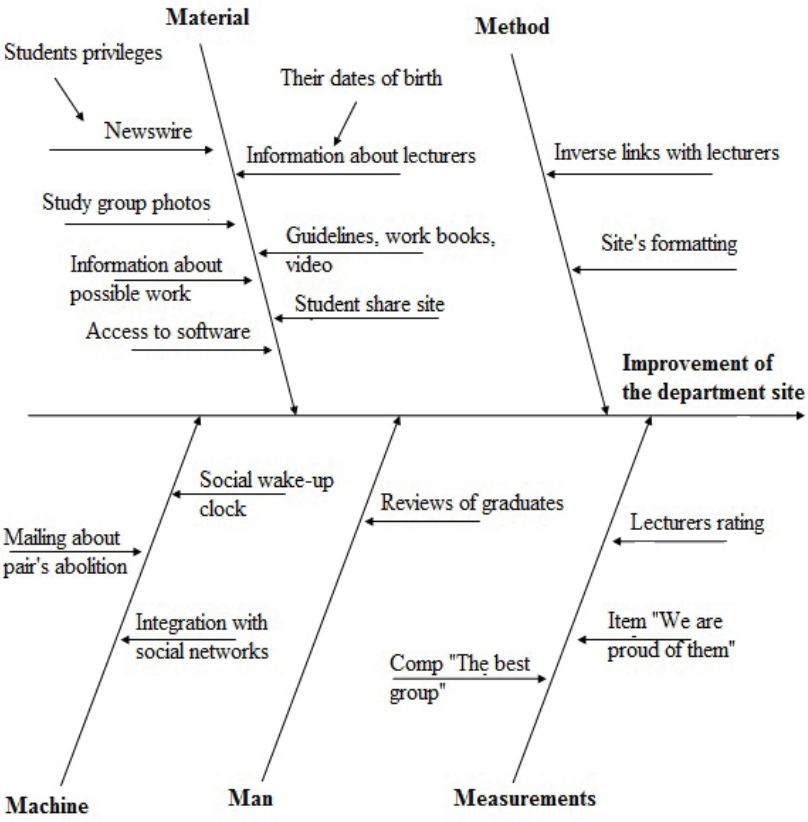

Fig. 1. Needs and desires of students on department's website filling.

In this article we analyzed the importance of information management and website as its instrument. Also we gave consideration to the department site and showed a few methods that could be used to improve it.

REFERENCES:

1. The Importance of a Good Information Management System [Электронный ресурс] // Blue Avenue Associates: [сайт]. URL: http://www.blueavenueassociates.com/insight-resources/online-resource-center/insights/importance-good-information-management-system (дата обращения 14.03.2013)
2. Cisco Connected World Technology Report [Электронный ресурс] // Cisco: [сайт]. URL: http://www.cisco.com/en/US/netsol/ns1120/index.html (дата обращения 14.03.2013)
3. Different Kinds of Website [Электронный ресурс] // Rose India Technologies Pvt. Ltd: [сайт]. URL:
http://www.roseindia.net/services/webdesigning/corporatewebsitedesign/Different-Kinds-of-Website.shtml (дата обращения 14.03.2013).
4. *Kolowich S.* No Laughing Matter [Электронный ресурс] // Inside Higher Ed: the online source for news of higher education. URL: http://app3.insidehighered.com/layout/set/popup/news/2010/08/04/websites (дата обращения 14.03.2013).

CELLS MORPHOLOGY INVESTIGATION IN WHOLE BLOOD SMEARS BY DIFFRACTION PHASE MICROSCOPE

N.A. Talaykova[1], A.L. Kalyanov[1], V.V. Lychagov[1], V.P. Ryabukho[1,2]

[1] Saratov State University
[2] Institute of Precision Mechanics and Control, Russian Academy of Sciences

INTRODUCTION:

Diagnosis for diseases of blood and blood-forming organs was set or confirmed for 1,288,460 people according to the statistics of the Ministry of Health of the Russian Federation (Aleksandrova G. A. et al., 2012). A change in morphology RBC measure of complete blood count is known and used in many countries around the world. Full blood count is essential for establishing a diagnosis of blood diseases.

At the present time there is a large number of techniques, which allow to measure the morphology of red blood cells (Ikeda T.et al, 2005; Mir M. et al., 2009; А. О. Таганов и др, 2011*)*. Diffraction phase microscopy is presented in this work. Diffraction phase microscopy is a method of optical microscopy,

which also allows measurement of cell morphology. However, each method has its own characteristics. Features of the diffraction phase microscopy will be described further in this paper.

The purpose of this work is to measure red blood cell morphology and its characteristics, which are used by physicians to detect abnormalities in the tissue and diagnosis.

DESCRIPTION OF EXPERIMENTAL SETUP DIFFRACTION PHASE MICROSCOPE:

Diffraction phase microscope (DPM) is an optical microscope, in which the diffraction phase module is installed in image plane (Талайкова Н. и др., 2012). Image of the object, resulting in the microscope, is combined with the image of the interference picture produced by the diffraction phase module in the plane of the detector matrix. Experimental setup DPM with double low-coherence lighting system is shown in Fig.1. We have combined both transmitted light and reflected light illumination schemes to make simultaneous measurements of relief and optical thickness of the object.

In case of transmitted-light illumination we have used green LED (λ_0 = 530 nm, $\Delta\lambda$ = 20 nm). Light from this low-coherent source is collimated by condenser and passes through the object (transmitted light). Then microobjective and tube lens construct an image of the object in the back focal plane of the latter (diffraction grating plane).

A feature of DPM is the principle of optical field division – the light diffracted by a diffraction grating generates diffraction orders. Only two orders pass through the spatial filter (spatial light modulator).One of them (+1 on Fig. I) contains complete data about the object and names object arm. Reference interferometry arm is zero-order, which filter spatial light modulator. Lens L1 and L2 form a 4-f system.

In case of reflected-light illumination we use red LED (λ_0 = 630 nm, $\Delta\lambda$ = 20 nm). This light is collimated by collector, condenser and microobjective (MO), reflected by the object, and keeps the data about it. Then reflected light, similarly to transmittion light, microobjective and tube lens construct an image of the object in the back focal plane of the latter (diffraction grating plane).

A light wave passing through a phase object, such as human blood cells, undergoes a phase change (amplitude-phase modulation), which is caused by the difference in refractive indices between the object and the environment and is shown in the curve of the interference fringes (Диков и др., 2012*)*.

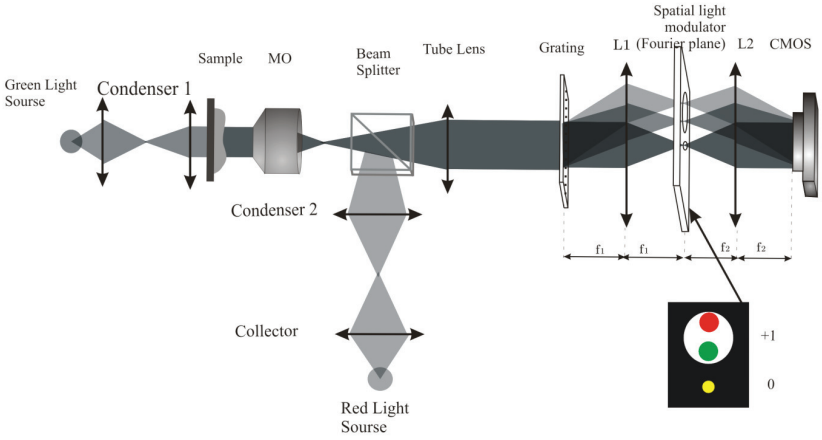

Fig. 1. DPM experimental setup with double low-coherence lighting systems. MO-microobjective, L1, L2 – lens, CMOS – CMOS-camera.

ALGORITHM PROCESSING INTERFEROGRAMM AND OBTAINING RESULTS:

The recorded interference picture (Fig.2 a) is converted into a phase portrait using the Hilbert transform (Popescu G. et al, 2005). The phase portrait results after the application of the operation sweep phase and detrend, and describes the change in optical thickness (COT) of the object. Phase of the object wave and this wave propagation across the entire image (phase map) has quantitative data about the object of study. All the morphological characteristics of the change in the optical thickness can be calculated from the quantitative information obtained from the phase object map.

The methods used to calculate the three dimensional parameter are volume COT RBC, and parameter COT, which were written on LabView. It calculates the test object data, for example, the change in optical thickness. From these data the three-dimensional map of the phase is constructed (see Fig. 2 b).

RBC volume is calculated after obtaining the phase map. This creates a «mask» that is superimposed on the original image, keeping only the red blood cell, which you need to obtain data from. The sum of the remaining values of the phase map is the volume of the object. Results of this calculation for each RBC sum for a large number of RBC. Then this sum is divided by the number of treated cells. As a result we have one of the erythrocyte indices – MCV. The shape of the volume distribution and its relative modifications with respect to

normal conditions have been widely used for clinical diagnosis and turn out to be a reliable indicator of various physiological conditions ranging from anemia and vitamin B12 deficiency to nicotine and alcohol addiction (F. Charriere et al., 2007).

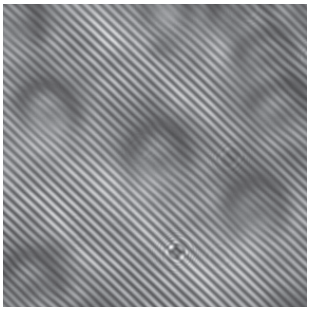

Fig. 2 a. Interferogram with RBC, obtained by diffraction phase microscope

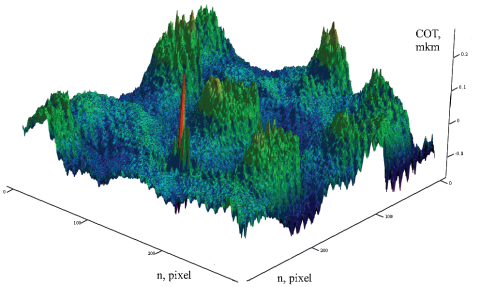

Fig. 2 b. Phase map has quantitative information about the object of study

The studies were carried out on 27 erythrocytes in whole blood smear 3 patients. Mean of COT is shown in Table I. The volume (V) is related to the COT as:

$$V = \frac{COT}{n_{erit} - n_0}, \quad (1)$$

where n_{erit} is the index of refraction RBC, n_0 – index of refraction environment.

Table I

Experimentally measured mean values of COT

	P1	P2	P3
Mean of COT, μ^3	3.51±0.32	3.6±0.42	3.69±0.4

In conclusion, we carry out measurements of erythrocyte COT by diffraction phase microscope. In this paper we give the formula for RBC volume measurement, and algorithm of recalculating the volume of MCV.

REFERENCES:

1. *Александрова Г. А. и др.* Заболеваемость всего населения в 2011 году. Статистические материалы. Часть I. 2012.

2. *F. Charriere et al.* // Opt. Lett. 2007. Vol. 32. P. 2456–2458.
3. *О. В. Диков, С. А. Савонин, В. И. Качула, О. А. Перепелицына, В. П. Рябухо* // Известия Саратовского университета. 2012. Т. 12. Сер. Физика, вып. 1. С. 13–17.
4. *Ikeda T., Popescu G., Dasari R., Feld M.* // Opt. Lett. 2005. Vol. 30. N. 10. P. 1165.
5. *Mir M., Wang Z., Tangella K., and Popescu G.* // Opt.Exp. 2009. Vol. 17. No. 4. P. 2579–2585
6. *Н. А. Талайкова, А. Л. Кальянов, В. В. Лычагов, В. П. Рябухо, и др.* // Проблемы оптической физики и биофотоники SFM-2012. 2012. С. 8-10.
7. *А. О. Таганов, А. В. Кретушев, Т. В. Вышенская, М. А. Стенина, Л. И. Кривов, В. П. Тычинский* // Сборник научных трудов НИЯУ МИФИ. 2011. С. 13–14.

CONTROL OF RBC FORMATION BY THE METHODS OF INTERFEROMETRIC MICROSCOPY

Y.V. Tarakanchikova, N.V. Tkachenko, V.V. Tuchin

Saratov State University

INTRODUCTION:

At the Department of Optics and Biophotonics, Saratov State University, we investigated photodynamic haemolysis of RBC sensibilized by carbon nanoparticles Astralene™. Initially, stable suspension of hybrid carbon nanoparticles based on Astralene™ sensitized nanographene in saline solution was developed. Further features of mechanism of photohetnolysis it for laser radiation (λ = 532нм) of rat RBC suspension sensitized by hybrids carbon nanoparticles was studied.

The purpose of our work is the research of dark interaction carbon nanoparticles of fulleroid types with RBC using digital holographic microscopy (DHM)

METHODS AND MATERIALS:

We took 50mg powder of Astralene™ and added it to 5 ml basic solution of nanographene. We obtained the basic suspension of hybrid nanoparticles. Basic suspension was diluted to physiological saline solution (0,9% NaCl) The solution was diluted 512 times to a concentration of 1.95 10-3C. Research of dark interaction of carbon nanoparticles with membranes of cells was studied with RBC of a rat. We took 4 ml of physiological saline solution and added it to 20 mcl of RBC suspension. Thus suspension of RBC 0.5% was developed (1).

Microscopic observation of dynamic of a form and the size of rat RBC at their dark interaction with suspension of hybrid nanoparticles was carried out

on a digital holographic phase microscope. The technique of the DHM carries out qualitative and quantitative estimate of the form and the internal structure of the transparent biological microscopic objects (Kemper B., von Bally G. 2008, Christopher J. Mann, Lingfeng Yu and Myung K. Kim, 2006).

The optical scheme of DHM is exhibited in Fig.1. The different feature of the scheme is rotary mirror. This is mirror turns the object and reference wave of light straightens up, which allows to place the monitoring phase micro-object in a horizontal plane [4].

The developed software allows realizing procedures of numerical reconstruction of complex amplitude and intensity of an objective field in a plane of image, from the written down digital hologram, and also the subsequent multiexposition interference analysis of dynamics of change of phase object (Ганжерли Н. М., Гуревич С. Б., Катушкина Н. В., Константинов В. Б. и др., 1984).

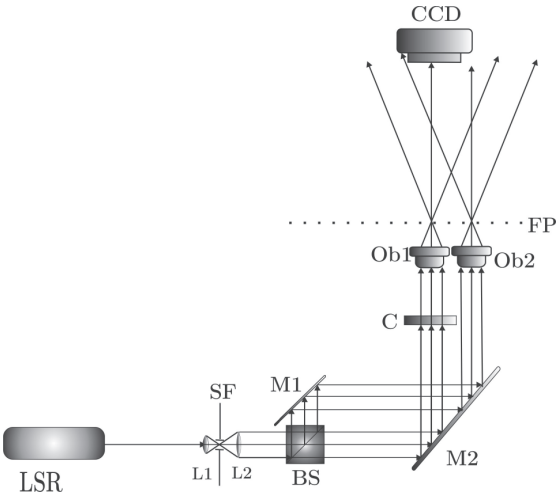

Fig. 1.The optical scheme of digital holographic microscope: LSR – He-Ne laser;BS –beam splitter;M1, M2 – turn mirrors; SF – spatial filter; L1-L2 – collimator; C – phase object; Ob1, Ob2 – microscope objectives; FP – focal plane of microscope objectives; CCD – digital camera.

RESULTS AND DISCUSSIONS:

A control of condition of RBC was measured with the help of DHM. Holographic images of rat RBC is shown in Fig.2. These images were obtained at various time intervals after mixing the suspension of RBC and nanoparticles.

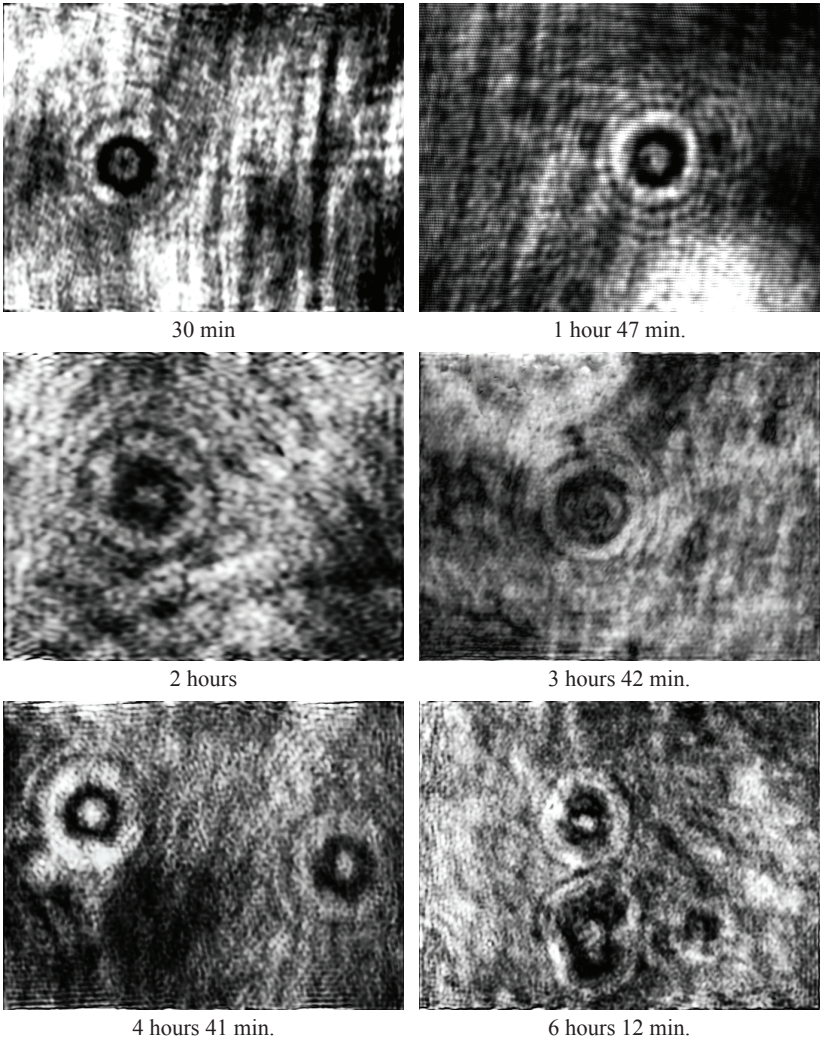

Fig.2.Holographic images of rat RBC was obtained at various time intervals after mixing the suspension of RBC and nanoparticles.

During the experiment, the sedimentation of carbon nanoparticles to membrane in area of concavity of RBC disc was observed. The size of RBC increased slowly on a time interval of 1 hour 47 minutes. Darkening of out-

side path of RBC membrane took place in a time interval of 4 hours 41 min (Ian J. MacDonald, Tomas J. Dougherty, 2001). It is possible to assume that it is bound to both redistribution of the adsorbed nanoparticles and to change of local adhesion properties of a membrane. These processes were accompanied by a lysis of RBC membranes with a release of cell contents and formation of empty membranous envelopes. (Bilgin M. D., M-Ali Al-Akhrast, M. Khalili, H. Hemmati, L.I., 2001; Leonard I.).

CONCLUSIONS:

The methods of DHM for control of changing conditions of membrane, size and shape of RBC were developed. The size of cells increased for time domain 1–3 hours. At the time of dark interaction of red blood cells with nanoparticles of 6 hours (when a steady decrease of the optical density starts) in observed suspension the appearance of red blood cells were lysis, and the formation of aggregates of RBC.

REFERENCES:

1. RusNanoNet http://www.nanoteh.ru/p2.html
2. *Kemper B., von Bally G. //Digital holographic microscopy for live cell applications and technical inspection //* Appl. Opt., 2008, Vol. 47, № 4, P. 52–61.
3. *Christopher J. Mann, Lingfeng Yu and Myung K. Kim // Movies of cellular and subcellular motion by digital holographic microscopy //* BioMedical Engineering OnLine, 2006, **5**:21 doi:10.1186/1475-925X-5–21.
4. *Соколов М. Э. // Современные методы визуализации фазовых объектов. Голографические методы и аппаратура, применяемые в физических исследованиях.//* М: Наука 1987.249 с.
5. *Ганжерли Н. М., Гуревич С. Б., Катушкина Н. В., Константинов В. Б. и др. // Применение методов оптической обработки изображений.//* Л., 1984. С. 88-90.
6. *Ian J. MacDonald, Tomas J. Dougherty // Basic principles of photodynamic therapy. J. Porphyrins Phthalocyanines//*, 2001, V. 5, p. 105-129
7. *Bilgin M. D., M-Ali Al-Akhrast, M. Khalili, H. Hemmati, L.I. // Grossweiner. Photosensitization of red blood cell hemolysis by Lutetium Texaphyrin. //* Photochem. Photobiol, 2000, V. 72(1), p. 121–127
8. *Leonard I.* Grossweiner. *//Photosensitization of Red Blood Cell hemolysis: A brief review. 1999, Internet Photochemistry&Photobiology. An international forum for virtual conferences //* http://www.photobiology.com/reviews/5/index.htm

A FAST AND EFFICIENT WAY TO OBTAIN LITHIUM-IRON PHOSPHATE WITH EXCELLENT ELECTROCHEMICAL PERFORMANCE

A.V. Ushakov

Saratov State University

Lithium-ion batteries (LIBs) are the most capacious commercially realized rechargeable electrochemical systems. LIBs provide longer operating time of the low-power portable devices such as mobile phones, e-books, notebooks. The electrochemical and operational characteristics of the battery primarily depend on the properties of the electrode materials. Lithium-cobalt oxide, traditionally used as a material for the positive electrode of the LIBs, is quite electric capacity material and its synthesis is not burdened with special difficulties. However, the high cost and toxicity of the initial substances and the material itself, danger of the quick charge or discharge determine that it cannot be used in large-size batteries for high-power devices such as electric motors.

The use of lithium-iron phosphate with the olivine structure will avoid these difficulties. However, the low electronic conductivity and the low diffusion coefficient of lithium ions are characterized for the pure $LiFePO_4$. The improvement of conducting properties is possible 1) by reducing the particle size of the material, 2) by the addition of substances with a high conductivity, 3) by making defects by heterovalent ions doping, and 4) the modification of the synthesis. Application of the most available iron oxide (III) for the $LiFePO_4$ synthesis can reduce significantly the cost of the desired material. Carbon is advisable to apply as a reducing agent for simultaneous conductive coating on the surface of $LiFePO_4$ particles and to control their agglomeration. Therefore, the carbothermal reduction method is selected as basis for developing a methodology for the synthesis.

Mechanical activation of starting materials mixture (lithium carbonate Li_2CO_3, iron oxide (III) Fe_2O_3, ammonium dihydrogen phosphate $NH_4H_2PO_4$ in the stoichiometric ratio, varying amounts of acetylene black and acetone) allows to reduce the time of heat treatment significantly. Activator mill AGO-2 used to perform this operation. Annealing of the dry mixture implemented in a tube furnace under an argon atmosphere at different temperatures and for different times to identify the optimal conditions of heat treatment. The phase composition of the products was controlled by X-ray diffraction anal-

ysis. The single-crystalline primary particles size was estimated by Debye-Scherrer equation, corundum was used as a standard with the particle size of 100 nm. The size and the shape of particles were determined using scanning electron microscope images. The evaluation of carbon weight fraction of the $LiFePO_4$/C material was implemented by defining insoluble residue at boiling in 37% HCl solution.

The electrochemical cycling performance of $LiFePO_4$/C powders was tested with electrochemical cells using metallic lithium film as the counter and reference electrode. The cells are based on the configuration of Li metal (−)|electrolyte|$LiFePO_4$ (+) with a liquid electrolyte (1M solution of $LiClO_4$ in propylene carbonate– dimethoxyethane (7:3, v/v). Slurries composed of 80 wt.% $LiFePO_4$/C with 10 wt.% acetylene black and 10 wt.% PVDF binder in N-methylpyrrolidone or 90 wt.% $LiFePO_4$/C with 10 wt.% PVDF binder were prepared, which were deposited on current collectors of aluminum foils by blade. The electrode was dried at 120 °C for 12 h before electrochemical evaluation. Cell assembly was conducted in a glove box filled with pure argon. The charge/discharge characteristics of the cells were recorded over the potential range between 2.6 V and 4.0V at different range of 0.1C –5C (1C = 170 mAh/g) at -10–55 °C. Cyclic voltammetry tests were performed over the potential range of 2.6–4.0V at the scanning rate 0.02–0.5 mV/s.

According to the X-ray diffraction data, the samples obtained by heat treatment above 600 °C are the phase-pure olivine $LiFePO_4$. Figure 1 shows the results of the electrochemical test of sample obtained by annealing at 750 °C for 3 hours. Olivine $LiFePO_4$ obtained under these conditions of synthesis has the best electrochemical properties. The carbon mass fraction in the sample is 11.0 wt.%. The coherence length for the sample is 65 nm.

The results match the performance of the best samples reported in many prior works. The reversible capacity is 157 mAh/g at 0.1 C and 65 mAh/g at 5 C (Fig. 1*a*); the voltage as a function of the lithiation/delithiation rate has a plateau at 3.4V, characteristics of the phase separation between Li-rich and Li-poor phases in well-crystallized samples. Fig.1*b* shows the principal need to introduce conductive additive despite the presence of carbon in the material $LiFePO_4$/C. The electrode with 10 wt.% acetylene black no degrades even at 1 and 5 C.

Cyclic voltammetry method makes possible to calculate the diffusion coefficient D of electroactive species using the linear dependence of the peak current on the square root of the potential sweep rate (Fig. 1*c*) and using the following expression for a reversible process (Churikov et al., 2008):

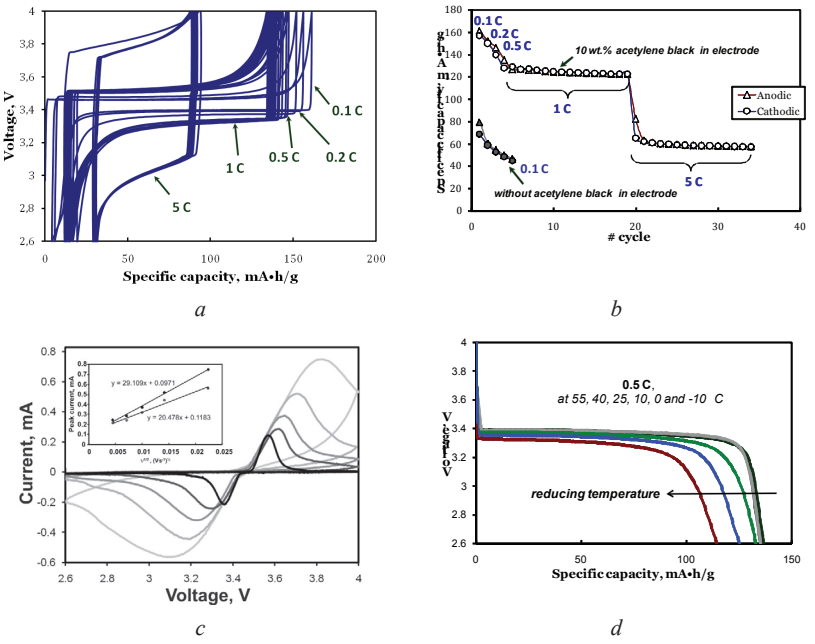

Fig. 1 (a) The galvanostatic cycling curve of the $LiFePO_4$/C sample at 25°C. **(b)** Cycling of $LiFePO_4$/C electrode (discharge rate = charge rate) with 10 wt.% acetylene black or without it. **(c)** Cyclic voltammograms of the $LiFePO_4$/C electrode at the scan rates of 0.02, 0.05, 0.1, 0.2, 0.5 mV/s between 4.0 and 2.6V and a linear relationship between peak current and square root of the scan rate. **(d)** The discharge curves of the $LiFePO_4$/C composite at 0.5C at various temperatures varied from -10 to 55 °C.

$$j_p = 0.4463\nu^{1/2}\frac{nz^{1/2}F^{3/2}}{R^{1/2}T^{1/2}}c_0 D^{1/2}.$$

This analysis gives the average estimate of the diffusion coefficient, which is assumed to be constant in the used range of potentials. For the cathodic process $c_0 = c_{Vac}$ is an initial concentration of available to fill vacancies for lithium ions in Li_xFePO_4. Anodic current $c_0 = c_{Li}$ is initial concentration of dissolving lithium in structure of $Li_{1-x}FePO_4$ (stoichiometric composition $LiFePO_4$ corresponds to the value $c_{Li} = 0.0228$ mol/cm^3).

The anodic and cathodic voltammograms give the same average coefficient of lithium diffusion $D = 3\cdot10^{-12}$ cm^2/s if $c_{Li} = 2^{½}\, c_{Vac}$. This value is near the upper limit of the range of values reported in most experimental studies (about

$10^{-11} \div 10^{-17}$ cm^2/s) (Churikov et al., 2010; Gopi Krishna Phani Dathar et al., 2011). High transport characteristics of discussed cathode material $LiFePO_4/C$ explain its ability to withstand the acceleration of the charge and discharge at low temperature (Fig. 1*d*).

ACKNOWLEDGMENTS:

We thank the Russian Foundation for Basic Research (project #13-03-00492) for financial support.

REFERENCES:

1. *ChurikovA.V., Ivanishchev A. V., Ivanishcheva I. A., Zapsis K. V., Gamayunova I. M., Sycheva V. O.* Kinetics of electrochemical lithium intercalation into thin tungsten (VI) oxide layers // Russian Journal of Electrochemistry. 2008. V. 44, № 5. PP. 530 – 542.
2. *Churikov A. V., Ivanishchev A. V., Ivanishcheva I. A., Sycheva V. O., Khasanova N. R., Antipov E. V.* Determination of lithium diffusion coefficient in LiFePO4 electrode by galvanostatic and potentiostatic intermittent titration techniques// Electrochim. Acta. 2010. V. 55. PP. 2939 – 2950.
3. *Gopi Krishna Phani Dathar, Sheppard D., Stevenson K. J., Henkelman G.* Calculations of Li-Ion Diffusion in Olivine Phosphates // Chem. Mater. 2011. V. 23. PP. 4032–4037.

DYNAMICS OF FLOOD PLAIN GEOSYSTEMS OF VOLGOGRADSKOE RESERVOIR

V.A. Zatonsky

Saratov State University

This article provides some research experience concerning flood plain geosystems on the area from Saratov to Marks. From 2006 to 2012 complex landscape-ecological studies were carried out by the stuffs and students of geografical an biological faculties of Saratov state university on this area of the Volga flood plain.

To understand the research object clearly we should give its brief physical and geografical characteristics in brief. Before creating of the hydro electrical station cascade the Volga velocity had been about three or four km per hour (near the city of Saratov). The Volga river carried out about 25 mln tons of sediment and 40-50 mln tons of dissolved mineral substance. The Volga stream was very narrow and winding and it didn't allow ships with large tonnage capacity pass throught. The river widely overflowed in spring and became shal-

low by the end of summer. New shoals appeared every year. The islands were not numerous islands but they were large.

The Volga banks vary in character in this area. The right bank has high and disjointed relief. The left bank is represented with low and flat plain. The asymmetric structure of the valley causes the definites of banks's destruction. The right bank slopes are rather steep, they rise from 5-10 to 20-40 m above floodplain level. Behind the slope the bank line rises more slowly up to 200-350 m. The top of the left bank slope usually rises up to 1–7 m and only sometimes reach 10-16 m over the water. As a rule behind the top of the slope usually the flat plain stretches (1).

There is vast area of island floodplain estimated about 650 square km in Saratov region (Fig 1). The islands occupy about 27% of the whole area of the river lake like extension. The Volga practically did not come out of it banks after overflooding to the north of Marks, but to the south of Saratov the floodplain of almost islands was overflowed nearly all the islands and nowadays it has a conderisable width. Geologically and geomorphologically this territory refers to the quarter period and it took 10000 years to form it. The islands can be divided in to three parts accoding to their genesis.

1. The right bank watercourse floodplain (the rest of the overflowed right bank).

2. The central floodplain in the center of the watercourse (the territory that had always been islands before overflowing).

3. The left bank watercourse floodplain (the flooded left bank of the Volga.

The islands geosystems of the researched area line of all other floodplain landscapes are found to be very dynamic. The relief is constantly changing here as well as vegetation. But there are some insensitive to changes territories which have been preserving their state for decades.

After creating of the hydro-electrical station cascades the islands area decreased as much as dozens times. Most of the sandy beaches and shallows were flooded and the main part of forests suffered as well. Oak forests of middle floodplain are getting perished after the increase of ground waters level because of high level of moisture in the soil. The oak forests were changed with willow and aspen trees as they more tolerant to water. Besides, ecosystems of inland island lakes have suffered dramatically as well.

Industry and agriculture of the region were widely enlarged after the creating of the reservoir. But at the same time the intensity of dangerous geological and geomorphological processes such as abrasion, landslides and flooding increased several times. Microclimatic conditions of the adjust territories and biodiversity have changed greatly. Particularly range of species of living

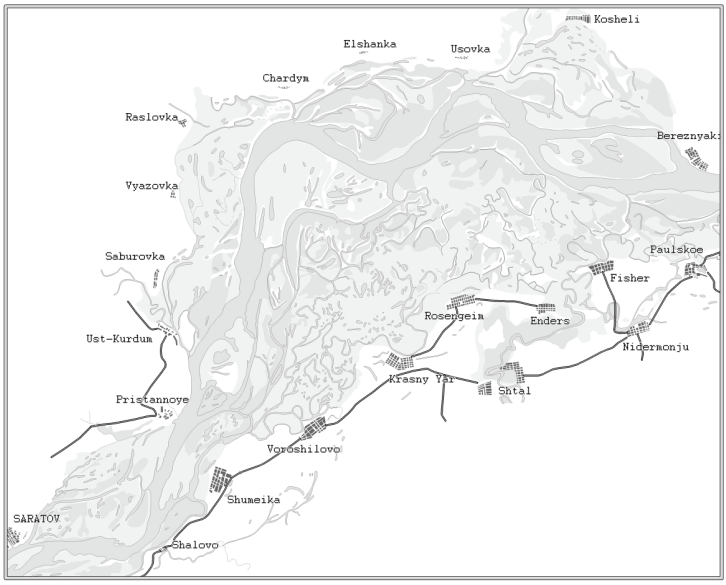

Fig 1. The Volga state in the beginning 20th and 21th centuries.

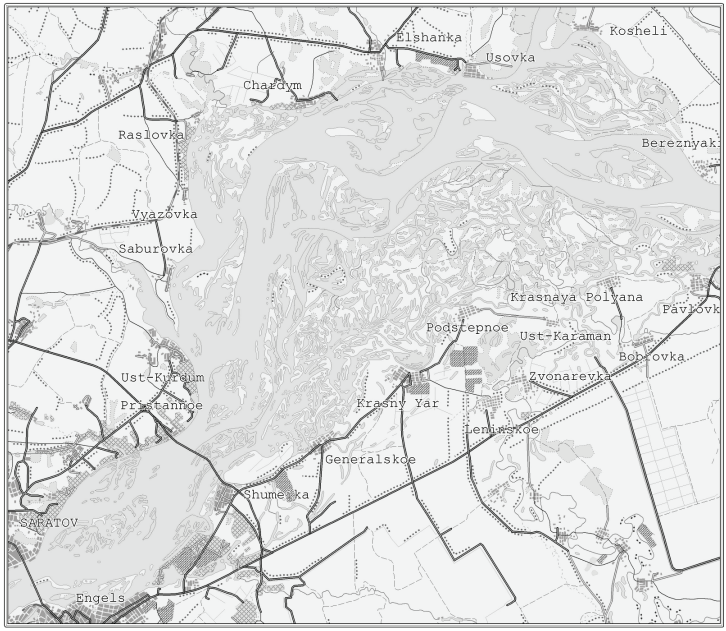

creatures, and fish populations of the floodplain decreased immensely as well. Recreation nature management improved but the river ability of selfclearing became very low. The silling of the Volga bed increased, but the silt is known to be a good sorbent for pollutants.

Until the 60 of the 20 century this natural territorial complex was subducted mainly to natural processes of floodplain creating and all the lanscapes component were under influence of watercourse and overflowing regime of the Volga. The proportion between soil-vegetational cover on the floodplain islands was the following: sands with rear vegetation -35%, meadow and meadow – steep vegetation -25%, forests -25%, the rest of the land – bushes and swamps -15%. Volgogradskoe reservoir has changed coexistence of watercourse processes, the level of overflowing, relations between different faces on islands. Nowadays 40% of floodplain is wooden vegetation, 20% – meadows, 30% – covered with cane and shallows, the rest 10% are sands and marshes (3).

About 30% of the territory was occupied by gardens, vegetable gardens, and grasslands before overflowing. But the recreation intensity wasn't considerable as there were other floodplain territories downstream opposite Saratov city. The forests arrays were subjected to cutting. There fish business existed. In the second half of the 20th century the structure of nature management was considerably transformed (Rodzevich N. N.,2003).

Developing of hydrocarbons mining worsened the ecological situation, and course decreasing of fish resources and excluded fishery here. Recreation intensity has increased greatly. Grasslands, gardens and orchars occupied significationly less area. Water transport influenced islands differently in different periods of time. If until 90 of the 20th century intensive large tonnage capacity ships movement facilitated destroying of islands banks situated on the root Volga. Nowadays this influence has almost disappeared because of sharp decreasing of the river fleet. At the present day there are only small sized crafts on the Volga (2; 5).

We can state that besides the main factor, which having changed the way of many landscape-forming processes on the researched area, name of created Volgogradskoe reservoir, the settlements and their recreation intencity influence geoecological situation of the Volga islands. Thus, dynamic change of floodplain landscape are subdinates both to the reseivour on one hand and total influence of the town ecology on the other hand (Zatonsky V. A., 2011).

The first factor leads to decreasing oak forests and increasing of the area with cane shallows, the second factor can lead to any littering territory till creating here national natural park projected by the state authorities.

The unique nature of floodplain lanscapes in Saratov region has been attracting attention of scientists for many years (7; 8). The 20th century has become crucial in the Volga river destiny. Namely during this period the Volga has become the object of multifaceted studies and at the same time the river image has changed greatly. The building of the Volga reservoirs cascade transformed the greatest European river thoroughly. The scientists gave lots of optimistic forecasts, concerning the river destiny, concerning recreation of its natural functions, but most of them have not come true. After two decades term for functioning those scientific forecast concerning the possibilities to reach a balance as well as possibility to stop abrasion failed.

REFERENCES:

1. Physiographic regions of the Lower Volga, Saratov, 1961.
2. WR Williams Selected Works, Vol. III, Scientific basis of grassland. Moscow: Academy of Sciences of the USSR, 1955.
3. Encyclopedia of the Saratov region. Saratov: «Privolzhskoye publishing house», 2002.
4. *Zatonsky V. A.* Volga floodplain landscape research as an example of. Green // Geology of the XXI century: Proceedings XII All-Russian scientific conference of students and young professionals. Saratov: Saratov State University in 2011. – S. 118–119
5. Scientific reading memory NF Reimers and FR Shtilmark. / / Anthropogenic transformation of the environment: Proceedings of the international. School-Seminar of Young Scientists (6–9 December 2011). Perm: Perm. State. nat. tests were performed. Univ., 2011. – 294 p.
6. *Rodzevich N. N.* Geo-ecology and environmental management. M. Bustard, 2003.
7. Report on the activities of the Volga Biological Station for 1905 Proceedings of the Volga Biological Station. Saratov, 1906 V.III, Issue 1. – 15 seconds.
8. Proceedings of the expedition for the study of Saratov University, Saratov and Volgograd reservoirs. No. I-VIII.

FOAM CONCRETE APPLICATION IN MANY-STORIED CONSTRUCTION

I.N. Zhakupova

Zhangir Khan West Kazakhstan Agrarian-Technical University

Construction of a many-storied building is today the main way of housing problem solution in the cities. It is a complex and responsible challenge, because the apartment house represents a difficult design. Special demands are made to construction of inhabited apartment houses (1). On the basis of geo-

logical researches, taking into account climatic features and a seismological situation, and also existence of own production of construction materials in the region the choice of the most optimum and economic technology of construction and a choice of construction materials is made. As the main problem of article is raised a question: it is possible to apply foam concrete block as a wall material at many-storied construction?

At construction of many-storied frame buildings foam concrete block is applied as a protecting design, a combination of its properties, namely: ease, zero water absorption, heat economic characteristics, convenience of processing allow to achieve good results (Akhmetov A. I., 2008). Wall products from cellular foam concrete make, as a rule, in the form of large blocks, all which allows to cope with a laying at construction from foam blocks even to one person. The big size and ease considerably simplifies and reduces the price of construction from foam concrete blocks. So, the speed of construction increases at 5-10 time, labor input – by 3–5 times, the economy of solution makes about 70%. The leading role is played here by quite low cost of technology in combination with unique properties of a material (Bagenov U. M.1983).

The important aspect in a question of construction of many-storied buildings with application of foam concrete blocks is dimension of thickness of external walls of the house and as climatic features of the built-up area. It is one of the most vital issues and to rely here on hearings and councils isn't necessary. Therefore it is necessary to use such calculation: by the formula given below we determine the demanded thermal resistance (R_{th}) of a wall for the West Kazakhstan region:

$$R_{\text{факт}} = \frac{1}{\alpha_{\text{в}}} + \frac{\delta}{\lambda} + \frac{1}{\alpha_{\text{н}}} = \frac{1}{8,7} + \frac{0,4}{0,21} + \frac{1}{23} = 2,06^2 \cdot °\text{C/Вт}$$

Where:

δ-thickness of a wall, m;

λ – coefficient of heat conductivity of a wall material, W/m • °C (see. Directory of the builder);

α_b, α_n – coefficients of a heat transfer of an internal and external surface walls, equal of respectively 8,7 and 23 W/sq.m • °C;

CONCLUSION:

As we see at the rate of the actual resistance of a single-layer wall from foam concrete blocks 400 mm thick and by density of D800 surpasses old standard indicators in heat savings, but doesn't satisfy to modern heat techni-

cal indicators toughening criteria according to heat preserving characteristics of protecting designs of buildings (Table 1).

Table 1

The actual resistance of single-layer protecting designs of walls from foam-concrete, gas-concrete blocks, R_{fact}, sq.m • °C/W.

Thickness of the wall, mm	Density of the blocksD, kg/m^3	Coefficient of thermal conductivity, Λ_0, Wt/m°C	Resistance of the wall, Rfact, m^2•°C/Wt
300	500	0,12	2,66
	600	0,14	2,30
	800	0,21	1,58
350	500	0,12	3,07
	600	0,14	2,66
	800	0,21	1,82
375	500	0,12	3,28
	600	0,14	2,83
	800	0,21	1,95
400	500	0,12	3,50
	600	0,14	3,01
	800	0,21	2,06

We take into account that settlement coefficient of heat resistance for external walls for the West Kazakhstan region: R_{acc} ~ 4,1 sq.m • °C/W. Apparently from the presented table blocks D500 400 mm thick density most close meet standards. From foam concrete blocks with a density less than 800 kg/m3 also it isn't recommended to erect the house without a monolithic framework. For construction of low houses to three floors possibly use of non-frame system with a density of gas-concrete D500-D600 blocks and foam concrete blocks D800 density.

We were convinced by a theoretical way that constructional solutions of single-layer external walls from foam-concrete blocks provide performance of modern norms on a heat-shielding.

Calculations showed that laying cost from high-precision foam-concrete blocks of not autoclave curing, executed with application of glue solutions, is 1,1–1,2 times cheaper, than the same products from autoclave foam concrete. Power consumption on production of not autoclave foam concrete makes 272–334 MDZh/m3, and on production of wall blocks of an autoclave gas concrete – on the average 1592 MDZh/m3.

Thus, on technical and economic indicators of production and application foam-concrete products and monolithic foam concrete are among the wall materials most demanded now even at many-storied construction. The solution of the problem of energy saving, durability, profitability, fire safety and low cost of protecting and heat-insulating designs of buildings and foam concretes allows to recommend not autoclave foam concrete and their production it for the broadest application.

Perspective also combined and monolithic option of protections executed from a fixed timbering from high-strength protective and decorative foam concrete 800 – 900 of factory production, a layer from foam concrete 600 and heat-insulating plates stacked between them or foam concrete 200 – 250 filled in built-up conditions also is provided. Taking into account the executed calculation it is possible to claim safely that construction of the many-storied building with foam concrete block application as a wall material in the West Kazakhstan region is possible.

REFERENCES:

1. *Kazakov A. S., Asimov B. K.* Modern technologies of a building, Saint Peterburg, 2004.
2. *Akhmetov A. I. Key* issues of foam concrete, Almaty, 2008.
3. *Bagenov U. M.* Concrete technology, Vysshaya shkola, 1987.

CONTENT

Научное издание

ПРЕДСТАВЛЯЕМ НАУЧНЫЕ ДОСТИЖЕНИЯ МИРУ. ЕСТЕСТВЕННЫЕ НАУКИ

Материалы IV международной научной конференции молодых ученых
«Presenting Academic Achievements to the World»

Выпуск 4

Ответственный за выпуск *Н. И. Иголкина*
Корректор *И. Ю. Астахова*
Оригинал-макет подготовила *Н. И. Степанова*

Подписано в печать 15.09.2013. Формат 60x84 $^{1}/_{16}$.
Усл. печ. л. XX,XX (XX). Тираж XXX экз. Заказ XXX.

Издательство Саратовского университета.
410012, Саратов, Астраханская, 83.
Типография Издательства Саратовского университета.
410012, Саратов, Астраханская, 83.